ALMA MATER STUDIORUM
UNIVERITÀ DEGLI STUDI DI BOLOGNA

Dipartimento di Elettronica, Informatica e Sistemistica

Dottorato di Ricerca in Ingegneria Elettronica, Informatica
e delle Telecomunicazioni – XX CICLO

SSD: ING-INF/01 - ELETTRONICA

Design of wireless sensor networks for fluid dynamic applications

Tesi di dottorato:
Rossano Codeluppi

Relatore:
Prof. Ing. **Roberto Guerrieri**

Coordinatore:
Prof. Ing. **Paolo Bassi**

Correlatore:
Prof. Ing. **Marco Tartagni**

Anno Accademico 2006 – 2007

To my family.

To Ale, Micky and Francesca .

To who hasn’t shared with me life and time in the last three years,
but who has been always in my heart.

Keywords

Wireless sensor networks
Capacitive pressure sensors
Fluid dynamics
FEM
Sensing
Embedded system

Contents

Introduction

In fluid dynamics research, pressure measurements are of great importance to define the flow field acting on aerodynamic surfaces. In fact the experimental approach is fundamental to avoid the complexity of the mathematical models for predicting the fluid phenomena.
It's important to note that, using in-situ sensor to monitor pressure on large domains with highly unsteady flows, several problems are encountered working with the classical techniques due to the transducer cost, the intrusiveness, the time response and the operating range.
For example sensors for aircraft design need high accuracy and precision, working in ranges up to ±2kPa. Otherwise the internal airflow sensor for automotive design requires a pressure operating range from ±10kPa to about ±30kPa. Considering sensors for nautical applications, they must detect pressure ranges up to only ±250Pa.
A common specification in fluid dynamics applications is to create a measurement system able to work over a large size surface, using a large number of robust and conformable sensors so that the required spatial resolution is achieved. Certainly a real-time pressure measure is an important tool for the aerodynamic behaviour analysis of the body and its correct design. The required sensor properties will be: small dimensions, high rejection ratio to temperature, robustness , low cost and low environment-invasion level. The latter characteristic can be satisfied only if the whole measurement system is not invasive. In fact, each sensor need a read-out circuitry and there will be cables to collect data and to supply the structure, embedded inside the body under test.
The above specifications point out that the classical measurement techniques are suitable in laboratories where the aerodynamic surface are designed, but it's rather unlikely to find them in the real environment where real bodies are used. An example can be to implement a classic pressure system on the top of a sail or on the racing car aerodynamic surfaces
To achieve a real and low invasive level it would be fundamental to remove every kind of wiring connection between the sensor and the device used to perform the data collection.
These remarks give the motivation to investigate the possibilities to change the classic sensor network implemented on the body under test in a sensor network based on wireless technology, without loss of robustness, number of measure points and real-time acquisition. Moreover creating a networks by means of wireless communication , on the top of aerodynamic surface is very challenging. In fact radio communication is an expensive energy process, the dedicated electronic increase the device dimensions and each measurement point must be a little system able to monitor the sensor, creating a digital data and managing a radio transmission.
The technological improvements of the last few years help to implement wireless communication. Wireless Senor Network platforms were born to perform an

environmental sensing (home control, security, health) but also are useful applications of the technology to allow exploring the technological challenges of further integration. Based on low power devices and miniaturized electronics, these structures are able to manage communications between sensors (set inside a wide area) and data collection point.
A interesting approach for satisfying the previously reported sensor requirements is the implementation of Micro-Electrical-Mechanical-Systems (MEMS). Using this devices small area occupation (tens of μm^2) and the proximity of the read-out circuitry to sensor can be obtained permitting to improve the spatial resolution.
However, aspects such as sensor packaging, time-consuming processes, robustness and costs cannot be neglected. In fact harsh environments or interfacial stress may be critical for the packaging procedure, limiting MEMS robustness.
The use of devices fabricated with polyimide or polyesters materials and assembled by means of micromechanical circuit board technology may represent a valid alternative to the MEMS solution, allowing sensors costs to be further decreased and providing features of environment-invasive-level and resolution fairly similar to the MEMS ones. Devices based upon the Printed Circuit Boards technology can be used for electro-mechanical transduction.
The purpose of this work is to design, build and test a sensor capable of acquiring pressure data on aerodynamic surface and to design and create a wireless sensor system able to collect the pressure data with the lowest environmental–invasion level possible.
The system is a network of electronics nodes able to sense pressure by means of developed sensor. The sensor is based on a flexible membrane changing the displacement because of fluid dynamics parameters variations. The membrane is an electrode of a capacitor, so that the displacement generates an electrical capacitance variation. The embedded electronics reads out such variations and translate them into a digital data and finally it transmits the information to a collection point. The wireless network must be able to manage several tens of nodes, guaranteeing a robust communication and a long life time of the system.
As a proof of concept, the monitoring of pressure on the top of the mainsail in a sail-boat has been chosen as working example.

Chapter 1

Fluid field measurement

Particular objects immersed in an ideal fluid and characterised by a geometry that determines a very small and attached vortical zone (non ideal fluid) are defined *aerodynamics* and the vortical zone around them is defined as a *boundary layer* [1].
Example of aerodynamic object are the aircraft wings or the boat sails. When an aerodynamic object passes through the air, it creates a pressure gradient distribution, due to its geometry, velocity and due to the direction with respect to the air motion.

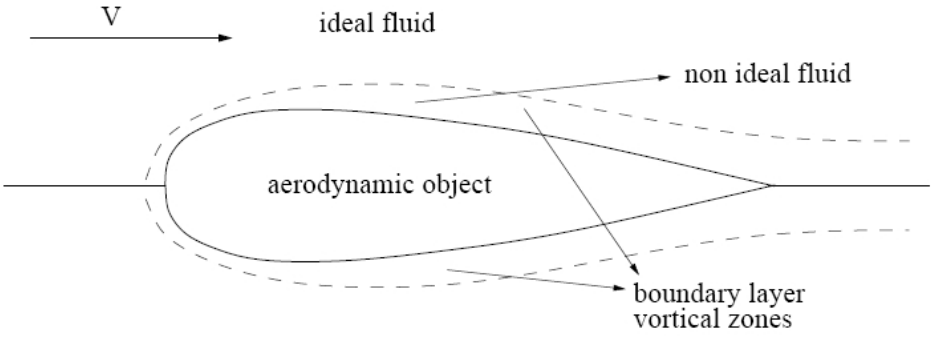

Fig.1.1 : Aerodynamic object moving through a real fluid

The boundary layer theory describes as if the boundary layer is sufficiently thin, there is no static pressure gradient, in the direction normal to the object surfaces: this means that the pressure just above the vortical zone is the same on the object surface. In this way, it is possible to obtain the pressure distribution at the object surface, using the Laplace and Bernoulli equations outside the boundary layer, on the aerodynamic object.
The aerodynamic loads acting on a body immersed in a flowstream are produced by the normal and tangential stresses over its surface due to the pressure distribution. When integrated, these stresses give rise to the resultant load components. These effects are strictly connected with the shape of the aerodynamic body.
It's understandable how important the knowledge of these forces is.
An active control of the magnitude of pressure, over the surface of an aerodynamic object, is useful both for the design and for the basic concepts of fluid dynamics [2].

1.1 Pressure measurement background

Pressure can be acquired with different methods depending upon the applications and the required fluid dynamic conditions. The measurement techniques can be generally classified as direct or indirect, depending upon whether the instruments are able to measure the required physical quantity or evaluate it from other measured properties. A wide number of fluid dynamic techniques are available for describing the fluid flow behaviour. Mainly we can divide them by: MEMS devices, conventional pressure transducer and imaging techniques.
The MEMS pressure transducers operate a capacitive, resistance or piezoelectric transduction. They have an excellent spatial resolution and a real low invasive level but they are still expensive. The output accuracy of the MEMS, in fluid dynamic measurements, strongly depends upon a correct calibration as well as upon the conditions in which they are used (harsh environments are not suggested)[3].
The conventional transducers (i.e. Scanivalve®, Setra® Capacitive Instruments) use fluid dynamic probes, such as Pitot or Prandtl tubes to sense the flow field. They have an good spatial resolution but and they are very expensive with an high invasive level.
Finally the imaging techniques, as Pressure Sensitive Paint (PSP) or Optical measurements based on laser Doppler velocimetry can be used. This techniques have an excellent spatial resolution and a medium-high invasive level but they are still very expensive. Moreover the particular measurement setup is suitable only inside a laboratory.
The above remarks depict a technical scenario where is possible to perform excellent measures, investigating carefully the fluid field, but only laboratories are environments suitable to perform the measurements.

1.2 Proposed pressure measurement

Starting from reflections discussed in the last paragraph, it's clear like, at moment, it's impossible to perform real time experimental tests in the real environment where the aerodynamic body is used. This is an important technological gap.
In the present work we suggest a solution and we describe a system able to overcome the bounds of the current pressure measurements.
The goal is to create a sensors network to acquire pressure values in the real environment over an aerodynamic surface. The system have to be robust, reliable, with a low invasive level and operating in real time.
We have chosen to apply the sensor network on the surface of sail.

Fig.1.2 : application field of proposed measurement system

1.2.1 Measuring system description

To perform the pressure sensing on the top of a sail, in the real environment, is necessary to create a sensor network with the lowest invasive level possible. Every network sensitive point, composed by the sensor and read-out circuitry, must be very thin minimizing the total area. To be implemented on the sail, the sensor network have to remove every kind of physic connection. In fact, the sail is too thin and tens of sensors necessary hundreds of wires, disposed along the surface or embedded in the sail. It's a quite complicated scenario.
The only solution is to perform a radio communication between every sensitive point and the network data collector. Therefore the sensitive point will be a wireless node housing the sensor, the sensing circuitry, the electronic dedicated to the radio transmission and node management, but also a power supply. The energy source has to be sufficient to allow node life time of several weeks

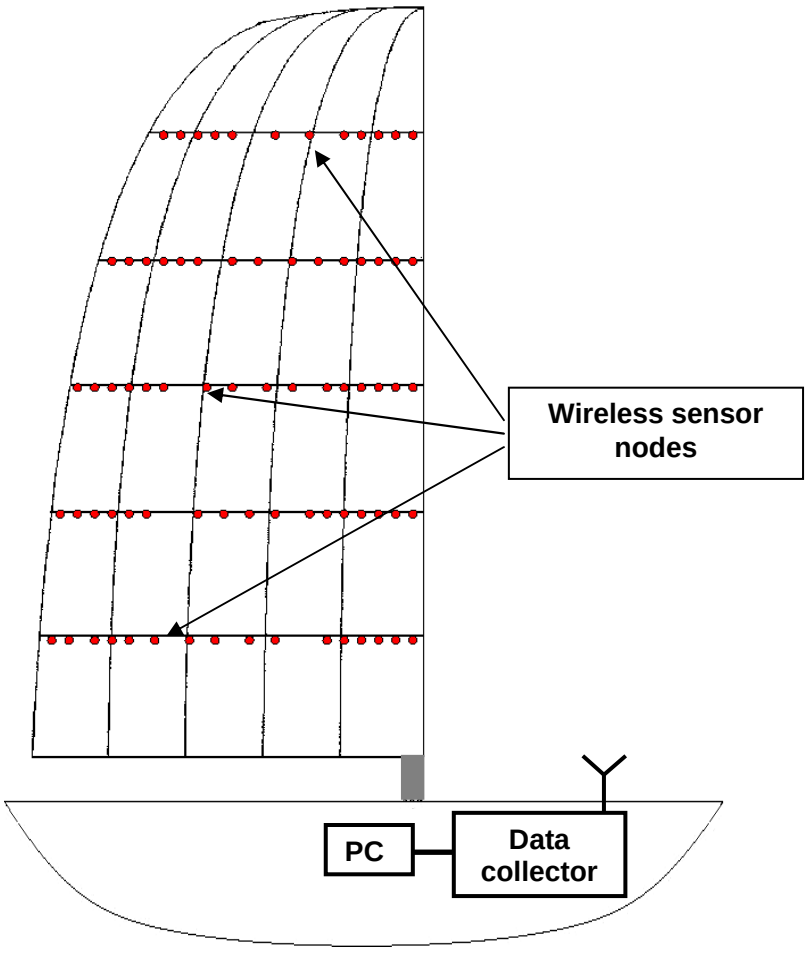

Fig.1.3 : system layout

The wireless sensor node will be a little system able to translate the data pressure in a digital information suitable to radio communication.

The sensor devoted to the application will be developed. The sensing will be done by the transduction of differential pressure between the sail leeward side and windward side (Fig.1.4) (an absolute sensor is not used because pressure variations on the sail are too small compared with atmospheric pressure) so an hole in the sail, below the sensor to create a static tap, will be necessary. Another opening, shaped like the sensor, must be created in the sail to allow the fluid field acting on the membrane sensor.

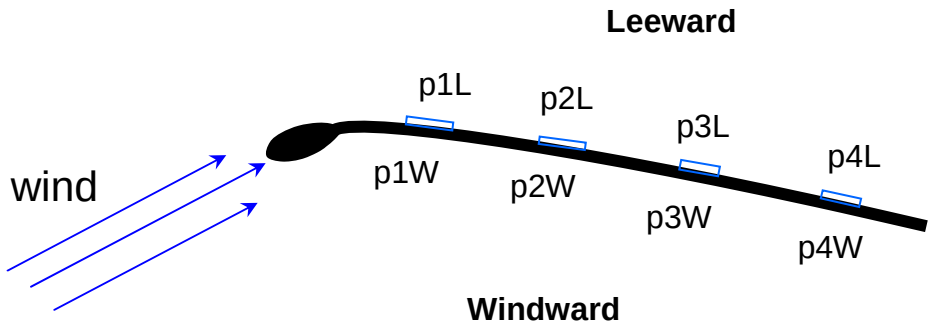

Fig.1.4 : pressure field detection

To obtain a low invasive level, the proposed wireless sensor network will be developed to be embedded in the sail battens. The wireless sensor node dimensions will be tuned on the batten shape and the number of nodes onboard each batten will be function of pressure map necessary (Fig.1.5).

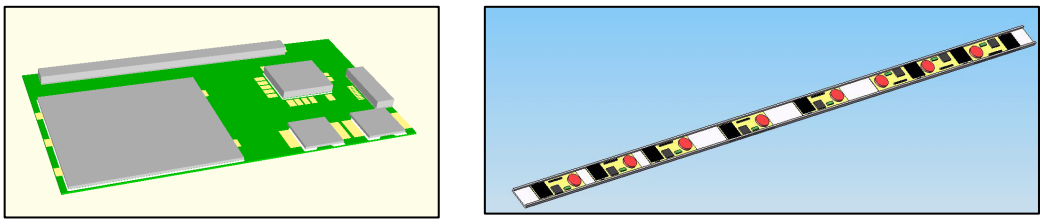

a) b)

Fig.1.5 : a) example of node , b) batten instrumented

Finally the node will have to be flexible so that will be able to follow the sail curving.

1.3 Additional considerations

The measurement system proposed is devoted to perform a real time pressure monitoring on the top of a sail, operating in the real environment. It can be useful to describe aerodynamic loads variations or drive force with relation to sail surface

trimming. Therefore the system can be an important means for analysis of the sail aerodynamic behaviour, helping the designer to optimize the aerodynamic object; otherwise it can be useful at the helmsman to improve sailing.

Chapter 2

Wireless sensor networks

The advances in radio frequency (RF) technology have created low-cost, low–power and multifunction miniature device. Low-cost, high performance RF devices and systems are finding their way in various applications. Some prominent applications include wireless LANs, portable GPS receivers, Bluetooth , RFID or wireless sensor networks (WSN). In particular WSN are applied to remote metering, home automation and large-scale sensor networks [4].
The wireless applications are classified by throughput and transmission range. If we compare the WSN with others applications, short range and low throughput are clear (Fig.2.1).

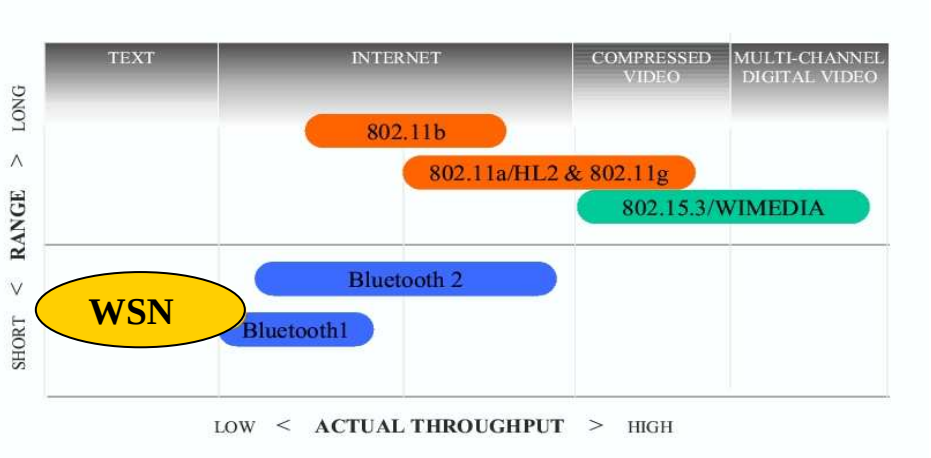

Fig.2.1 : comparison between WSN and others wireless applications

In fact, the wireless sensor networks have been created to collect sensors data (few bytes) using limited energy (low power transmission), so that to implement the network over a wide region it will be necessary a huge number of sensor nodes.
The architecture of the hardware sensor node consists mainly of five components: sensing hardware, processor, memory, power supply and transceiver (with antenna). Therefore the sensor node is able to sense, compute and actuate into the physical environments [5].
The wireless sensor networks can be an interesting solution to perform the wireless communication inside the proposed pressure measurement system.

2.1 Features

Operating into ISM (Industrial, Scientific and Medical) band ,the wireless sensor networks have several transmission frequency with different data rate (Fig 2.2). The transmission frequency is a very important parameter choosing the WSN platform suitable for the application, because it changes not only the data rate, but also the transmission range.
In fact, considering the Frijs transmission formula (2.1) that models the theoretical free-space loss between isotropic radiators in a communication system [6] , we have the relation between transmission frequency and power received into a transmission range.

$$P_R = P_T G_T G_R \left(\frac{\lambda}{4\pi R} \right)^2 \qquad (2.1)$$

In the (2.1) P_R is the received power, P_T is the transmitted power, G_T is the gain of the transmitting antenna, G_R in the gain of the receiving antenna, λ in the operating wavelength and R is the distance between the TX and RX antennas. It's clear as using the same transmission power but increasing the transmission frequency, it will be possible to obtain the same received power only into a shorter transmission range. The Fig.2.2 describes the available transmission frequency.

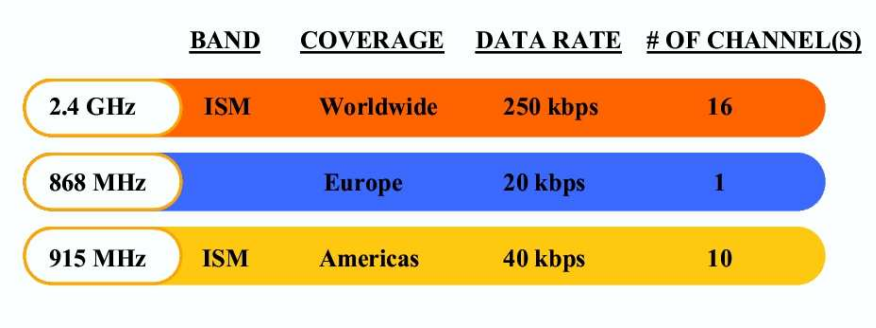

Fig.2.2 : ISM band : coverage, data rate and frequency

Changing transmission band, we find different data rate and the maximum is 250kbps. Therefore the WSN works with low data rate and this is a suitable characteristic of networks with low duty cycle like them . The sensor nodes can be active few tens of milliseconds over wide period like minutes or hours, because it has to monitor just a sensor. It's important to note that low date rate allows to save energy and so it helps to have low power devices. In fact, to create a wide network with a large number of nodes, it's necessary to have devices with long time life using common battery. To save energy, the wireless sensor networks have short transmission range (low P_T) : 30-50metres indoor range, 100-200metres outdoor range. Moreover to have long battery life low power electronic is used Another important characteristic are the node dimensions: a small form factor is necessary to allows the system embedding it the operating environment so single chip with processor and transceiver embedded or miniaturized board are used[7] [8].

2.2 Network topologies

The wireless sensor networks are composed by two types of devices:

- Full Function Device (FFD)
- Reduced Function Device (RFD)

The FFD are devices able to perform the data sensing but also to manage data routing inside the network. They are the routers or controllers network
The RFD are devices devoted to perform only the data sensing. They are the slaves device (or network end points).
Every network needs at least one controller working like a network coordinator. There will be a large number of slaves able to communicate with the controller and, dependently from network topology, router can be used. The differences between the RFD and FFD are the amount of memory and the software programmed. In fact, the data routing functions are based on wide routing table (memorized) and a particular software management.
The WSN can have hundreds of network nodes, so it is important to find the best network topology to create the system. The three most common topologies are : star, mesh and hybrid.[9]

2.2.1 Star

In the Star topology all nodes (slaves) communicate directly with the network coordinator (Fig.2.3) . This type of network is very simple and the most suitable for short range applications.

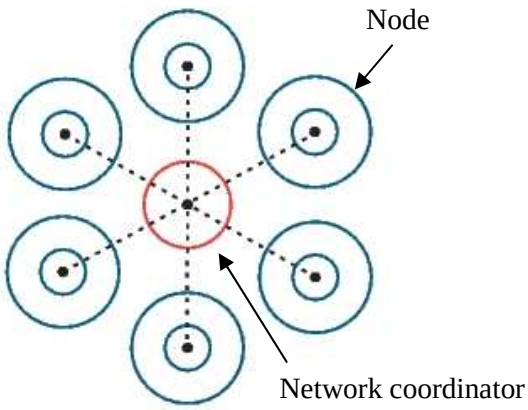

Fig.2.3 : Star topology

The single-hop approach for communicating between each slave and the controller is the lowest overall power consumption [10]

2.2.2 Mesh

In the Mesh topology all devices are FFD. In fact, every node con communicates with all devices (into its transmission range). This is a multi-hop approach for

communicating between each node and the controller. This topology is suitable to implement large-scale networks, with hundreds of nodes.
It's energetically expensive and the transmission time is increased by each hop. In fact, every node employs some tens of milliseconds to transmits a received data.
The communication is really robust, because each node can use many routes to reach the network coordinator.

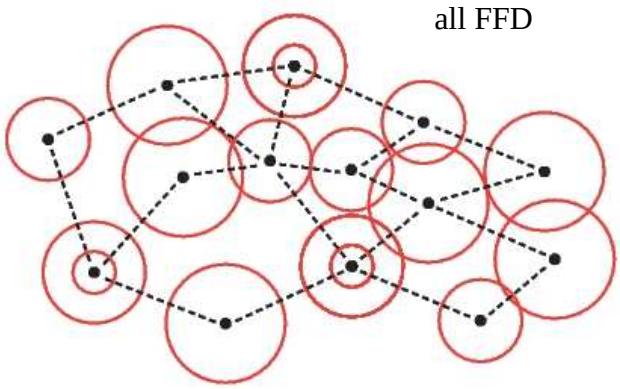

Fig.2.4 : Mesh topology

2.2.3 Hybrid

The Hybrid topology mixes Star and Mesh topology. This is a multi-hop approach for communicating between each node and the controller, but not all nodes can transmit to every device into transmission range. In fact this topology is useful to shape network on the environmental geographic bounds. This topology is suitable to implement large-scale networks, with hundreds of nodes.

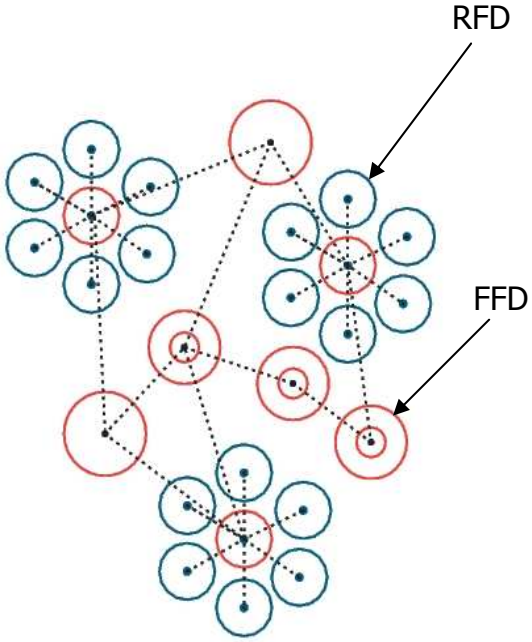

Fig.2.4 : Mesh topology

2.3 Network and Data management

To manage the wireless sensor networks it's necessary a RF protocol. Nowadays the user can choose between two options: ZigBee protocol or a proprietary solution based on the RF standard IEEE 802.15.4. It's important to note that not all WSN platform can use the two solutions, but just one is implemented. Usually the platform it's chosen also dependently from used protocol [11].
The ZigBee solution is the WSN standard, and huge number of companies cooperate to develop it. Using ZigbBee the user creates a self-organizing sensor network, really reliable , flexible and easy to deploy [9]. This standard appears very interesting when a Mesh network with hundreds node has to be created over a wide area. If the network is small with tens of nodes creating a Star network, using ZigBee can be too complex.
Proprietary solutions, appear real interesting to develop a WSN simple or where the self-organizing property is not important [12]. In fact,programming the nodes is simple and faster than a ZigBee solution.
The RF protocol provides to the user an API (Application Programming Interface) command data base necessary to develop the WSN management software.
It will be necessary to program the controller, the slaves and finally the router with devoted software.
It's interesting to describe the basic methods to acquiring and propagating sensor data. There are three common classes: [13]

- *periodic sampling* : useful where the process needs to be monitored constantly. Sensor data is acquired from a number of remote points and forwarded to a data collection center on a periodical basis;
- *event driven* : the sensor data is transmitted only when a certain threshold is reached;
- *store and forward* : the sensor data is captured and stored by a remote node before it is transmitted to the network coordinator.

The right method to acquire and propagate the sensor data is necessary to perform the best monitoring but also to minimize the power consumption. In fact, save transmission or power on the node only if necessary is basic to obtain long battery life.

2.4 The wireless sensor network chosen.

In the chapter 1 the measuring system is described. It's clear that a wireless sensor network can be used to remove every cable and deploying a sensor network on the top of a sail. This is a shot-range application, because the nodes are deployed into a small area (few tens of square metres) and the fastest communication between slaves and controller has to be performed. Finally the energy consumption is basic because the environmental bounds limit also the battery dimension.
Using the above remarks we have studied many platform based on ZigBee protocol or a proprietary solution. We have chosen a proprietary solution: the Z-WAVE™ platform by Zensys.
We have chosen Z-WAVE™ ZM0201 single chip solution because it was the first single chip on the market allowing to create a very small sensor node. In fact, into a

5x5mm QFN package there are a 8051 compatible microcontroller, a 868MHz RF transceiver, a 12 bit rail to rail ADC and ten configurable general purpose I/O pins.
The power consumption is small : 2.5µA in sleep mode and 5mA n normal mode.
The transmission power is programmable in the range -20dBm to 0dBm allowing to save energy in the transmission.
Finally it is interesting to note like in the Zensys developer kit are available different types of board to simplify the hardware and software test before the full customized electronic is created (Fig.2.5).

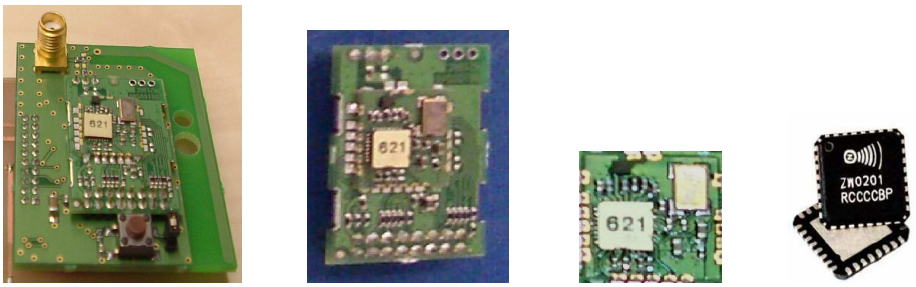

a) b) c) d)

Fig.2.5 : Zensys boards: a) ZW2106, b) ZW2106c, c) ZW2102, d) ZM0201

Working in the 868MHz ISM band Zensys platform allows to use less power to cover the same radio link compared with the 2.4GHz ZigBee solutions.
The very low data rate (9.6kbps) appears a limit , and so we will have to use carefully the available band.

Chapter 3

Design and simulation of Wing Pressure Sensor

The strip pressure sensor for aeronautical use, described in the following section, has been developed in strict collaboration with other colleagues. In particular the project has been led off and developed by Dott. M. Zagnoni from the Phd thesis of whom [14] and Eng. A.Rossetti.
The author has been involved only in the sensor structure optimization, in the fabrication of sensor and in the test. The design and optimization of single sensitive unit have been performed by Mr. Zagnoni and Mr. Rossetti.
The performed activity, concerning the aeronautical pressure sensor, has been preparatory to be able to develop the sail pressure sensor, thus the behaviour of materials, the simulation methods and the fabrication technology are reported

The aeronautical pressure sensor is a conformable thin film strip, designed for aerodynamic applications. It is a capacitive differential pressure transducer aimed at monitoring the pressure profile on an aerodynamic body. Capacitive sensing has been chosen because of distinct advantages when compared to other, such as higher sensitivity, lower power consumption and better temperature performance. The differential pressure sensor approach has been preferred to absolute pressure sensors for overcoming altitude problems due to barometric pressure gradients.
The sensor was built using PCB (Printed Circuit Board) technology. This choice has been done because it allows the manufacture of the sensor by fast prototype machine directly into our laboratories so we obtained a technology independence in the development of the device. The materials used are perfect to achieve a good transduction by sensitive units created, and they allow to build a low cost device because cheap. Moreover, in the future, the PCB technology can allow the hosting of electronic sensing and signal processing components by means of smart packaging, (such as the chip on board) directly inside the sensor.
The proposed sensor is able to operate in a pressure field with the range of ±2000Pa and a resolution of units of Pa.
The device developed must be suitable for conforming to the profile surface and must be characterised by a total thickness that will not alter the fluid flow condition. This requirement is satisfied if the sensor is comprised within the boundary layer of the profile.

3.1 Sensor working principle

The pressure sensor system presented, is meant to produce an electric output related to the pressure distribution that is applied to the sensor strip surface. The fluid dynamic variables act on the deformable part of the sensors, where an electrode is placed, which, changing its geometry, leads to an electrical capacitance variation (Fig.3.1).
The latter can be electronically read in order to collect a set of surface pressure points, through a multiplexed switch capacitor sensing scheme.

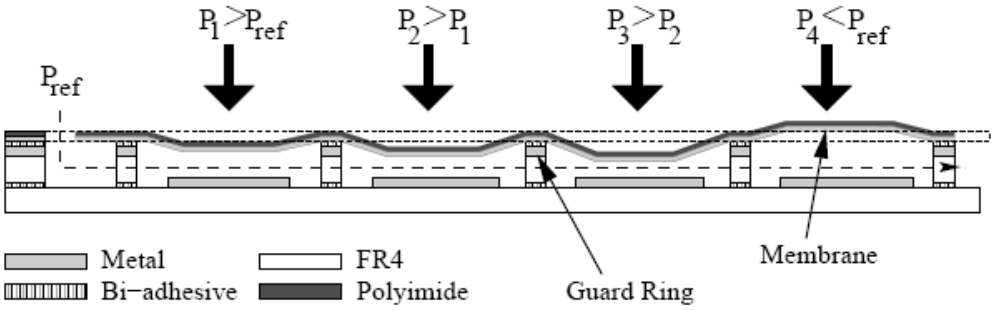

Figure 3.1: Differential pressure sensor strip principle of operation. Membranes deflect upward or downward with respect to the gradient of pressure between the outside and inside of the chamber.

As illustrated in Fig.3.1, the membrane at each point of sensing deforms itself downward or upward with respect to the static pressure reference taken by means of the holes. Since the membrane area is usually much smaller than the aerodynamic surface to be monitored, the corresponding pressure distribution over the deformable film can be considered constant with a good approximation, however the importance of the surface occupation of every sensing element in terms of spatial resolution becomes evident.

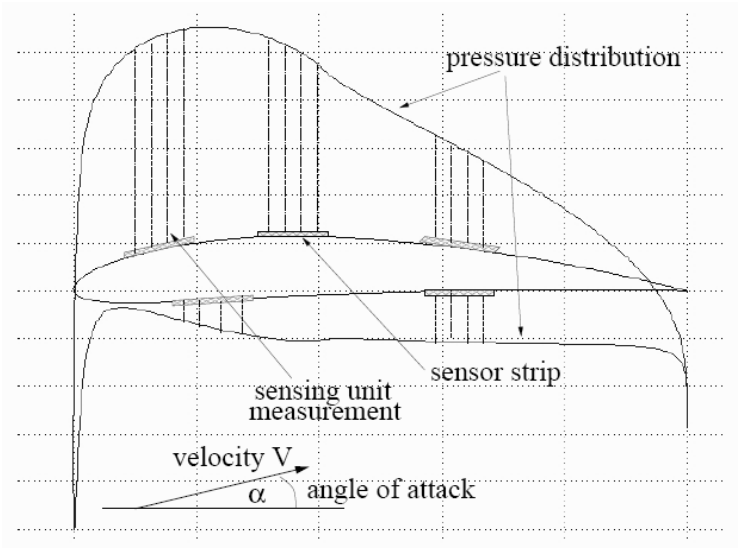

Figure 3.2: Application example: monitoring pressure distribution over a wing profile.

An application example is to investigate the pressure distribution over a wing profile. It depends on free stream velocity V and angle of attack α: a variation in the (α, V) field leads to a different pressure pattern (Fig.3.2).

3.2 Sensor structure and optimization

3.2.1 Original sensor structure

The sensitive unit consists of a three layer structure in a stack: Base, Spacer and Conductive Membrane (Fig.3.3):

- the Base layer is a rigid copper-clad glass-fibre composite layer. This layer hosts as many pads as pressure measurement points. Pads represent the lower plate of every capacitor (fixed electrode).VIAs (particular D) enable the addressing of every pad through the connection to a flat cable;

- the Spacer layer is a rigid glass-fibre copper-clad composite layer which is glued both to the top of the base layer and to the bottom of the membrane layer, forming the cavity within the membrane is deflected by the pressure input. All unity chambers are connected by miniaturised pipes, patterned in the spacing layers, in order to share the same internal pressure, forming a unique bigger chamber.

- the Membrane layer is a 25 µm thick deformable copper-clad (17 µm) Kapton® polyimide composite layer. Small holes (particular A) are drilled on the proximity of one the ends of the sensor, before the first sensing element and act as a pressure reference. A VIA (particular C) is designed for the connection of the upper electrode, through the same flat cable used for connecting the Base.

Layers are attached to each other by means of some 50 µm thick bi-adhesive tape, patterned in the same shape as the spacing layer. As shown in particular A of Fig. 3.3, a small chamber is realized for allowing the pressure reference to be shared in every sensing element chambers.
Exist also a copper layer acts as a guard ring, for reducing the coupling effects between the upper electrode on the membrane and the routes, on the top of Spacer. Particular B and C show how the spacer guard ring and the membrane can be electrically connected.
The device length and width can be set according to the application: the measurements and simulations reported here in this work are related to devices that are from 13 to 16 cm long and from 1.8 to 3 cm wide. The total thickness is comprised within 700 µm and 1 mm, as shown in Fig.3.4.

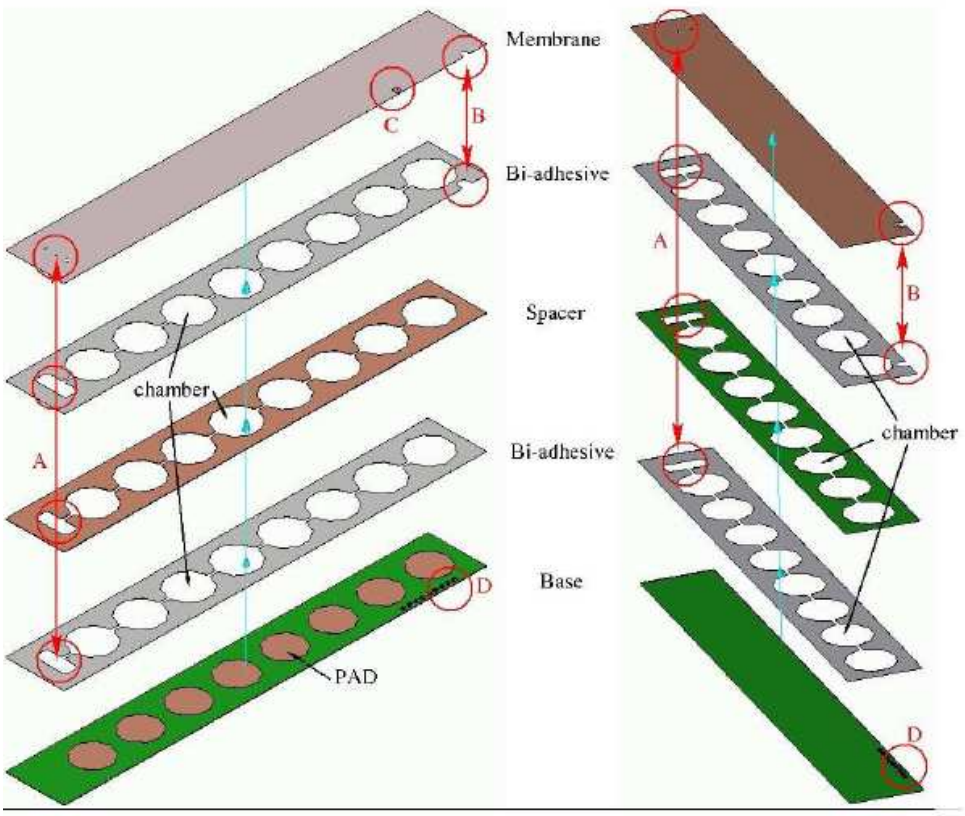

Figure 3.3: Pressure sensor strip structure: exploded top view (left side), exploded bottom view (right side).Membrane, spacer and base are connected by means of bi-adhesive layers. A: small chamber for allowing the pressure reference to flow in the spacer chamber. B: spacer guard ring electrical connection. C: membrane electrical connection. D: base electrical connections.

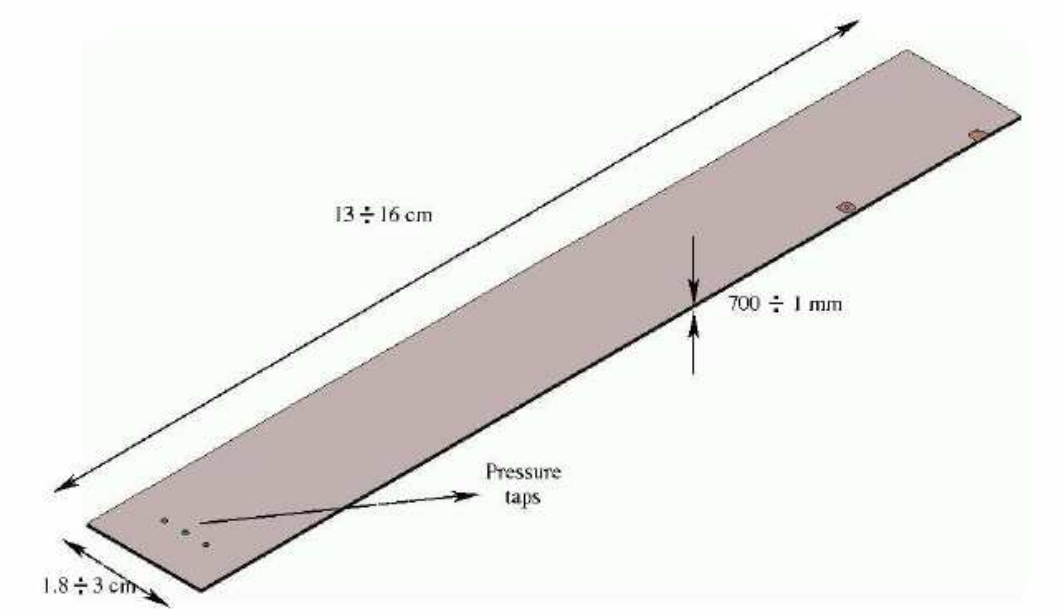

Figure 3.4: Pressure sensor strip structure: assembled view and dimensions.

3.2.2 Layout optimization

The sensor has been built using PCB (Printed Circuit Board) technology. This choice, allowing the manufacture of the sensor by fast prototype machine directly into our laboratories, let to reach a technology independence in the development of the device but also it needs to pay attention during the design. In fact, not all manufacture solutions will be possible.
The sensor design depicted above showed some critical characteristics:

1) there is a guard ring ground connected in front of moveable electrode divided by bi-adhesive layer. If Spacer shape process (milling of rigid glass-fibre copper-clad covered by bi-adhesive layer) is not perfect, we can have small rips in the bi-adhesive and so creating short cuts between guard ring and membrane;
2) the guard ring contact is on the top side of sensor. The VIA is critical to solder because Kapton® surrounds and it breaks the flatness around the VIA area;
3) the electrical routes are on the top side of Base layer around the fixed electrode (Fig.3.5). The Base-Spacer junction, created by a 50um bi-adhesive, can be dangerous for sealed cavity within the membrane is deflected by the pressure input. In fact the un-flatness of the Base layer can create small pipes around electrical routes and connecting the inside chambers with external pressure. The pressure shared in every sensing element chambers could be different from the pressure reference.

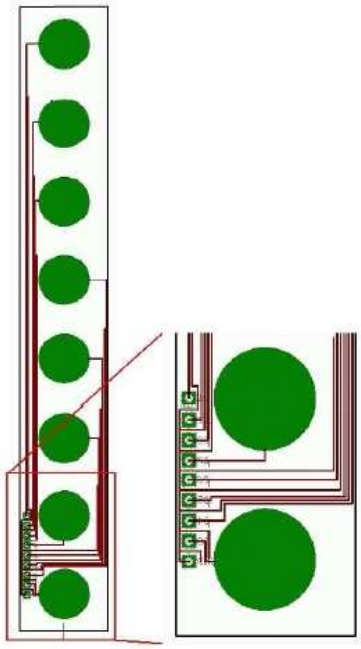

Figure 3.5: top side of Base layer in the original pressure sensor

To avoid critical features we have changed the Base layer and simplify the Spacer layer.
To obtain a perfect flatness around the fixed electrode, we have translated the electrical routes in the bottom side of the Base layer (Fig.3.6). To perform the electrical connection with the fixed electrodes on the top side we have created a drill plated in the centre of each pad. To note that the drill plated is a pipe to external

environment: we have provided a cover by a Kapton® layer on the bottom side of the Base layer to close every drill.

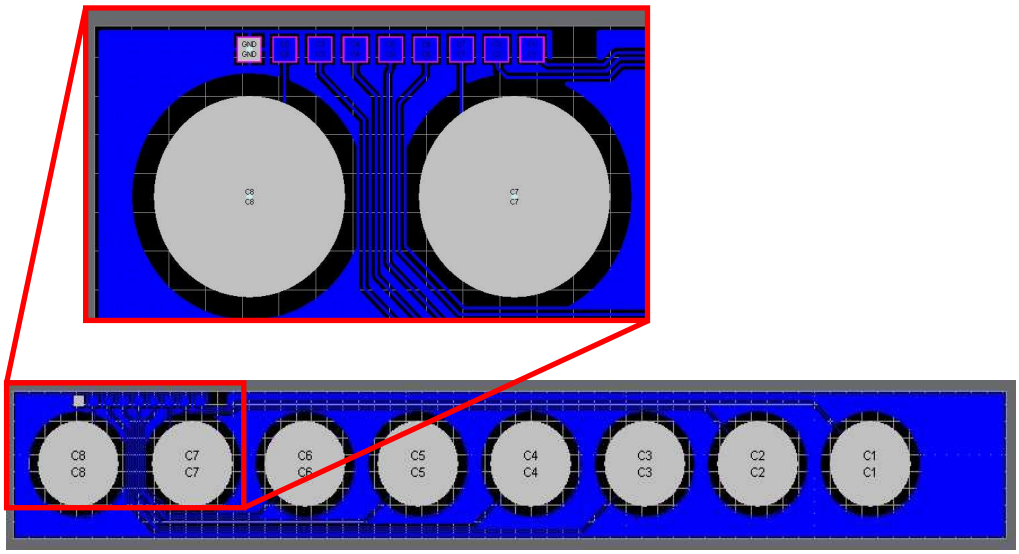

Figure 3.6:bottom view of the Base gerber file

The second change has been to remove the guard ring from the Spacer layer and to translate it on the top side of the Base Layer (Fig. 3.7). This solution avoid every short cut chance between membrane and guard ring, and it removes the problem about the electrical connection. In fact, having the guard ring on the top of the Base layer a simply VIA is sufficient to lead the electrical contact on the bottom side, simplify the soldering. All electrical contacts will be in the bottom side of the Base layer.

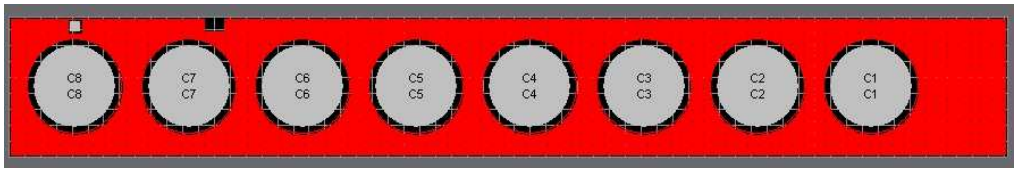

Figure 3.7:top view of the Base gerber file with guard ring (red part)

The Spacer layer will have the same shape but without guard ring. The Membrane will not need the particular B of Fig. 3.3.

3.3 Designing methodology

3.3.1 Mechanical model compared with FEM simulation

The first designing step has been to develop an analytical sensor model for modelling the sensor and for identifying the parameters.
A cylindrical structure has been chosen for the sensing element. Such geometry considerably simplifies the model description, since a three dimensional axial symmetric configuration can be easily expressed in two dimensions, allowing much simpler equations to be considered both for the mechanical and the electric model representation.
The mechanical model is based on the classical mechanical theory of large deflection where a linear stress-strain relationship for matters (Hooke's law) describes the linear displacement of plates with respect to the exerted pressure.
Afterwards Finite Element Method Simulations (FEM simulation) have been performed.
Aim of FEM simulations is to describe more efficiently the physical and structural sensor features, because of the sensor analytical formulation the behaviour might be not sufficiently accurate. To achieve a good design of the device due to the non linearity present both in the pressure-deflections transduction and in the electric capacitance relationship, other approximations are then introduce by means of the model used in the rule of mixtures, these topics lead to a non neglegible error in the capacitance integration.
Studying the result of comparison between FEM simulation and analytical model, the latter appears unsuitable to design the sensor, as Fig 3.8 and 3.9 show.

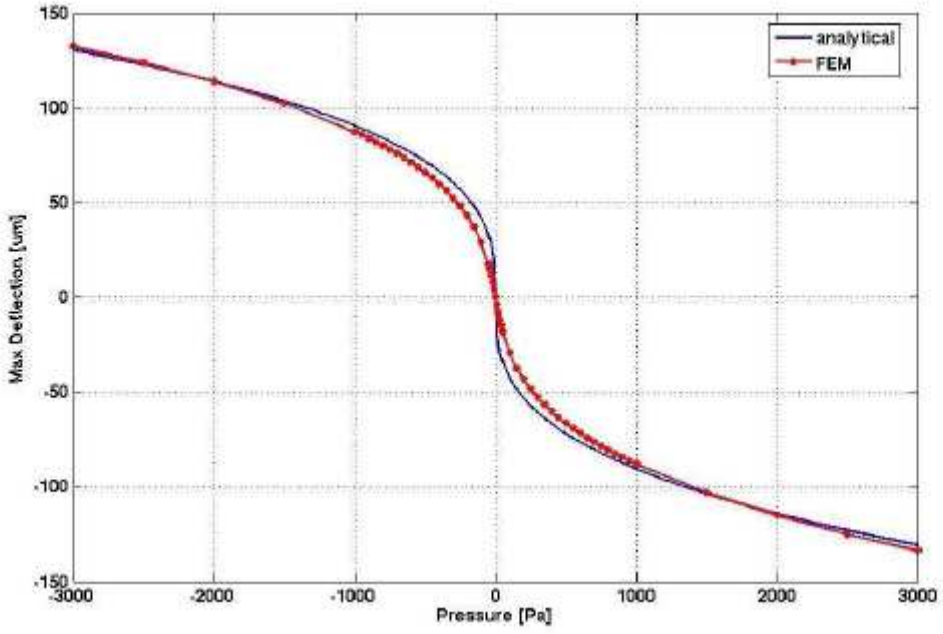

Figure 3.8: deflection; analytical an FEM simulation

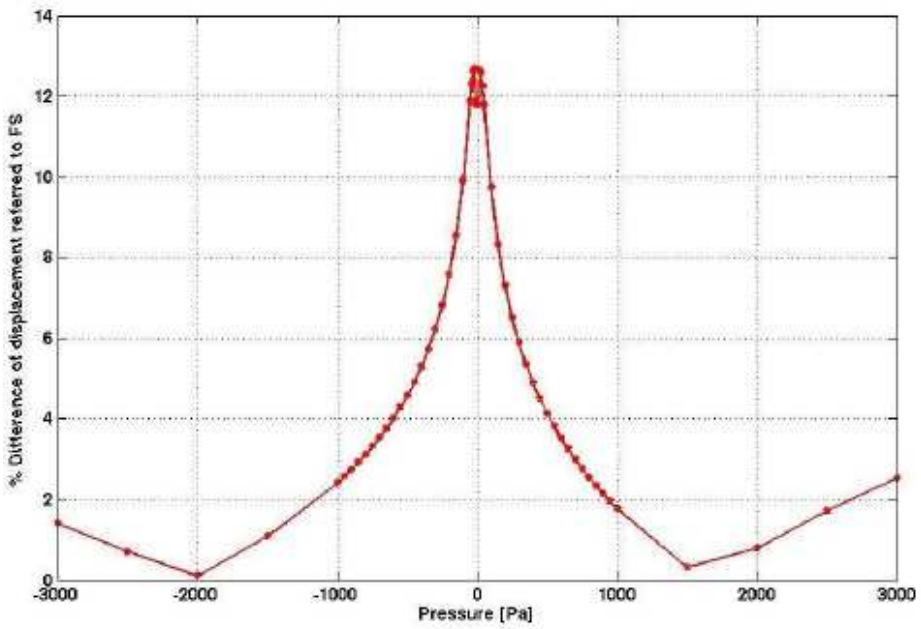

Figure 3.9: difference (%) of displacement between analytical an FEM simulation

3.3.2 Creep : viscoelastic phenomena

Some materials subject to an external load can be considered, in the range of small deformations at ambient temperature whenever the internal stresses don't exceed the yield and therefore can be treat as linear elastic solids. This assumption implies that the Hooke's law can be used and that there is no time-dependent relationship between stress and strain. When a material is subjects to tension exciding the yield point or to lower tension but at high temperature then the relationship between stress and strain strongly depends on the size of the applied load, on the temperature, and crucially on time. This effect is usually referred to as viscoelasticity [15]. Materials as metals or ceramic manifest viscoelastic phenomena at very high temperature and load while other materials as polymers or polyester are still concerned with this phenomena at ambient temperature and low stress levels. An important implication of viscoelastic behaviours is that the stress-strain characteristic cannot be rigorously considered a static (i.e. memory-less, though nonlinear) relationship. Conversely, the stress-strain characteristic exhibits behaviours that appear highly non linear, even for small deformations, and that, most importantly, depends on the derivatives of the stress and strain functions. This phenomenon is well evidenced by the analysis of two cases.

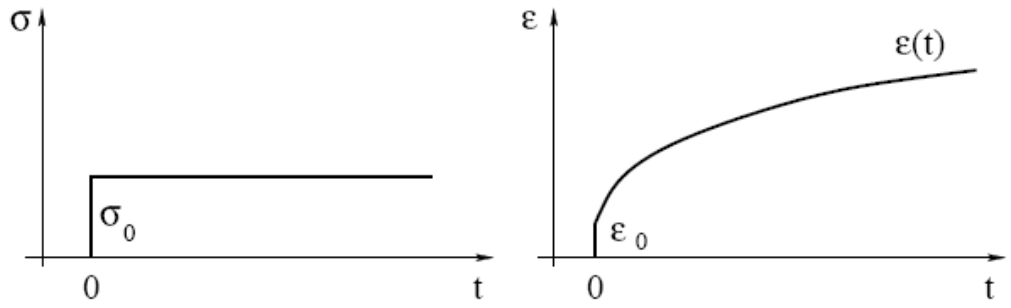

Figure 3.10: Response to an applied constant stress.

As shown in Fig. 3.10, if a stress function step (σ_0) is applied to a sample of material subject to creep, a sudden elastic strain is followed by a viscous and time dependent strain with an increasing trend ($\varepsilon(t)$). This phenomenon is referred as "compliancy" as is defined as:

$$D(t) = \frac{\varepsilon(t)}{\sigma_0} \tag{3.1}$$

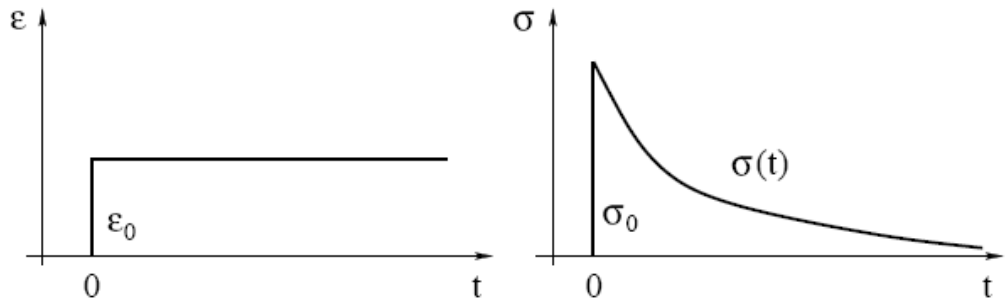

Figure 3.11: Response to an applied constant strain.

Conversely, if a strain step is applied, the stress decreases as a monotonic function (Fig. 3.11) and is commonly referred as "relaxation", defined as:

$$E(t) = \frac{\sigma(t)}{\varepsilon_0} \tag{3.2}$$

This type of behaviour is usually present in polyimides at ambient temperature and for stress bigger than 1 MPa [16] and is conventionally known as creep, where the common trends followed by materials are shown in Fig. 3.11. In viscoelastic material

the stress is a function of strain and time and so may be described by an equation of the form:

$$\sigma = f(\varepsilon, t) \tag{3.3}$$

This is known as a non-linear viscoelasticity, but as it is not amenable to simple analysis it is frequently approximated by the following form:

$$\sigma = \varepsilon \cdot f(t) \tag{3.4}$$

This response is the basis of linear viscoelasticity and simply indicates that for a fixed value of elapsed time the stress will be directly proportional to the strain.

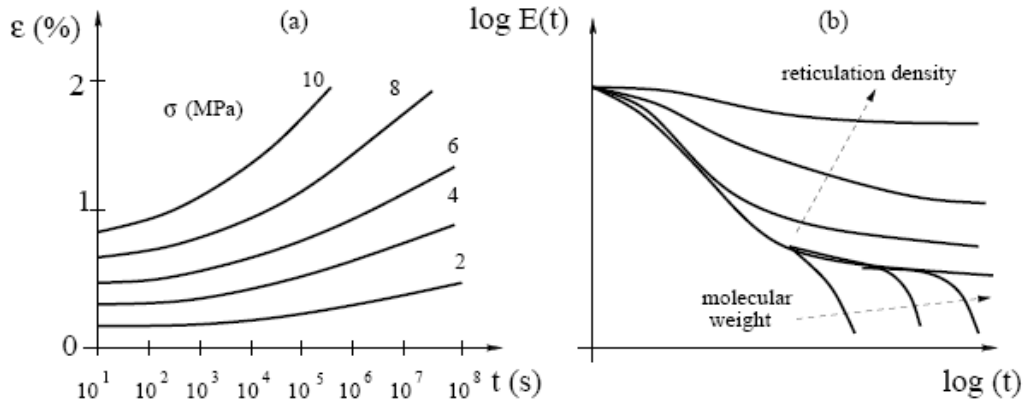

Figure 3.12: a) Creep deformation for different applied stresses. b) Qualitatively behaviour of the relaxation modulus as function of time and molecular structure.

However, this doesn't imply that the time function is linear. First of all, it can be observed that the mechanical deformation of a body subject to creep phenomena is a function of the entire loading history of the body itself. In other terms, thanks to viscoelasticity the system gains memory: all previous loading steps contribute to the final response, as shown in Fig. 3.13.

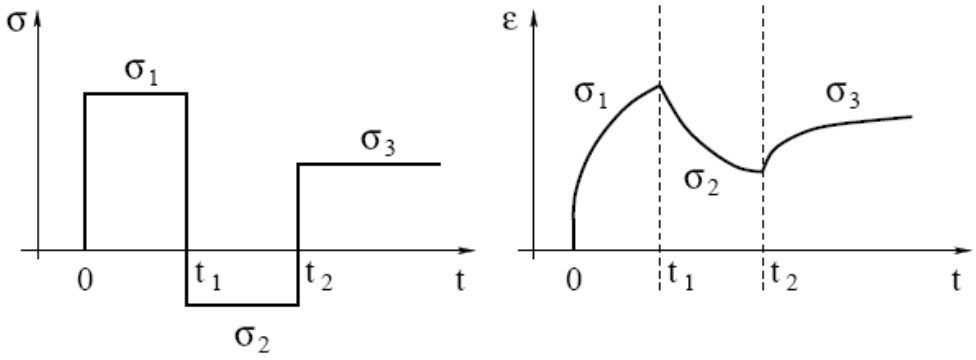

Figure 3.13: Presumed creep response when different stresses are applied

Creep affects the proposed structure, causing membrane deflections of some μm, manifesting themselves in time-scales of tens of minutes. The above observation implies that in order to know the exact response of a structure subject to creep, a model of its excitation should be available, describing the evolution in time of input stress (or strain). This is normally not possible in fluid dynamic applications where the input loading and its dynamic is unknown. In this case, the best that can be achieved is a bound on the maximal deviation that creep may introduce with regard to static models. Such bound can be roughly interpreted as an uncertainty that should be taken into account when using the sensor as a measurement device in a dynamic environment. A convenient way to obtain such bound consists of realising that creep can be approximately classified as a low-pass phenomenon, so that a typical experiment to estimate its extent consists of applying, at t = 0, a step-like excitation in stress spanning the whole allowable stress range and in evaluating the difference between the response at t = 0+ and the response at t $\rightarrow\infty$, where, of course, t$\rightarrow\infty$ means a temporal value for which the experiment can be considered settled or the viscoelastic effect has reached more than 90 % of his relaxation behaviour.
The major reason to practise this kind of analysis is to understand how actions on the geometry and materials employed in the sensor fabrication can reduce the extent of the viscoelastic response and thus tighten the error bounds.
In the modelling of creep [17], the deformation model of a membrane changes from a static, non-linear, time-invariant model to a dynamic, non-linear, time-invariant model. In other terms, one could in principle model the viscoelastic behaviour by introducing time derivatives into the system of partial equations that rule the membrane deformation. In many conditions it is useful to model creep by using equations where time-varying parameters take care of describing the dynamical effects. A particularly effective way of doing so is by the introduction of a time dependent module of elasticity, obtained starting from Kapton® data sheets [16]. As shown in Fig. 3.14, from strain versus time curves, given by different applied stresses, the corresponding time dependent modulus of elasticity have been calculated, interpolating the strain curves, as:

$$E_r(t) = \frac{\sigma_i}{\varepsilon_i(t)} \tag{3.5}$$

where $\varepsilon_i(t)$is the time dependent strain, σ_i is the corresponding stress and the index "i" represents different values of stresses and temperature conditions. The approach

is convenient because it leads to equation sets which fit more easily into an analytical and conventional FEM simulation structure than models with explicit time derivatives. In other terms it allows creep to be obtained by a sequence of static simulations referring to different time instants. These curves (Fig. 3.14.b) have been fitted by :

$$E_\tau(t) = \sum_j \left(A_{ij} e^{B_{ij} t} \right) + k_i \tag{3.6}$$

where Ai_j , Bi_j and Ki parameters are representative of the elastic and viscous behaviour of the membrane in particular condition of exerted stress and temperature. The expressions obtained in Eq. 3.6 will be used for time dependent mechanical simulations and for analytical approximation in the design phase. The approach followed is an alternative and easier way to reproduce creep behaviour without differential equations, basing the estimation of the coefficients of Eq. 3.6 by means of interpolation, depending upon the stress and the temperature. Since the maximum membrane relaxation, due to creep, is obtained for the maximum pressure value, a time dependent capacitance variation can then be calculated until the transient response can be considered as finished or no longer relevant for the proposed application.

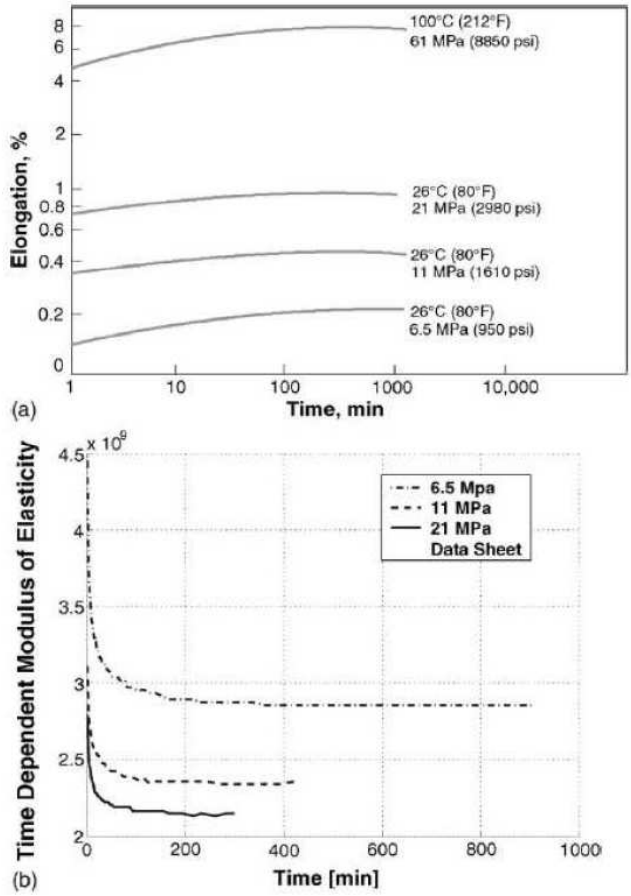

Figure 3.14: Kapton® creep: a) strain versus time behaviour from datasheet for particular temperature and stress conditions. b) time dependent modulus of elasticity Eτ(t), as described in Eq. 2.18 for particular temperature and stress conditions.

3.3.3 Electro-Mechanical model compared with FEM simulation

The electric model has been developed considering the axial symmetry of the sensor and a parallel plate capacitor structure with electrodes of the same area The capacitance C is given by:

$$C = \frac{\varepsilon A}{d} \tag{3.1}$$

where ε, A and d are the permittivity of the gap, the area of the plates and the distance between the plates, respectively. For moving circular diaphragm sensor, the capacitance becomes:

$$C = \iint \frac{\varepsilon}{d_0 - w(r)} f dr d\vartheta \tag{3.2}$$

where d_0 is the distance between the plates when no pressure is applied and w(r) is the deflection of the diaphragm . Due to the axial symmetry of the structure there is no dependence on the angle θ.
Developing the expression 3.2 it's possible obtain a math relation between sensor capacity and pressure applied in function of the membrane Young's modulus E .The creep behaviour in the membrane is evaluated with a first order approximation, using two different values for the Young's modulus, E_{Max} and E_{Min}.
The FEM simulation has been performed using modulus of elasticity Eτ(t) obtained from Kapton® data sheets.

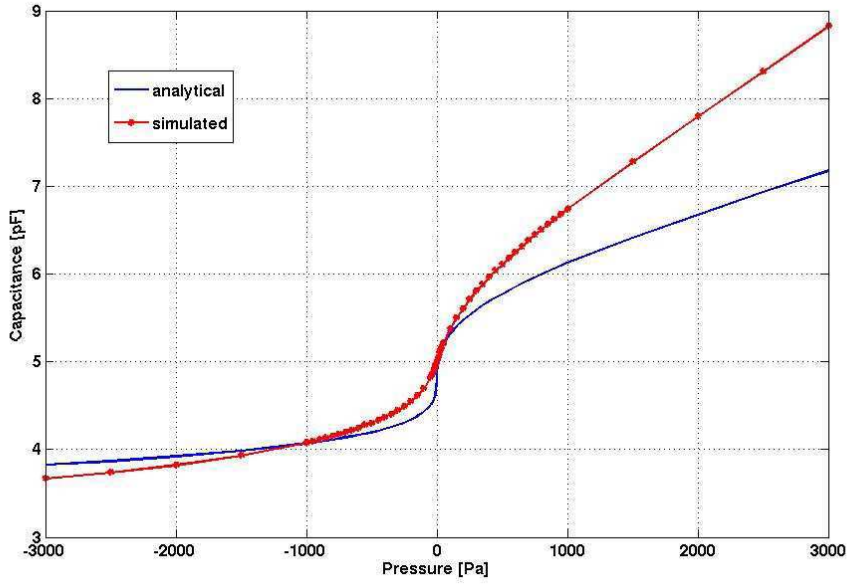

Figure 3.15: Electro-Mechanical model compared with FEM simulation

As Fig.3.15 shows, the analytical and simulated methods presents a significant difference, especially for pressure values that lead the plates to get closer. The FEM

model remains a useful mean for a qualitative interpretation and it allows the designer to understand which effects are produced by changing the sensor parameters.

3.3.4 Conclusion

During the designing of sensor the best tool has been FEM model. It's important point out that the design created without viscoelastic phenomena consideration (creep) appears unless. In fact, the creep change radically the behaviour sensor. Thus to perform a correct analysis we must to know modulus of elasticity $E\tau(t)$; for the wing pressure sensor we have used the $E\tau(t)$ obtained from Kapton® data sheets[16].

Chapter 4

Fabrication of wing pressure sensor

For assembling the sensor we have chosen standard printed circuit board technology. This choice has been done because it allows the manufacture of the sensor by fast prototype machine directly into our laboratories so we have obtained a technology independence in the device development. The materials used are perfect to achieve a good transduction by created sensitive units, and they allow to build a low cost device because cheap.
Manufacturing the rigid part of sensor, fibreglass epoxy layers were used. They low thickness and stiffness guarantee both a low total thickness and a strong frame above which to stretch the membrane. The membrane is a Polyimide layer, a polymer commonly used for obtaining flexible connections in devices where a moveable part is utilised, i.e. inject printers, due to its resistance to cyclic stresses. Bi-adhesive tapes habe been used for assembling the three main parts of sensor (base, spacer and membrane).

4.1 Materials

4.1.1 Epoxy resin

FR4 laminate is the usual base material from which plated-through-hole and multilayer printed circuit boards are constructed. ”FR” means Flame Retardant, and Type “4” indicates woven glass reinforced epoxy resin. The laminate is constructed from glass fabric impregnated with epoxy resin and copper foil. Foil is generally formed by electro-deposition, with one surface electrochemically roughened to promote adhesion. FR4 laminate displays a reasonable compromise of mechanical, electrical and thermal properties. Dimensional stability is influenced by construction and resin content.
We used a two types of FR4 laminate:

- FR4 DURAVER-E-CU 104ML : 200 μm thick with copper 35 μm thick (both side)
- FR4 DURAVER-E-CU 104ML : 125 μm thick with copper 17 μm thick (both side)

4.1.2 Polyimide

Polyimides are a very interesting group of incredibly strong and astoundingly heat and chemically resistant polymers, which are often used for replacing glass and metals, such as steel, in many demanding industrial applications. They can also be used in circuit boards, insulation, fibres for protective clothing, composites, and adhesives.

Aromatic heterocyclic polyimides are typical of most commercial polyimides, such as DuPont's Kapton®. In this work we used:

- AKAFLEX KCL: a composite laminate made of a Kapton® VN layer and copper layer, whose thickness was 25 μm and 17 μm respectively, was used for the sensitive membrane.
- A generic 50 μm Kapton® layer : it was used like protective clothing of the sensor bottom side, where there are the electrical paths.

4.1.3 Bi-adhesive

We have used, for assembling the sensor layers, 3M Acrylic Adhesive 200MP in the format 7962MP. 200MP tapes are usually employed for bonding a variety of substrates, including most metal, sealed wood and glass, as well as many plastics. They are characterised by specific features such as high tensile strength, high shear and peel adhesion, resistance to solvent and moisture, low outgassing and conformability. The 3M Acrylic Adhesive 200MP in the format 7962MP is a 50 μm adhesive layer double coated by two 100 μm protective layers, presenting a total thickness of 150 μm (± 10% tolerance). It's ideal for selective die-cutting.

4.2 Tools

The sensor fabrication consists of two steps: the first one produces the BASE, the SPACER and the MEMBRANE layer of the pressure sensors; the second step concerns to assemble the parts. Every layer is designed by CAD software and it's created by PCB fast prototyping techniques. The layers have been bonded together by bi-adhesive films. To perform the layer bonding we have built a particular assembler device working with a vacuum table.

4.2.1 Fast prototype machine

To create every sensor layer the LPKF Protomat S62 fast prototype machine has been used.

Figure 4.1: LPKF Protomat S62

This machine by means of milling tools, it's able to draw, on a FR4 substrate or on other material (sheets of plastic, aluminium, copper) electronic circuit, and mechanical structures.
To use the fast prototype machine, we have created a project where the action of every machine tools are described by a dedicated software (CircuitCam) able to translate a generic CAD design in a project to be used by the prototype machine. To carry out the project we must use a particular management software (BoardCircuit): it creates the job machine which describes the number of devices and where the devices will be created, but it allows also the machine setup.
The LPKF Protomat S62 is a three axis (X,Y,Z) machine able to work with a maximum of 10 different tools in the same job, creating holes with different diameters and drawing lines of 100 um wide with a working precision of 10 um on the horizontal surface (X,Y). It isn't a full 3D machine: in Z direction it's possible to set only the tool working depth.

4.2.2 Assembler Device

The assembly procedure has been performed by means of special assembler built in laboratory of the faculty. The assembly device is presented in Fig. 4.2 a), it is composed by three floor of which just the middle one is movable. The bottom floor is fixed (Fig.4.3 a))on the ground and by means of three reference pivots allows the alignment of the base layer settle on it. The movable floor is actuated by a circular crank handle, and it houses also three reference pivots to perform the layers alignments . Moreover the movable floor is a suction surface, in fact it is connected, by means of a rectangular sealed chamber and a circle plug, to an extractor fan. It is thus possible to lay subsequently both the spacer and membrane layers to the movable floor, and to lower the floor to perform first the base–spacer junction and then the spacer-membrane junction to complete the assembly procedure. In Fig.4.2 b) the assembler device completely lowered is shown.

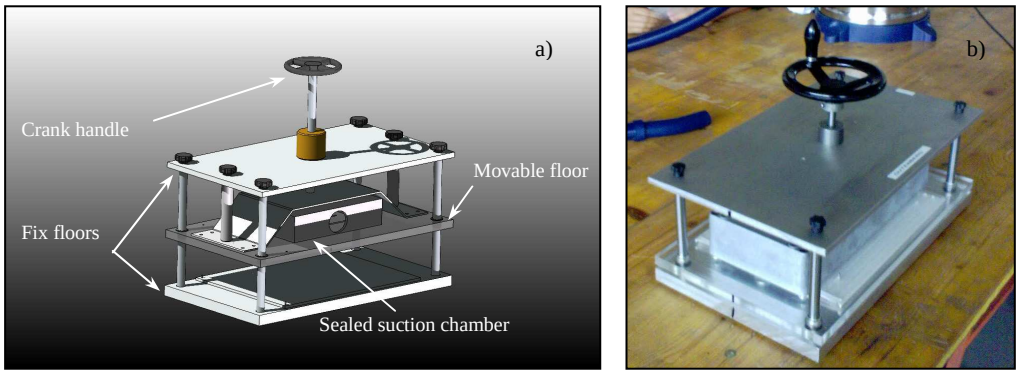

Figure 4.2 : a) assembler device sketch, b) created assembler device

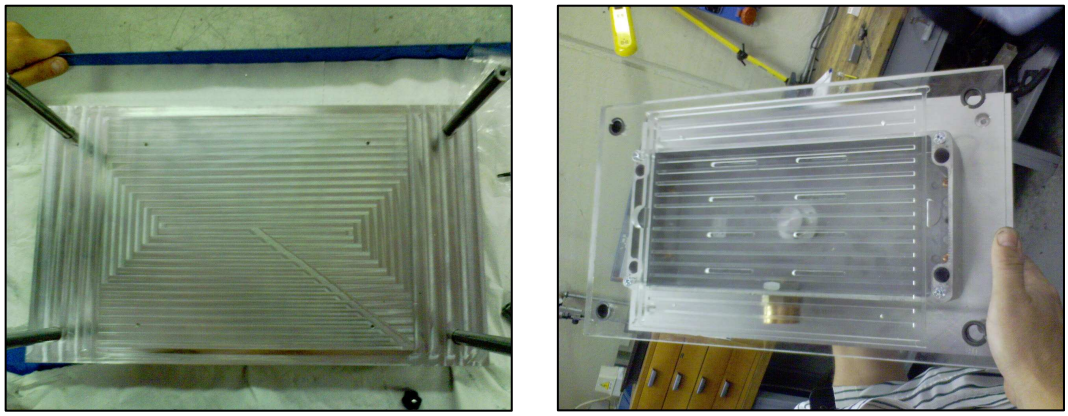

a) b)

Figure 4.3 : assembler device a) bottom floor, b) top and movable floor

4.3 Layers

The sensing unit is a three layers stacked structure:

- BASE : rigid part of the sensor built using a FR4 layer
- SPACER : rigid part of the sensor built using a FR4 layer
- MEMBRANE : deformable part of the sensor built using AKAFLEX KCL

The sensor vertical section is presented in Fig.4.4 : it's possible to note the structure of every layer.

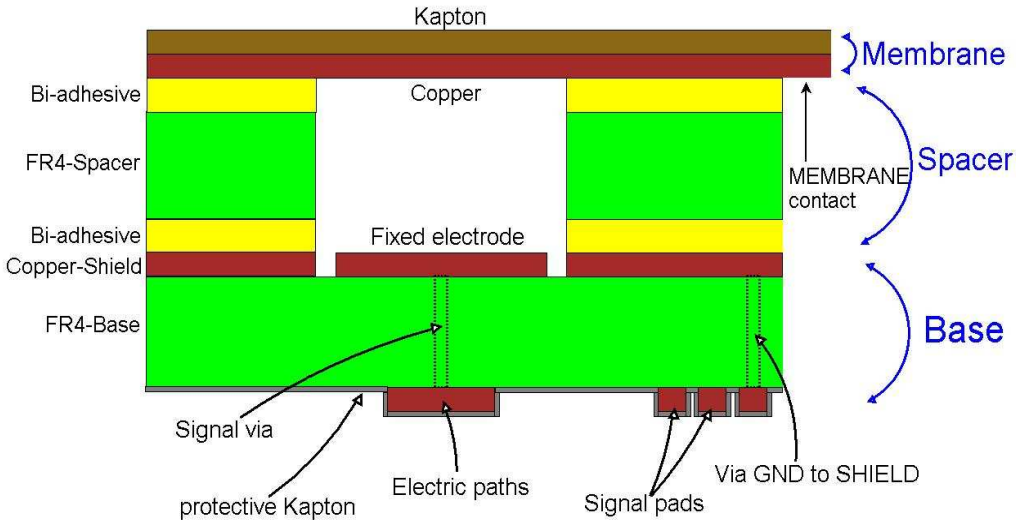

Figure 4.4 : three layers stacked structure

4.3.1 BASE

The BASE layer is an FR4 substrate covered by a double layer of copper. The copper thickness on each side of FR4 is 35um, the FR4 is 200um thick. After the creation of project by means of an electronic CAD, the sensor sketch is exported into the prototype machine management software.

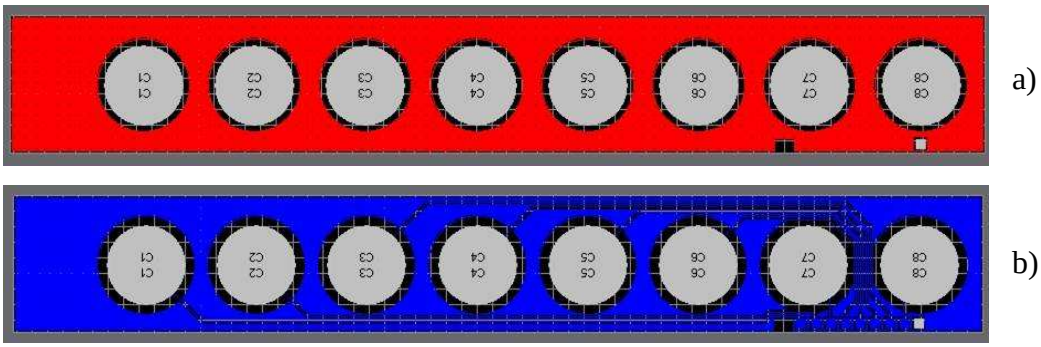

Figure 4.5 : Base gerber files: a) top view , b) bottom view

The fast prototyping machine area has been able to milling seven sensor layers at once (maximum working area is A4 size). The three different layers have been realized and bonded in the assembly procedure all at once, and subsequently divided by each others.
In the BOTTOM side of the BASE layer the electronic paths and the pads to carry out the electronic signals are present Fig.4.6 a). In the TOP side of the BASE layer the fixed electrodes of the capacitors are milled as shown in Fig.4.6 b). The signal of every fixed electrodes in the upper side, is routed to the electric paths on the bottom, by means of drills plated. It's important point out that all fixed electrodes are enclosed by ground plane (shield) : it's important to flat the junction surface between BASE and SPACER to obtain the best peel adhesion and to protect the fixed plate from electromagnetic interferences. The shield has been connected to ground by a devoted via near others fixed electrodes signal pads. Near the signal pads a square cut has been realized to allow the signal of the conductive membrane to be lead to the bottom side of the BASE through the thickness of the whole sensor. (Fig. 4.7)

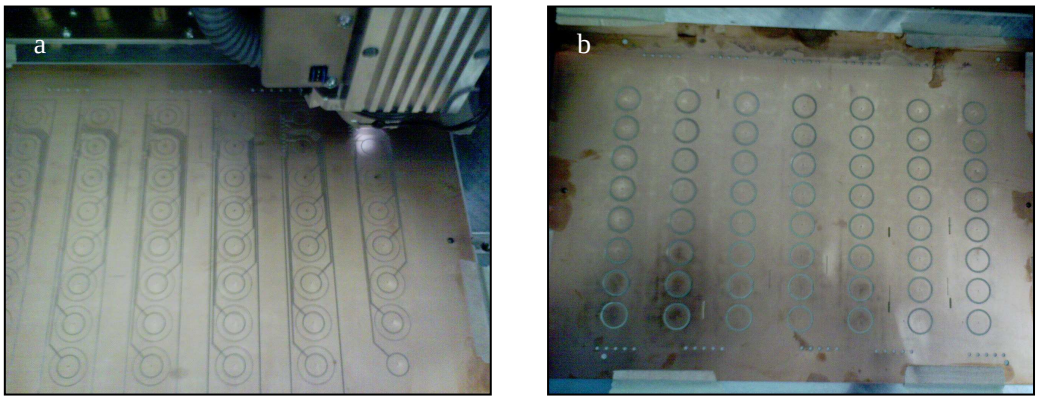

Figure 4.6 : BASE layer: a)bottom side, signal routing, b)top side, fix electrode

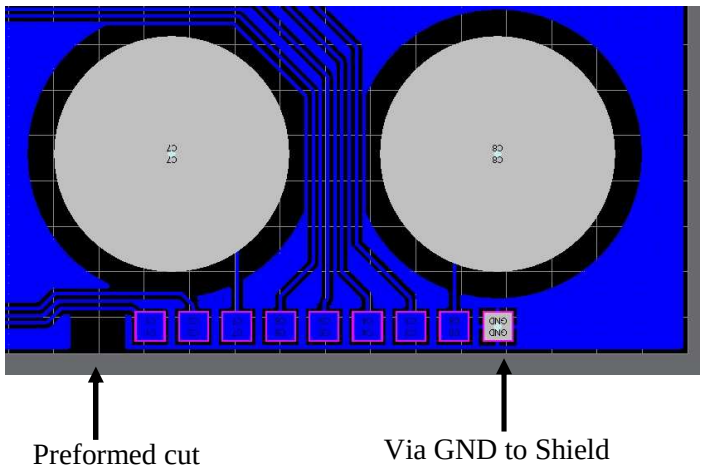

Figure 4.7 : BASE gerber file: zoom of signal pads side

Drills holes between every internal cavity sensor and the external environment have been closed by means of a Kapton® layer set above the bottom side of the BASE, to avoid air to penetrate inside the cavity of every sensing unit. The Kapton® layer is also useful to preserve, the electronics path in the bottom side of the base, from oxidation (Fig. 4.8).

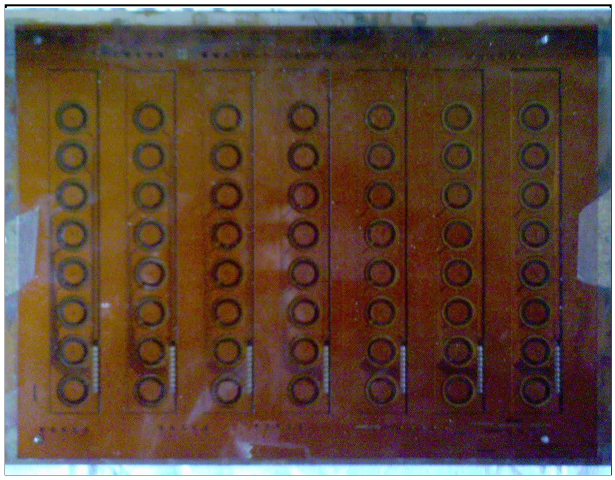

Figure 4.8 : Bottom side BASE sensor covered by Kapton® layer

4.3.2 SPACER

The SPACER layer is an FR4 substrate covered by a double layer of copper. The copper thickness of every layer is 17um, the FR4 is 125um thick. After the project creation by means of an electronic CAD, the sensor sketch is exported into the prototype machine management software.

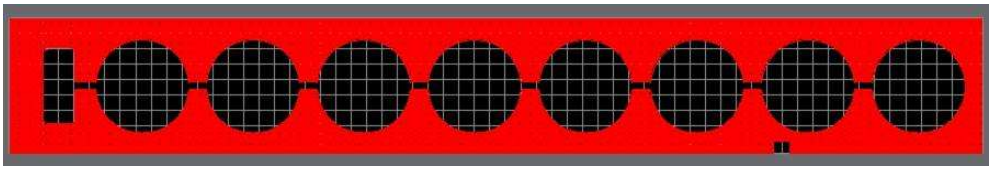

Figure 4.9 : SPACER gerber files

All unity chambers are connected by miniaturised pipes, patterned in the SPACER layers, in order to share the same internal pressure, forming a unique bigger chamber. It's possible to note that in the BASE gerber file, a square cut has been realized to allow the conductive membrane signal to be lead in the bottom side of the BASE through of the whole sensor thickness. (Fig. 4.9)

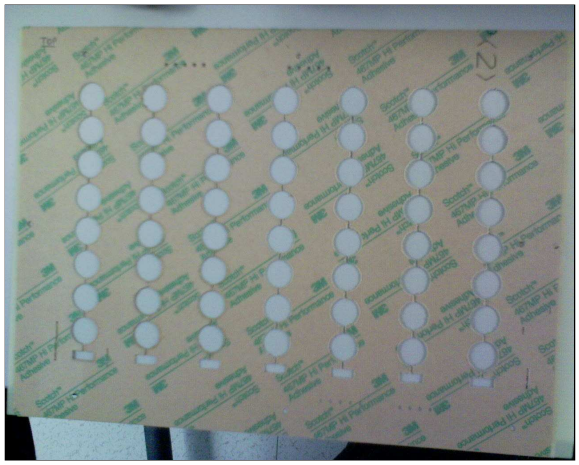

Figure 4.10 : SPACER layers covered by bi-adhesive

The SPACER layer is an FR4 substrate where the copper layers has been chemically removed, this layer when bonded to the base create the inner circle cavities where the circular electrode are present and the membrane is deflected. In order to create the internal chamber between the BASE and the MEMBRANE, the bi-adhesive layer has been bonded in upper and lower side of the FR4 SPACER layer before the milling process (without peeling off the remaining external coating protection). Acting in this way the spacer and the two bi-adhesive layers are shaped at once (Fig.4.10).

4.3.3 Membrane

The MEMBRANE layer is a 25 μm thick deformable copper-clad (17 μm) Kapton® polyimide composite layer (AKAFLEX KCL). After the creation of project by means of an electronic CAD, the sensor sketch is exported into the prototype machine management software.

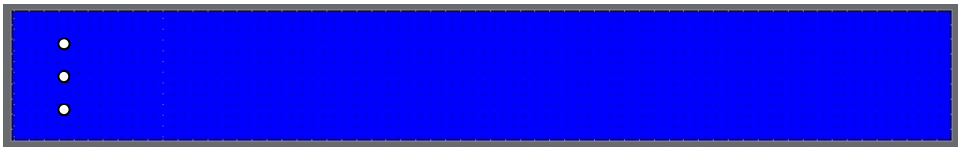

Figure 4.11 : MEMBRANE gerber file

Three small holes are drilled on the proximity of one the ends of the sensor, before the first sensing element and acting as a pressure reference. The MEMBRANE was a AKAFLEX KCL sheet with the same dimension of sheet containing the seven SPACER layers.

4.4 Methods

4.4.1 BASE – SPACER bonding

The BASE-SPACER bonding is performed aligning the sheet containing the seven BASE layer, above the fixed floor, of the assembler device, by the three reference pivot. The BASE layer is arranged to share the top side (the one with the fixed electrode) towards the movable floor (Fig.4.12 a)). The SPACER layer is aligned above the movable suction floor (Fig.4.12 b)), the bi-adhesive protective film is removed and subsequently the movable floor is lowered to perform the bonding process.
To obtain optimum adhesion, the bonding surface must be well unified, clean and dry. At room temperature, approximately 50% of the ultimate strength will be achieved after 20 minutes and 100% after 72 hours. In Fig.4.13 the BASE and SPACER layers are shown after the bonding process. The top side of the SPACER layer still present the bi-adhesive protection film, that will be removed in the following SPACER-MEMBRANE bonging.

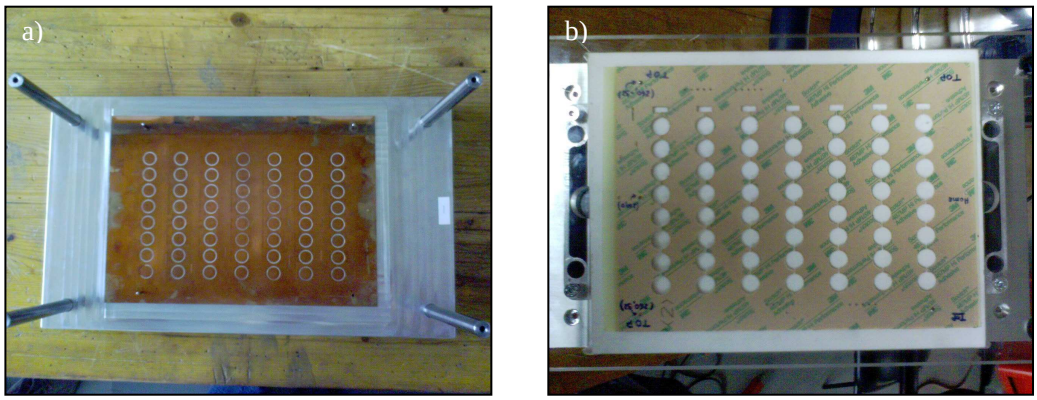

Figure 4.12 : a) BASE layer above the fixed floor, b) SPACER above movable floor

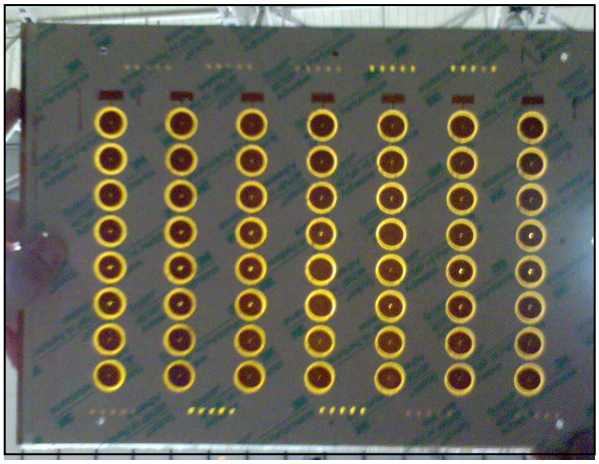

Figure 4.13 : BASE and SPACER layers after the bonding

4.4.2 MEMBRANE – SPACER bonding

The MEMBRANE-SPACER bonding is performed aligning the previously bonded BASE and SPACER layers above the fix floor. The bi-adhesive protection film is removed from the upper side of the SPACER (Fig.4.14 a)). The MEMBRANE layer is aligned above the movable floor and is arranged to share the bottom conductive side toward the bi-adhesive layer. The suction performed by means of the suction surface ensure the planar shape of the flexible membrane (Fig.4.14 b)).
Subsequently the movable floor is lowered to perform the bonding process, in Fig.4.15 a) and b) the bottom and the top side of the assembled array of strip sensor are shown.

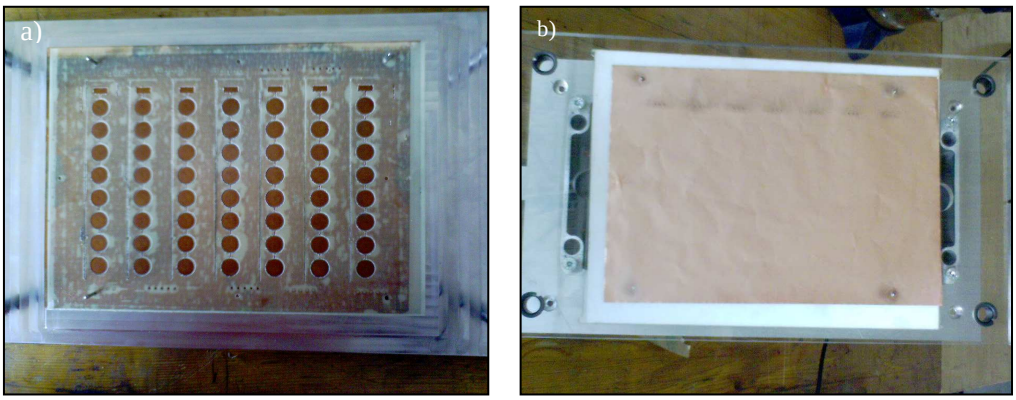

Figure 4.14 : a) BASE layer above the fixed floor, b) SPACER above movable floor

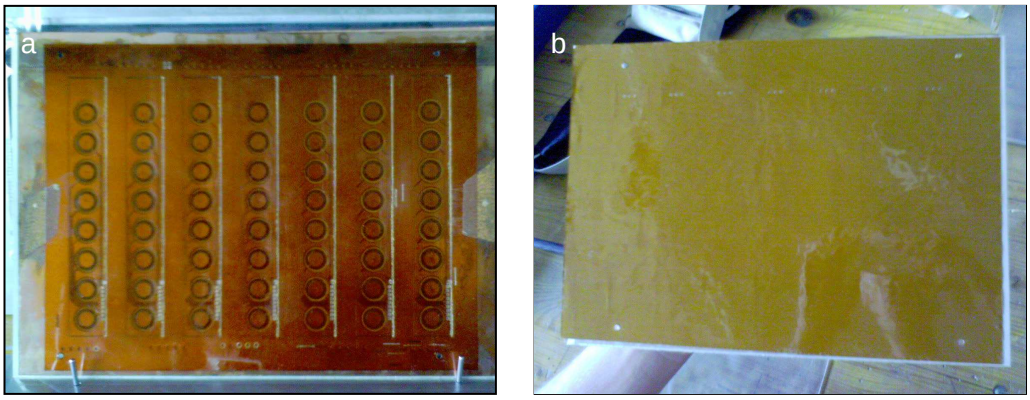

Figure 4.15 : assembled array of strip sensor a) bottom side , b) top side

Finally the array of strip sensor is aligned inside the PCB prototyping machine, to separate along the edge the single sensor unit. In Fig. 4.16 one of the final strip sensor is presented.

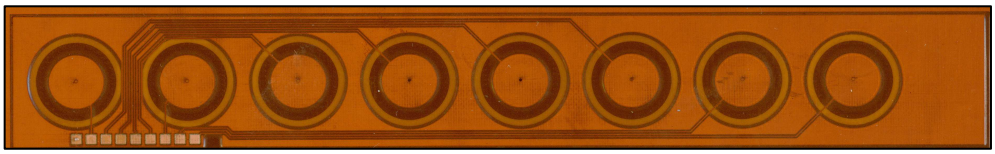

Figure 4.16 : final strip sensor - bottom side

The final size of strip sensor are: 158mm long, 22mm wide and only 0.6mm thick.

Chapter 5

Experimental results of wing pressure sensor

The fabricated strip sensor in laboratory, as described in chapter 4, has been tested. The analysis set up intended to validate large deflections and creep simulation models for the sensitive unit in the array: this has been obtained by applying several pressure values (in the range from tens to hundreds of Pa) on the device membrane by means of sealed chambers that allow an independent measurement to be conducted on each sensing unit.
The test results have been compared to the first sensor series prototypes built by a PCB Swiss manufacturer, since in the laboratory where this work was originally developed, there were not the facilities for assembling the devices.[14]

5.1 Experimental setup

The experimental test targets were to obtain the static characteristics of the sensor and testing the long term behaviour of the sensor in order to depict the viscoelastic behaviour of sensor membrane. The setup to perform the tests is composed by:

- a wind tunnel,
- a Pitot tube,
- sealed chambers for applying loads independently on the sensor membranes,
- a conventional silicon-based pressure transducer,
- an LCR meter,
- a Labview® interface control system.

The complete setup is shown in Fig. 5.1.

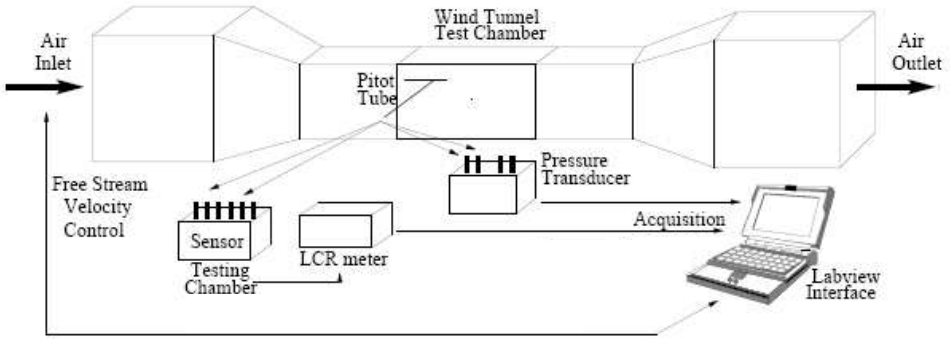

Fig 5.1 : the measure setup

5.1.1 Wind tunnel and Pitot tube

A system composed by a wind tunnel and a Pitot tube has been used, to apply different pressure values on the membranes. Low pressure values, into a range of units to hundreds of Pascal, are very difficult to obtain statically acting on small volume variations. Indeed the temperature drift and of the pressure waves propagation create instabilities in the resulting thermodynamic pressure.
The problem depicted above has been avoided using, as referenced applied load, the dynamic pressure obtained from a Pitot tube in the wind tunnel test chamber inserted. Varying the wind tunnel free stream flow velocity, various pressure values can be achieved as the difference between the static pressure and the total pressure, as shown in Fig. 5.2.

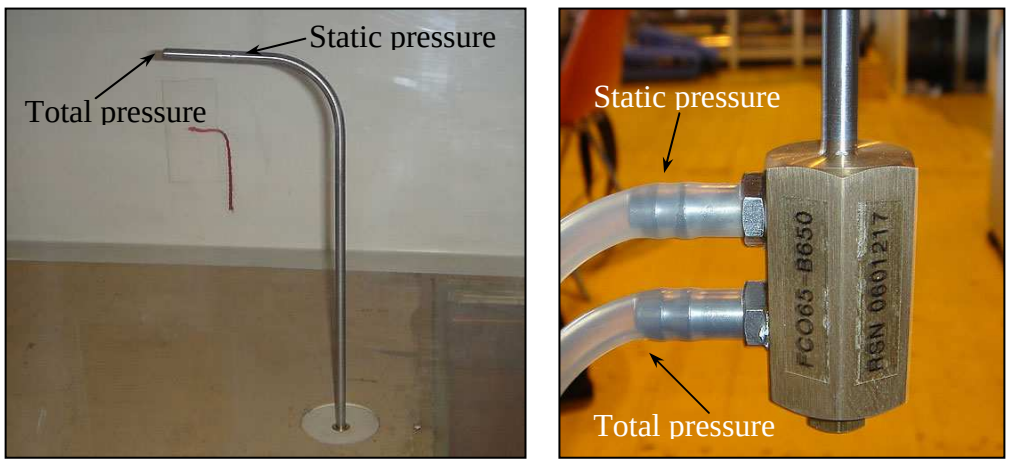

a) b)

Fig 5.2 : Pitot tube a) into wind tunnel , b) output pressure channels

5.1.2 Sealed chamber

The sealed chambers for applying loads independently on the top of the sensor membrane has been built using PVC by means of a numeric-controlled milling machine in our laboratories. The PVC device is composed by a base (Fig. 5.3) where the sensor is leaned (like above an airfoil surface) and a lid where two sealed chamber have been milled. In the smaller sealed chamber by means of three static taps in the forward part of sensor, the reference pressure is led inside the internal chambers of all sensing units. In the larger sealed chamber a different pressure value is led, thus each sensing unit share the same differential pressure.

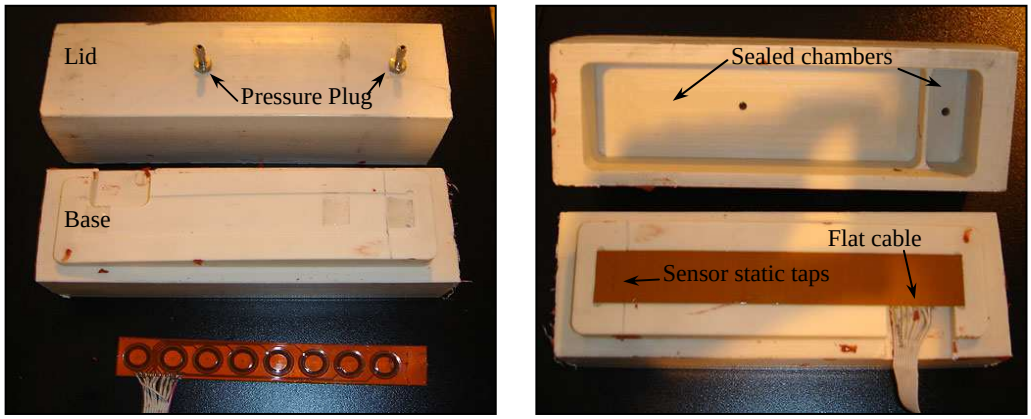

Fig 5.3 : sealed chamber

Every capacitor of the sensor is connected electrically to the measure instrument by a flat cable, soldered to the array.

5.1.3 Data read-out system

The conventional silicon pressure transducer, a Setra® Capacitive Instruments, connected to an National Instrument acquisition board, is used for measuring the pressure every time that the wind tunnel free stream velocity is varied by the dedicated control panel.

Fig 5.4 : Setra® Capacitive Instruments

An Agilent 4284A Precision LCR meter has performed the data acquisition. The instrument is used for measuring directly the capacitance values to estimate the accuracy of the characteristic evaluated by the theory and by the FEM simulations. Data have been sampled by a National Instrument PCI-6070E High Performance 1.25 MS/s 12-bit multifunction acquisition board, controlled by a Labview program (Fig.5.5)

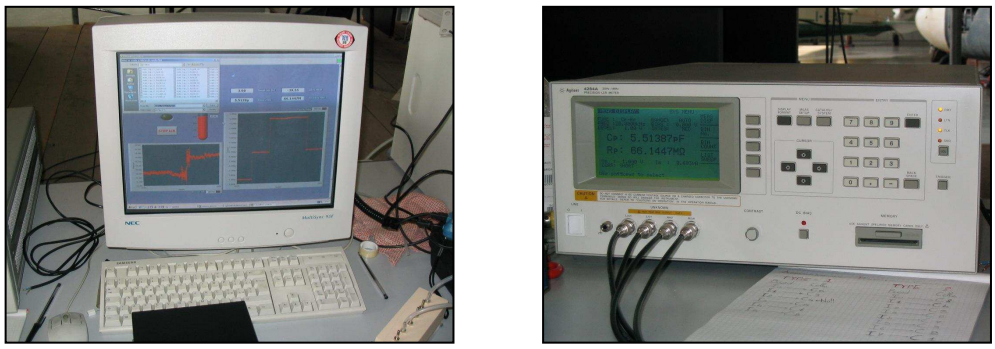

a) b)

Fig 5.5 : a) Labview programm ;B) Agilent 4284A Precision LCR meter

5.2 Static characteristic

A set of different constant pressure values have been exerted on the sensor membrane, each value being applied for an acquisition period of about sixty second , by mean of the sealed PVC chamber shown in Fig. 5.3. The static sensor characteristic and the creep drift was obtained by the modelling procedure described in chapter 3.

The fabrication process and the material employed are crucial issues in obtaining an reliable pressure sensing device; therefore a certain fabrication experience must be achieved. Tests on the first home made prototypes have shown a lack of repeatability in the static characteristic behaviour of the eight sensing unit of which the strip is composed (the results in Fig.5.6 are presented).

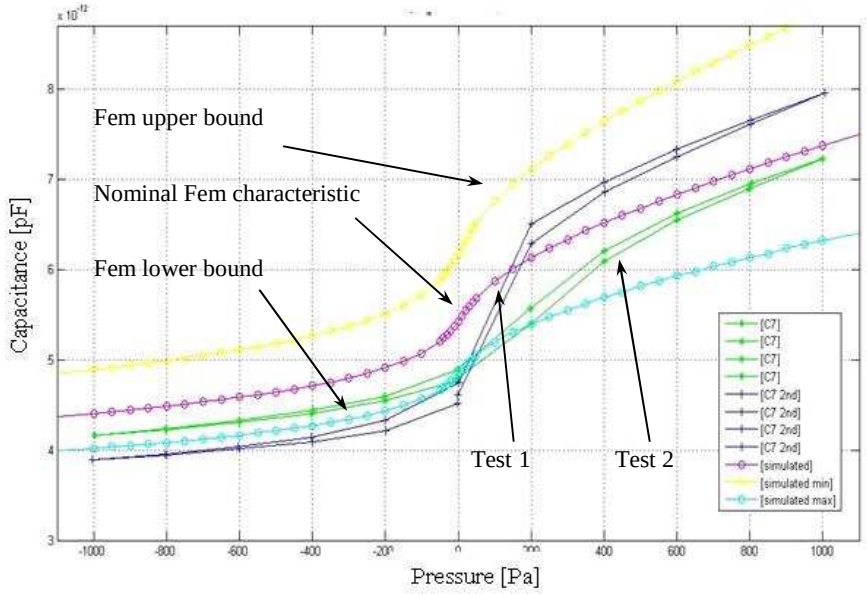

Fig 5.6 : two experimental static characteristics

Two experimental static characteristics of the same sensing unit have been extracted and compared with the Fem nominal characteristic and the two Fem bound related to materials tolerance.
The two experimental function, performed at different time instants, show a completely different behaviour. For low values of pressure between (+/- 200 Pascal) the function slopes are different. At higher pressure values the slopes of the two tests share the same trend but the absolute value of capacity is different. Further investigation has revealed how the lack of long term repeatability is due to the lack of a pre-stress level in the diaphragm of the strip. This cause a lack of planarity in the membrane causing different membrane equilibrium shapes for low pressure value.
Trying to overcame the problems, the assembly device described in chapter 4 has been modify to provide a pre-stress level in the Kapton® membrane before bond it to the SPACER layer.

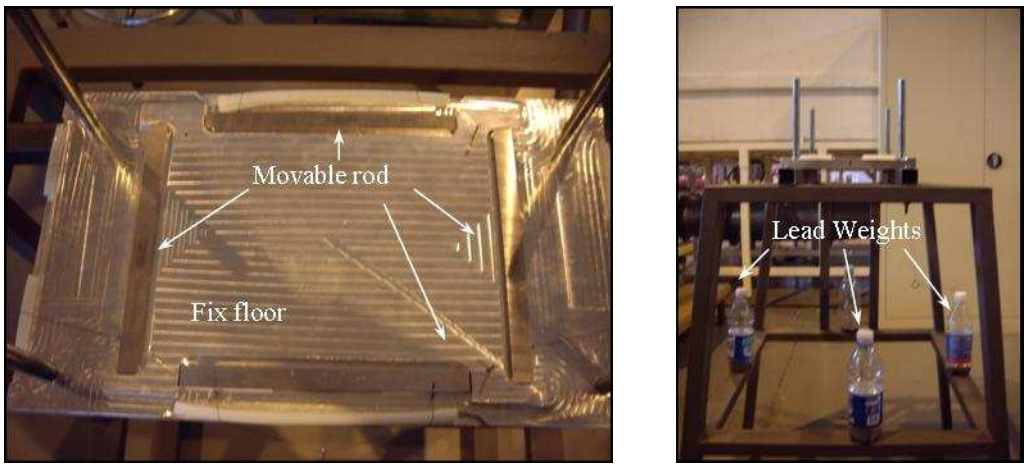

Fig 5.7 : assembler device modification

Four movable rods have been set at the same level of the fix floor, in the assembly device; any rods has been linked by means of wires to four known lead weights. The Kapton® sheet is first placed on the fixed floor and bond with an adhesive tape to the four movable rods, the lead weights are then applied and the kapton is pre-stressed. Subsequently the SPACER layer set on the movable suction floor describe in chapter 4, is lowered and bonded to the stretched membrane (Fig.5.7).
New test have been performed with the pre-stress membrane and an acceptable repeatability is gained (Fig.5.8).
Unfortunately the pre-stress procedure doesn't guarantee an uniform strain of the Kapton® sheet moreover if the lead weight is too big the sheet shape is not anymore planar. The pre-stress assembly device described has been suitable to understand that a certain level of pre-stress is necessary to let the sensor be repeatable in the whole full scale input and stable when low pressure input values are applied. Being able to understand the role of pre-stress a new device able to perform a known and repeatable stress-strain level in the membrane must be developed.

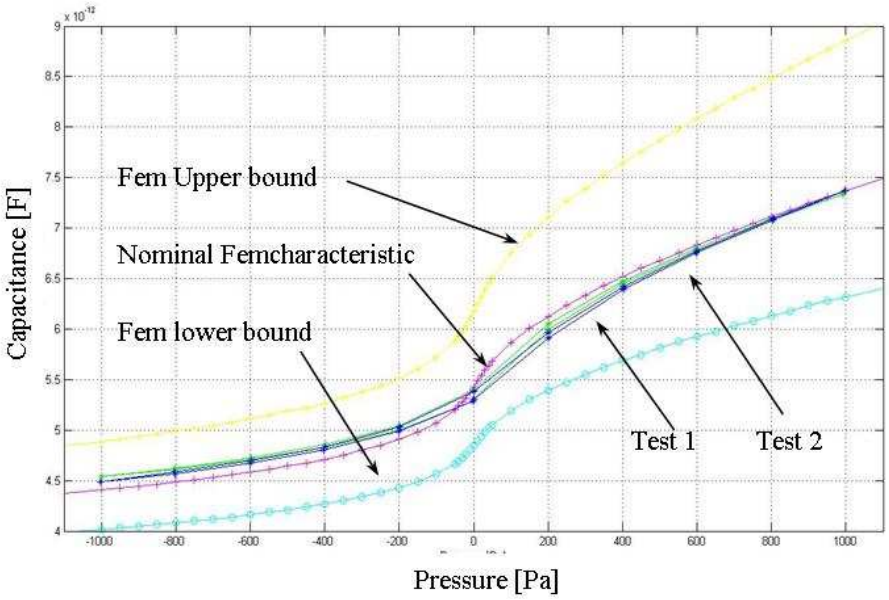

Fig 5.8 : new test with pre-stress membrane

5.3 Creep measurement

The response to a constant load of an ideal sensor and the response of sensor affected by viscoelastic phenomena are different. When a constant pressure load is applied it is possible to distinguish two dynamics: an instantaneous response due to the elasticity of the membrane and a slower response due to the viscoelastic behaviour.

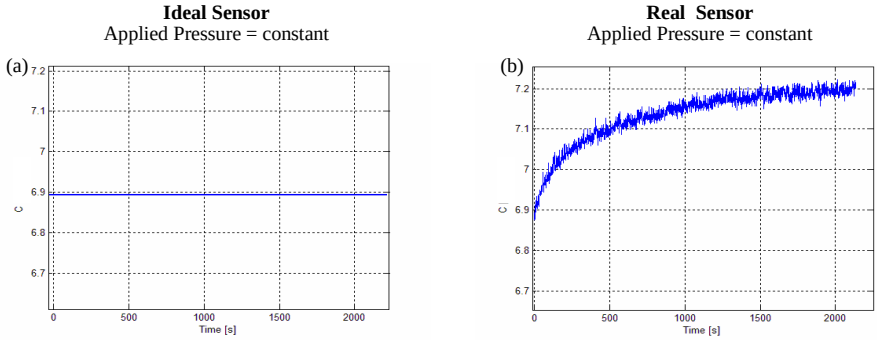

Fig 5. : response to a constant load: a) ideal sensor b) real sensor

In order to understand the viscolelastic behaviour of the sensor a series of long term experimental tests has been performed. The experiments has been carried out by applying four different steps of constant pressure over the membrane, for the whole time interval required to reach an asymptotic constant value of capacitance output. The four pressure loads imposed in the test procedure have been +200, +400 +600 +800 Pascal. The loads chosen are defined positive when the membrane deflect itself inside the cavity of the sensor, producing the higher value of capacity output.

The creep measurements on sensor reveal the worst viscoelastic behaviour if compared with previous sensor type designed (built by a PCB Swiss manufacturer)

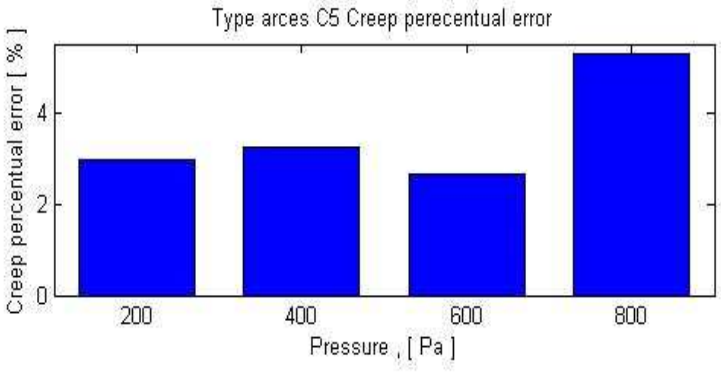

Fig 5.12 :creep % error

The maximum creep drift is 5% of the full scale output for a pressure of 800 Pascal.
The main reason for the worst behaviour of the home built sensor has been identified in the material employed to create the device.

5.4 Conclusions

If we compare the test results on home built sensor type with the sensor prototypes built by a Swiss manufacturer, we discover the best behaviour in the last one (Fig.5.13).
The static characteristic of Swiss sensor, if compared with static simulations, show a very good agreement and confirming the FEM models as a reliable mean for the sensor design.
About the creep measurements show a maximum error of 1,1% of the FSO for a pressure of 800 Pascal.
Observing the static characteristic we have the confirmation that the fabrication process is a crucial issues to obtain an reliable pressure sensing device.
Moreover the material employed in the fabrication of the device are really important. Indeed has not been possible to find on the market the same type of Kapton® used for the Swiss sensor type.
Kapton®, as many polyamide products, is made in a wide variety of blend and thickness and even if the copper layer employed has the same thickness the mixture of copper bonded to the Kapton® layer is slightly but crucially different.
Depending on the materials, viscoelastic behaviours can manifest at ambient temperature and for stress bigger than 1MPa [17,18,19,20,21] : copper thick, crystal copper size, gluing substance used to bond Copper to Kapton® and finally the polymer macromolecules are component able to modify the membrane behaviour .

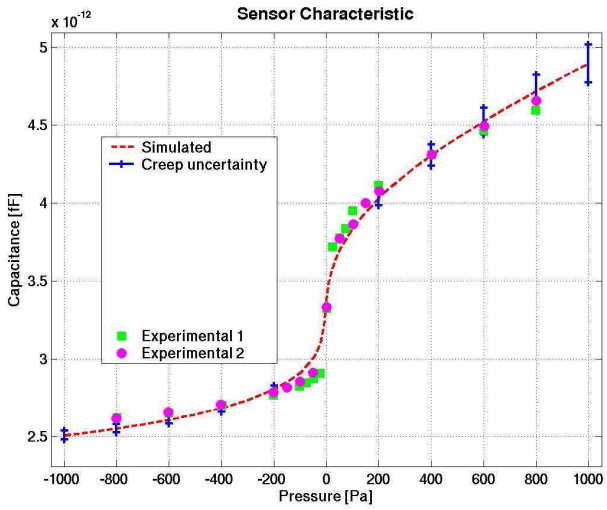

a)

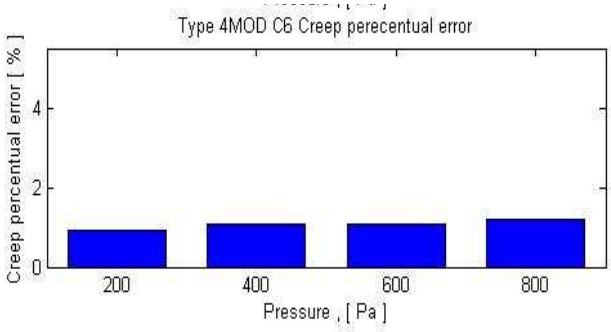

b)

Fig 5.13 : Swiss sensor a) static characteristic b) creep % error

It's important point pout that other tests have been performed to study the sensor behaviour. These have been accomplished by other colleagues in laboratory group and the author has been involved only marginally, because not interesting to develop other type of strip pressure sensor for aeronautical application.

Chapter 6

Design and simulation of sail pressure sensor

6.1 Fluid dynamic input variable

To perform the simulation to achieve the best geometrical definition of the sensor, first we need to define the range of fluid dynamic input variable (pressure range).
In many sailing contest the higher limit of the wind above which the regatta is aborted is usually twenty knots for this reason the full scale pressure input of the wireless sensor network has been developed to operate in a true wind ranging from zero to twenty knots. A safe factor to allow overpressure has also been considered.
The related differential pressure has been calculated for two conditions of apparent wind of 10 kts and 20 Kts. (Among the different fem codes the results from MacSail® a vortex-lattice (VLM) methods developed at the Helsinki University of Technology [22]], has been analyzed to infer the bound of the pressure field acting over a maxi yacht with mainsail and head sail)

$\vec{V} = 10\ Kts$	$\Delta p_{Max} = 38\ [Pa]$	Mainsail
$\vec{V} = 20\ Kts$	$\Delta p_{Max} = 160\ [Pa]$	

$\vec{V} = 10\ Kts$	$\Delta p_{Max} = 23\ [Pa]$	Headsail
$\vec{V} = 20\ Kts$	$\Delta p_{Max} = 204\ [Pa]$	

The maximum value of the differential pressure exert over the headsail is about 200 Pascal in a true wind of 20 Kts, with both the sails working. For this reason the full scale input of the pressure sensing unit implemented in the wireless network has been set to a value of +/- 300 Pascal to let the device able to sense the pressure field and to prevent unwanted overpressure.

6.2 Preliminary geometry definition

The proposed wireless sensor network has been developed to operate over sails, it's aim is to detect the pressure field without to be invasive. Invasivity is an important issue of the network cause geometrical variations or discontinuity over sail surface may affect the characteristic of the flow and, as a consequence, to modify the pressure field of the sail. For these reasons the most convenient way to take the measurement network above the sail is to integrate it in the battens of sail. This topic due to the natural shape and dimension of battens will dramatically affect the design of every nodes of network and the sensing units. As reported in chapter 3, the sensing unit is a circular diaphragm created by the union of three layer, the base the spacer and the membrane. The spacer create the circular cavity where the membrane deflect while the base, which is the thicker layer, has a square shape, as shown in Fig.6.1. In a first design phase the allowed maximum and minimum dimension for the frame square base L , the circular cavity of the spacer D , and the initial distance between plate H have been set.

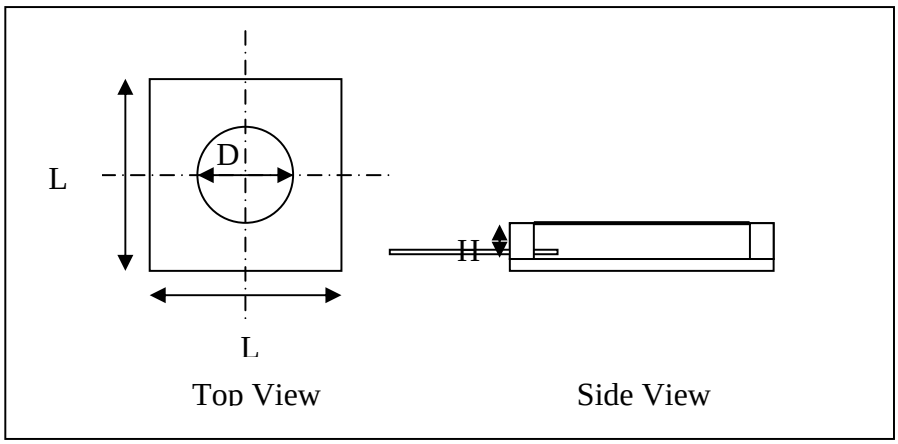

Figure 6.1: Sketch of sensor

Battens width usually ranges from 20 to at least 40 millimetres , for the design of the battens the higher limit of 40 millimetres has been chosen. The width L of the sensing units must lay between this two bounds and the round diameters D must be chosen as trade off among two requirements:

- it has to be as large as possible to guarantee a certain mechanical sensitivity;
- it has to be as small as possible to guarantee a wide free surface able to ensure a safe and robust adhesion of the glue employed to joint the membrane to the spacing layer.

The maximum lateral dimension L will also have to be some millimetres shorter than the width of the battens external edge, to let the sensor not to be damaged when the battens are inserted inside the apposite pockets in the sail.

Starting from the above considerations the maximum dimension allowed of the round cavity of the sensor D has been set to 20 mm while the external width L to 40 mm . Acting in this way the sensor can be house inside the battens, and a useful free surface for the layers adhesion is present. The minimum diameters for the membrane is set by the mechanical sensitivity of the membrane: the minimum diameters of 4 mm must be set to be able to sense the pressure field. According to the previous consideration the sensor edge length L, must be lower than 40 mm and radius of the membrane must be 4 mm<D<20 mm .
The last parameters is the initial distance between plates of the capacitor, the bounds within it can be chosen depend on the allowed maximum thickness for the battens and the minimum distance of the electrode at which the electrostatic force is no more negligible. The maximum thickness of a batten is about 4 millimetres but it doesn't affect the dimension H of the sensor cause for values of H greater than 500 um the sensitivity of the device is not appropriate to the FSI (Full Scale Input) proposed. The lower limit of H is limited by the magnitude of the electrostatic force that would cause the conductive membrane to be attracted to the lower electrode, this phenomena imposes to chose a value for the parameter H higher than 10 um.

6.3 FEM simulation

Numerical FEM simulations are then a fundamental task for the understanding of the sensor. The aim of FEM simulations is to describe more efficiently the physical and structural sensor features in order to find an optimum geometry and to satisfy the specific application. Since the output of the sensor is a capacitive information, coupled electrical and mechanical simulation have to be taken into account. It's also important to remember as a difficult issue is due to viscoelastic behaviour of polymers, that an over-simplified analysis could lead to large errors. A fem static model of the sensor has been realized by means of a static non linear coupled model able to predict the mechanical deformation of the membrane an the related capacitance change induced between the two plate of the capacitor.
The Fem static model is a suitable tool to predict different topic concerning the sensor behaviour, as the mechanical and electrostatic sensitivity, potential conditions of saturation, dead band zone and full scale output and resolutions. By means of the fem static tool is then possible to choose the appropriate geometrical dimensions in terms of radius and initial distance between plates related to the pressure field. Anyway the static fem model is not useful to estimate the error of the sensor in terms of accuracy and repeatability. This problem is due to the non linear and viscoelastic time dependent behaviour of the thin diaphragm (Creep).To be able to estimate the inaccuracy bound associated to each geometry tested with the static model and to be able to sense the proposed pressure field, a time dependent model of the error affecting the diaphragm is necessary. Unfortunately poor data concerning the creep behaviour of Mylar® are available in open literature or technical datasheet. Thus it has been necessary to develop an experimental procedure able to extract this data and to infer a time dependent error model to predict the inaccuracy of the device, introducing in the fem static model, time dependent parameters to reproduce, with a certain degree of confidence, the inaccuracy bounds related to the pressure input.
Both the fem static model and the time dependent error model have been used to choose among many potential geometries for the sensor. Finally the one associated with the better trade off , in terms of sensor figure of merits parameters, has been chosen.

6.3.1 Modelling and design

A multi-physic coupled mechanical load-deflection and electrostatic deflection-capacitance numerical analysis of the diaphragm and variable capacitor is necessary for the modelling and design of the sensor structure.
A FEM-based software tool such as FEMLAB® [23] has been used to perform a static non-linear analysis of the multilayered structures under a uniform load. The modelling of the diaphragm deformations with respect to the pressure load has been carefully considered (Fig.6.2).
The mechanical module output is the deformed shaped for each pressure load of the membrane, the latter is the input of the electrostatic module (Fig.6.3).The electrostatic module estimates the space charge density in the internal chamber of the sensor, therefore it's possible to evaluate the capacitance related to every pressure load of the full scale input.
Acting in this way it is possible to evaluate, by means of the mechanical module, the membrane deflection in response to the applied pressure load finding out, through the electrostatic one, the respective capacitance variation (Fig.6.4).

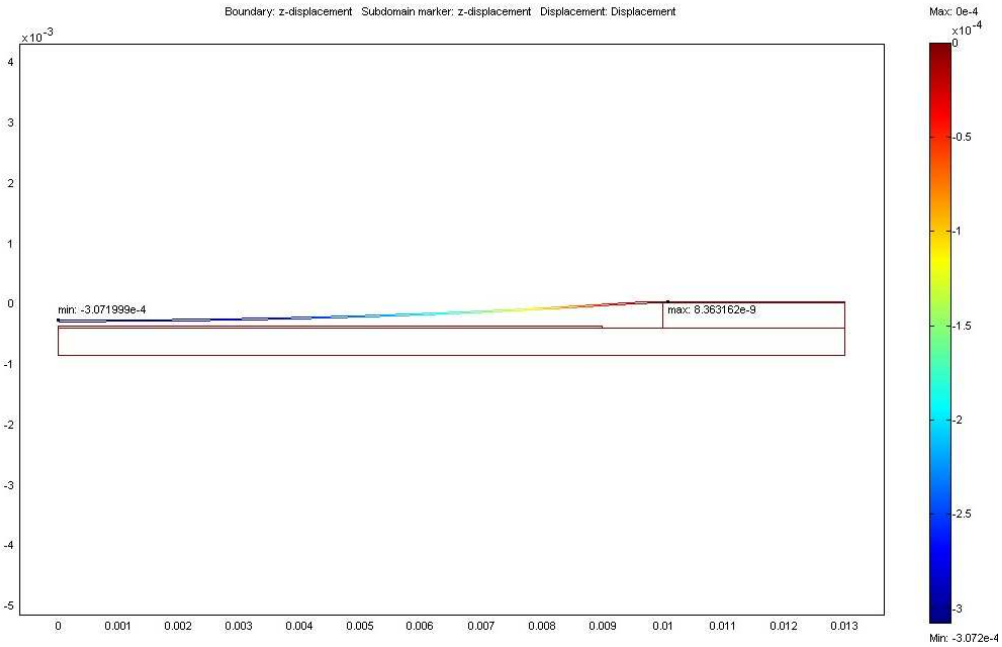

Figure 6.2: Diaphragm deformation

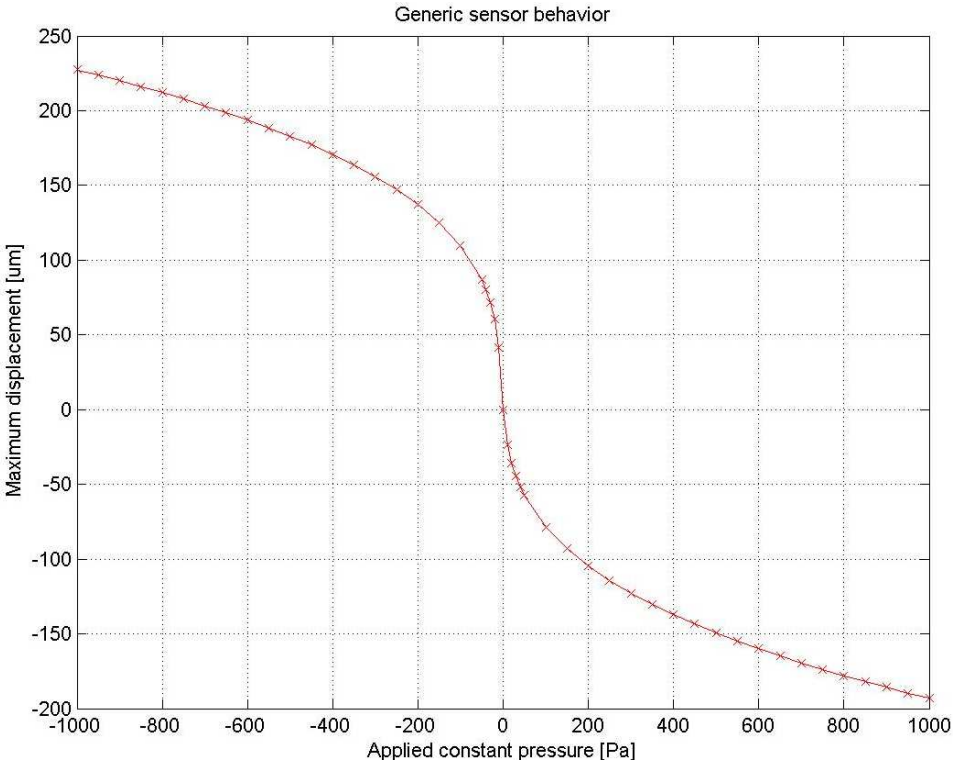

Figure 6.3 : Maximum displacement versus Pressure input

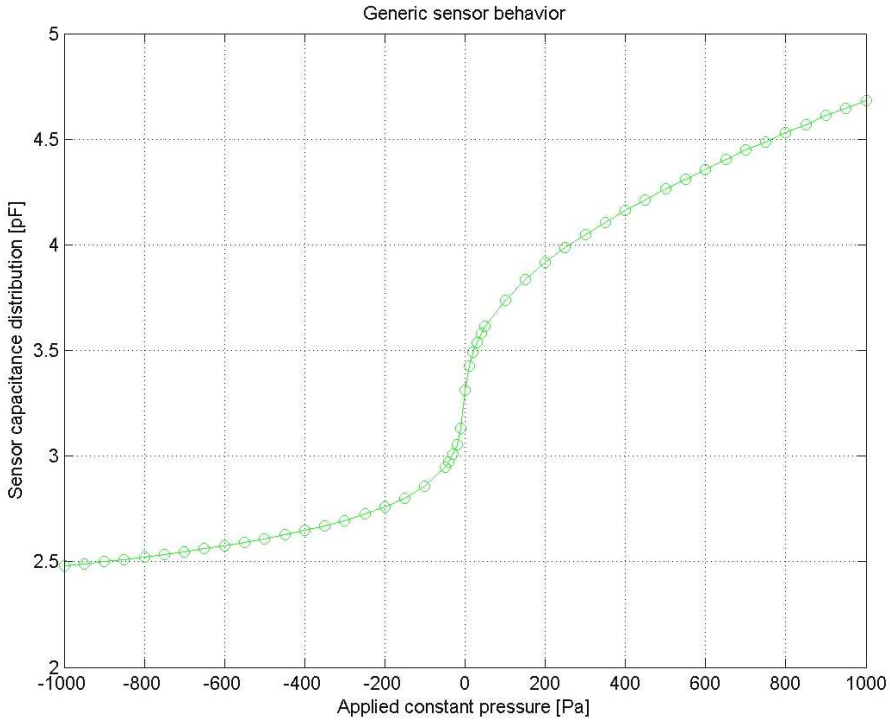

Figure 6.4 : Sensor capacitance versus pressure

.

A campaign of finite element test has been performed to investigate the behaviour of the sensor in full scale pressure input with different geometry and pre-stress level of the diaphragm.
The independent variable of the campaign are :

- ***p**: pressure load*
- ***r** : radius of the cavity*
- ***h** : initial distance between electrode*
- ***T** : initial pre-stress level*

while the dependent variable are :

- ***w** : maximum displacement of the membrane*
- ***C** : capacity*
- ***σ** : Von mises stress*
- ***σmean** : Mean Von Mises stress*

} Parameters used to describe pre-stress membrane

By means of the numerical output provided by the model is possible to obtain the classic figure of merit of the sensor as: full scale output, sensitivity, transduction function, saturation, dead band etc.
Aim of the numerical simulation is to find the best trade off of the independent variable of the sensor varying the dependent ones.

6.3.2 Fem data analysis : unstressed and stressed diaphragm

In the chapter 3 we described like bonding a membrane above the spacer guaranteeing only its flatness, it exhibits different equilibrium shapes when the pressure load is low. This problem manifest high level of hysteresis at low values of pressure. A radial pre-stress tension is therefore necessary to reduce diaphragm instabilities when the differential pressure is close to zero. This helps the membrane to preserve a steady planar shape in the absence of pressure input
In the condition of total absence of pre-stress load, when a pressure load is applied on the top of the membrane the mean local stress changes, as showed in Fig.6.5.

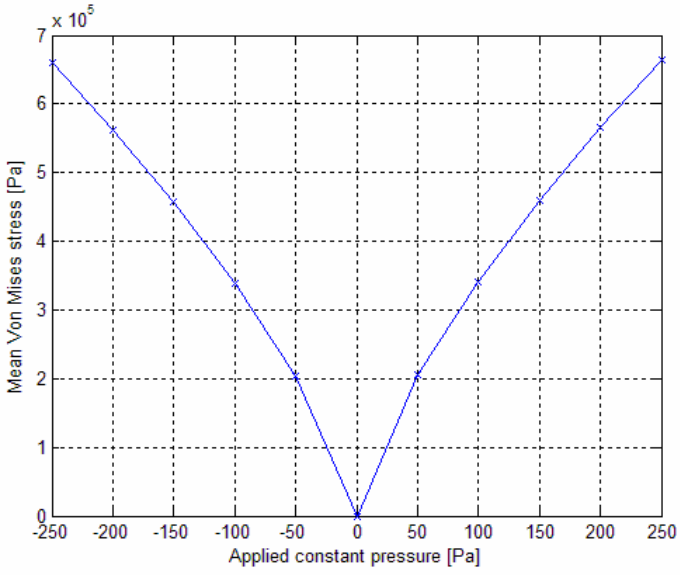

Figure 6.5: Mean von Mise stresses in the full scale input

This phenomena affects the displacement of membrane. In Fig.6.6 (a) and (b), half of deformed shape of Mylar layer is shown for five step of pressure, each one spaced of 50 Pa starting from 0 Pa to 250 Pa. The left plot (a) is related to a value of *T* equal to zero the right plot (b) to a value of *T* equal to 4 MPa. It's worth to note as above a certain level of stress the relation between load and deflection tends to a proportional behaviour (Fig.6.6 b)).

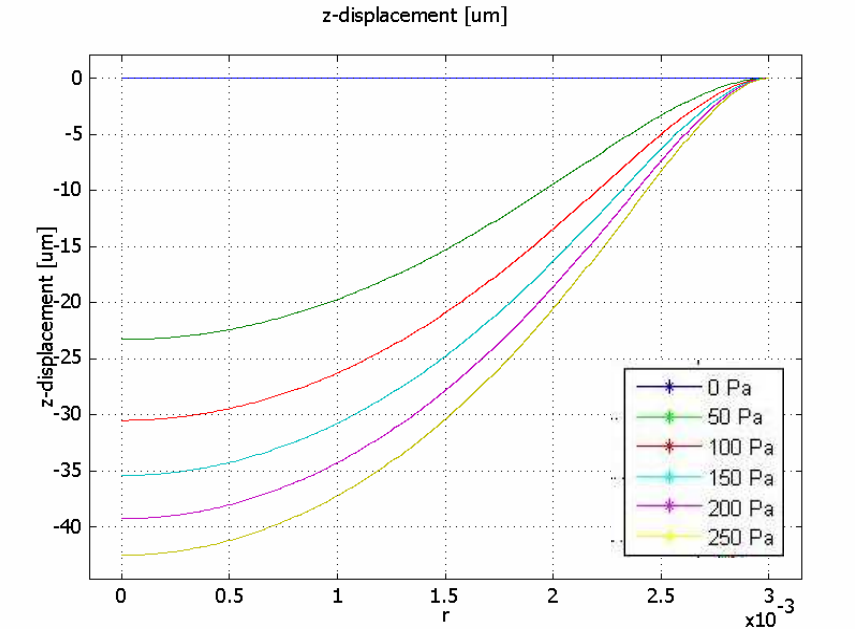

a)

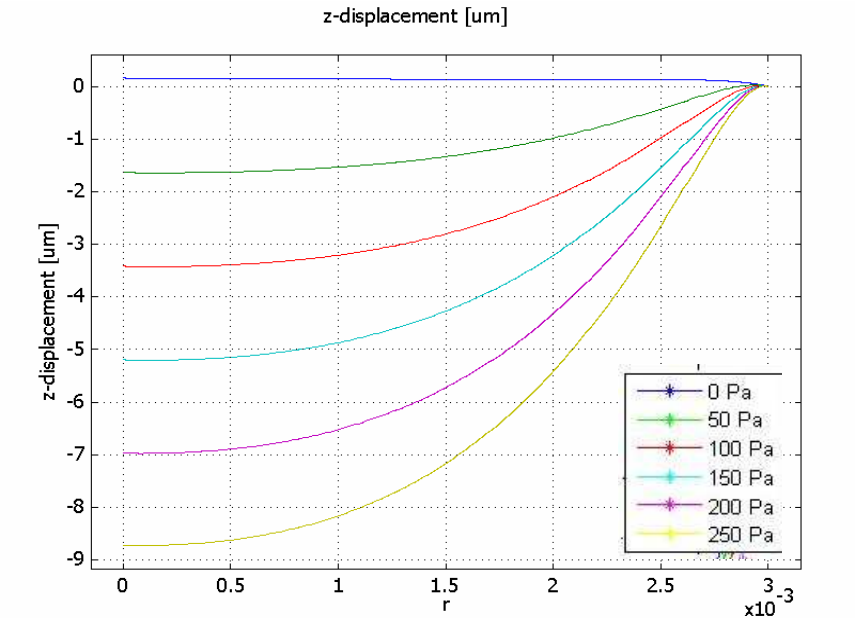

b)

Figure 6.6 : deformed shape of Mylar layer; a) absence of pre-stress, b) pre-stressed

The presence of a pre-stress in the membrane material, tends to increase the stiffness of the membrane and to reduce the mechanical sensitivity to the pressure load. Increasing the stress in a certain way acts as increasing the thickness or the material Young's module: even if subjected to the same loads the maximum displacements of the diaphragm decrease and its behaviour doesn't tends to the membrane model but to the one of a thin plate. This behaviour is shown if Fig 6.6 b) where the maximum displacement is expressed as a function of the full scale pressure input for different pre-stress level. When the induced stress in the diaphragm is close to 1.5 Mpa the magnitude of maximum displacement is equal to the thickness of the diaphragm (20um) and the maximum displacement is proportional to the pressure loads as in the thin plate theory.
The presence of a pre-stress in the Mylar plate decreases the mechanical sensitivity of the sensor but increase the linearity of the relation between displacement and pressure load Fig 6.7 a). A similar trend can be observed if the transduction curve of the sensor for the same level of tension is plot. The higher tension levels strongly decrease the overall sensitivity of the sensor reducing the full scale output but the transduction curve tend to a linear relation.

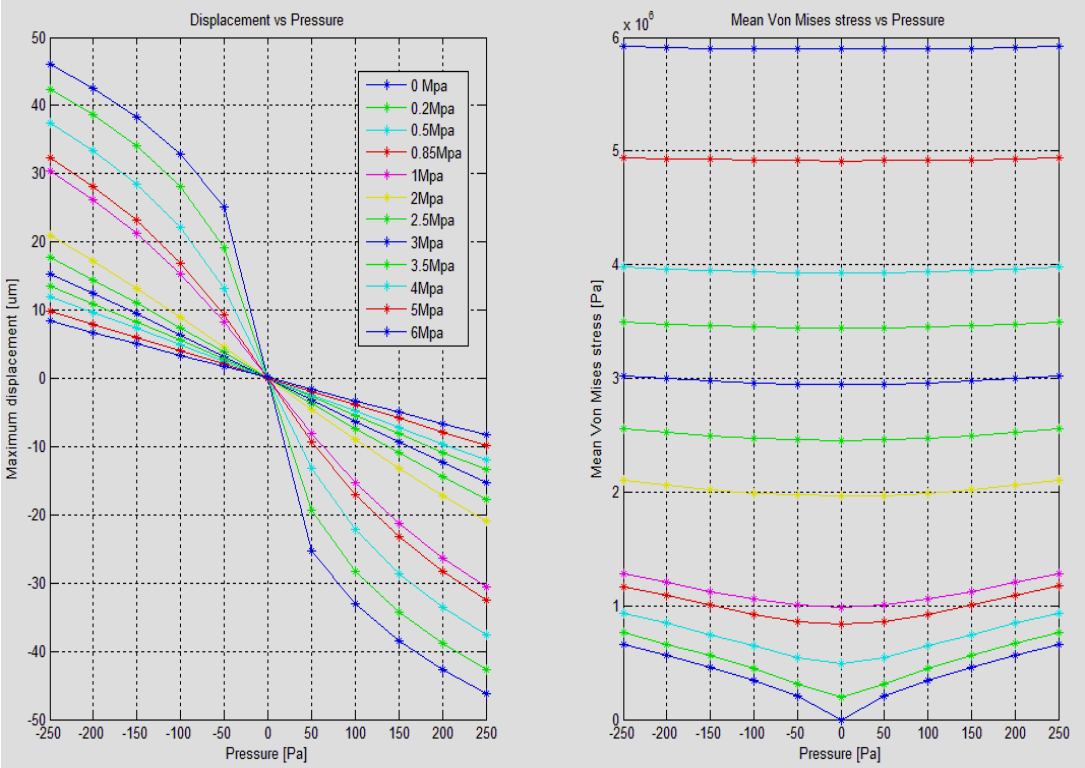

a) b)

Figure 6.7: a) Maximun displacement, b) Mean stress as function of pressure

The Mean stresses are dependent to pressure input loads until the parameters *T* reaches a certain value. In particular the stress for which this phenomena takes place is around the pre-stress tension for which the behaviour of the diaphragm change from membrane to like a thin plate subjects to large. This trend is depicted in Fig 6.7 b), where the maximum deflection and the mean stresses are plot as function of the pressure input load. For the particular geometry chosen, the pre-stress value, at which

the maximum deflection is equal or lower to the diaphragm thickness, is within 1,5 MPa and 2 MPa. Above these values mean stresses are not dependent on the pressure load and the percentage variation of mean stresses in the diaphragm is below 15%.

6.3.3 Viscoelastic phenomena: creep

The main consequence concerning the invariant behaviour of stresses with pressure is how the viscoelastic phenomena take place. As described in Chapter 3 the time dependent deformation of the diaphragm depends on stresses.
To be able to estimate the behaviour of each geometry tested with the static model and to be able to sense the proposed pressure field, a time dependent model of the error affecting the diaphragm is necessary. Unfortunately poor data concerning the creep behaviour of Mylar® are available in open literature or technical datasheet. . Thus it was necessary to develop an experimental procedure able to extract this data so that it was possible to infer a time dependent error model E(t).

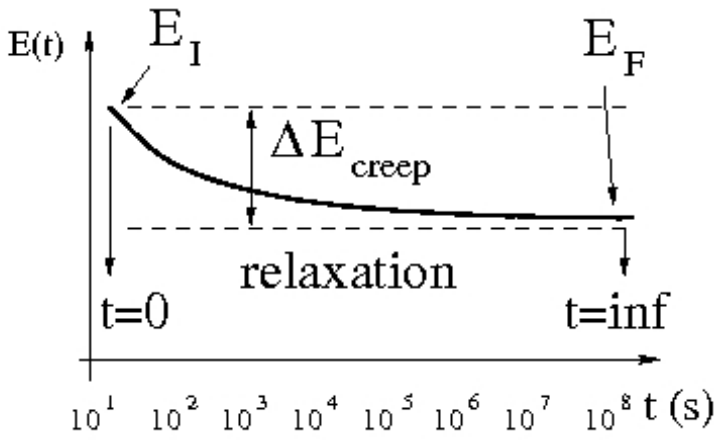

Figure 6.8: Example of E(t) function

The experimental procedure developed is an iterative process where performing tests to explore behaviour viscoelastic of prototype sensors, it has been possible to modify the static model.
Inserting time dependent parameters achieved into the static model it possible to reproduce, with a certain degree of confidence, the real behaviour of prototype sensors[18,24].The FEM static model and the time dependent error model achieved have been used to choose among many potential geometries for the sensor with the better trade off , in terms of sensor figure of merits parameters.

6.4 Electro-mechanical plan

Performing the iterative process briefly depicted above, we have developed four sensors type.

	Type 1	Type 2	Type 3	Type 4
With	24 mm	24 mm	24 mm	24 mm
Length	24 mm	24 mm	24 mm	24 mm
Cavity Radius	5 mm	3 mm	5 mm	3 mm
Fixed Electrode Radius	4,5mm	2,5mm	4,5mm	2,5mm
Spacer Thickness	110 um	110 um	75 um	75 um

Tab 6.1: four types dimensions of sensors developed

The best sensor type it was the type four: the sensor parameters are described in chapter 8.
The plan of the sensor and the fabrication are described in chapter 7 .

Chapter 7

Fabrication of sail pressure sensor

For assembling the sensor, standard printed circuit board material layers have been used. As described in the Chapter 5 “Fabrication of wing pressure sensor”, we have used the printed circuit board (PCB) technology because it allows the manufacture of sensor by fast prototype machine directly into laboratories and the materials used are perfect to achieve a good transduction by sensitive units developed. Finally the PCB technology it’s really low-cost.
If you compare the bill of materials used for wing pressure sensor with the list below you can note as we have changed the adhesive: we used an high resistance spray glue for assembling the three main part of the sensor.
A new material used in the manufacture of unit it has been the Mylar®. It’s a polyester layer commonly used for a broad array of applications in the electrical/electronics, magnetic media, industrial specialty, imaging/graphics, and packaging markets and wherever flexible surface with high resistance to cyclic stresses is required.
The rigid part of the sensor have been built again using fibreglass epoxy layers. Their low thickness and stiffness guarantee both a low total thickness and a strong frame above which to stretch the sensing Mylar® film.
It’s important point out that the sensor will not be bonded directly on final electronic board, but it will be soldered by a plinth. The reasons of this choice will be described in Chapter 11 “Wireless sensor node”. In this chapter we will describe only the plinth and the manufacture methods.

7.1 Materials

7.1.1 Epoxy resin

FR4 laminate is the usual base material from which plated-through-hole and multilayer printed circuit boards are constructed. ”FR” means Flame Retardant, and Type “4” indicates woven glass reinforced epoxy resin. The laminate is constructed from glass fabric impregnated with epoxy resin and copper foil. Foil is generally formed by electro-deposition, with one surface electrochemically roughened to promote adhesion. FR4 laminate displays a reasonable compromise of mechanical, electrical and thermal properties. Dimensional stability is influenced by construction and resin content.
We used three types of FR4 laminate:

- FR4 DURAVER-E-CU 104ML : 460 μm thick with copper 35 μm thick (both side)
- FR4 DURAVER-E-CU 104ML : 760 μm thick with copper 35 μm thick (both side)
- FR4 DURAVER-E-CU 104ML : 1.6mm thick with copper 35 μm thick (both side)

7.1.2 Mylar

Mylar® is a biaxially oriented, thermoplastic film made from ethylene glycol and dimethyl terephthalate (DMT). It is one of the most environmentally safe polymer products made today. Mylar® polyester film, only by DuPont Teijin Films, is available uncoated or coated and in a broad variety of gauges and widths.
The overall sensibility of the sensor is a trade off problem concerning the membrane mechanical sensitivity and the modulation of deflection actuated by the capacitor. To be able to improve the mechanical contribution to the overall sensibility of the device, a thin film is required.
Others important requirements are : a good dimensional stability, due to low thermal expansion coefficients and resistance to viscoelastic phenomena. Moreover the thin film must be conductive by its nature or able to be coated with conductive coating and nevertheless cheap, to respect the project guideline related to the development of a working macro pressure sensor, realizable with very low economics efforts.
Many of the already mentioned features are typical of metals but are more appreciable in special steels which are often employed as sensing element of typical commercial pressure sensors. The only mismatching features is the high manufacturing cost of such thin metal films.
A suitable alternative to thin steel film is represented by Mylar, it posses features similar to steel but with a cheaper costs. A wide variety of Mylar are available on market, each one of them have differences in the mechanical characteristics, anyway as indicated in the Dupont Mylar datasheet [25], it is generally not so sensitive to creep.
Unfortunately poor data about Mylar viscoelastic behaviour are present in open literature, as consequence an estimation of the viscoelastic behaviour of the thin film is not so easy to be inferred and the inaccuracy bounds of the sensor, largely dependent on these effects, are not predictable with finite element analysis. The particular Mylar chosen for the membrane is a Mylar840® type, 20um thick, coated on the bottom side with an aluminium deposition of few Armstrong. The coating let the membrane to be conductive and to operate as the movable plate of the capacitor.

7.1.3 Adhesive

We have used a spray glue: the Scotch-Grip Spray 77 Adhesive. It is a multi-purpose aerosol adhesive. It is fast tacking and it has a long tack range when applied to both surfaces. It is characterised by specific features such as high tensile strength, high shear and peel adhesion, resistance to solvent and moisture, low outgassing and conformability. It is usually employed for bonding a variety of substrates including lightweight boards, foams, plastics, fabric, paper and insulating materials. It is also used for bonding fabric backcloths in studios and window dressing, and bonding polystyrene foam in fabricating packaging units.
The solvent is a petroleum distillate/cyclohexane its colour clear/pale cream, it shows very good water and UV light resistance but a poor resistance to fuel solvent and oil, this characteristic fit well with the experimental procedures where different pre-

stressed membranes where easily glue to the same sensor frame once a quick solvent clean.

7.2 Layers

Four distinct prototypes, differing by dimensions and structures have been designed and tested. Since the viscoelastic behaviour has been underestimated and a correct procedure was not developed at the very beginning of the project. The first experimental attempts and results were initially useful for validating and optimising the FEM simulation models. However, their main use has been to provide a better understanding of the sensor transduction mechanisms from the physical point of view and for shedding new light even on the aspects that regard the parasitic capacitance and the optimisation of the sensor structure and its working principle.
The sensing unit consists of a three layers stacked structure:

- BASE : rigid part of the sensor built using a FR4 layer
- SPACER : rigid part of the sensor built using a FR4 layer
- MEMBRANE : deformable part of the sensor built using Mylar®

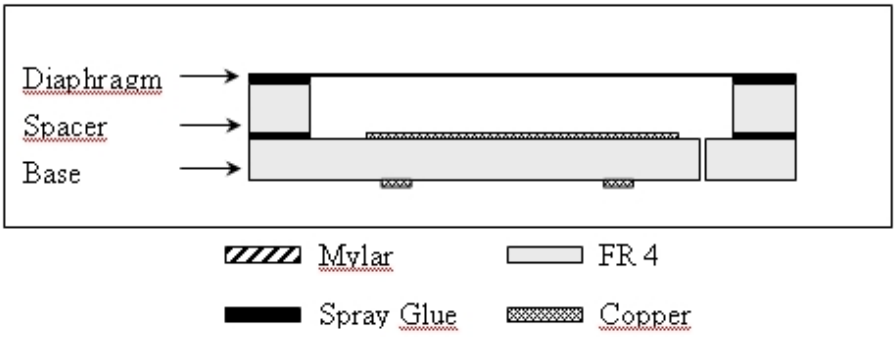

Figure 7.1 : Sensor layers sketch

Fig. 7.1 shows the sensor layers sketch. Layers have been attached to each other by means of either a 5 +/-2 um thick layer of spray glue, patterned in the same shape as the SPACER. To create BASE and SPACER layers we have used the fast prototype machine LPKF Protomat S62 like it has been for wing pressure sensor.

7.2.1 Base

The BASE layers has been created using the 760 um FR4 laminate. It is the bottom part and the thicker layer of the sensing units, and it have to guarantee different topics. First of all the base, due to its high thickness, has to act as frame above which the other layers such as the spacer and the diaphragm are glue and pre-stressed.
In the upper side of the BASE, the round fixed plate of the capacitor is realized, and a circular static tap of 1 mm is presented Fig. 7.4 (a) The static tap is a drill plated, so it leads the pressure inside the sensor cavity and it lets the electric signal of the fixed plate to be routed to the electric paths in the bottom side of the BASE layer. In the bottom side of the BASE layer Fig. 7.4 (b) two pads allow the contacts for the two

electrodes of the capacitor (deformable membrane, and round fixed plate), a rectangular shield is also present to protect the fixed plate from electromagnetic interferences.
In the shield ten copper connector are realized. They let manly the sensing unit to be stiffly bonded to the plinth, but also they connect to the ground the rectangular shield through the plinth.
One of the edge of the base perimeter presents a semicircular cut, realized to allows the signal of the conductive membrane to be lead to the bottom side of the base by means of conductive glue, routing the signal through the thickness of the whole unit Fig. 7.4 (a), Fig. 7.4 (b).
The first step to create the BASE it has been to design the structure by a CAD software. The Fig. 7.2 shows the gerber files produced. The second step has been to drill and to plate the hole. Final step has been to etch, by prototype machine milling tools, the top and bottom FR4 surface. In the upper side of the BASE we have etched not only the copper but also the glass-fibre inner layer around the fixed electrode, in order to lowering the base-spacer junction surface. This action has been crucial to set the initial distance between the plate of the capacitor. The precision of this manufacturing is +/-10 um.

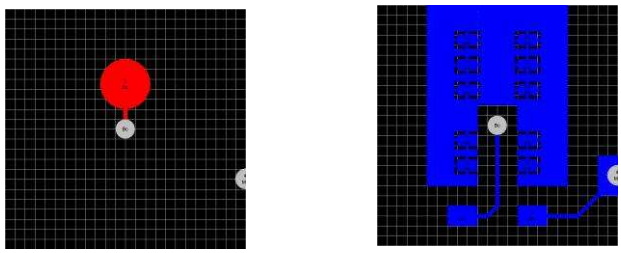

(a) (b)

Figure 7.2 : Sensor: BASE gerber file; upper side (a), bottom side in top view(b).

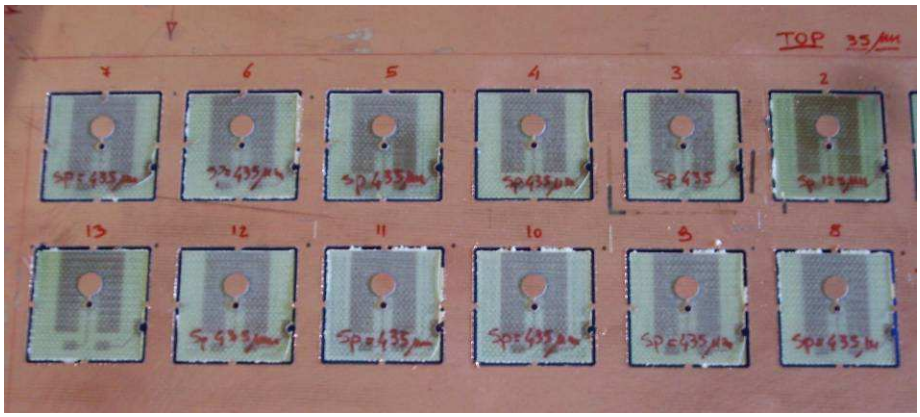

Figure 7.3 : Sheet of processed FR4 laminate to create the BASE layers

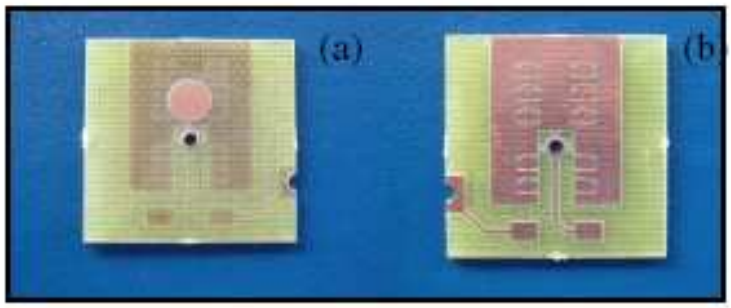

Figure 7.4 : Sensor upper side (a), Sensor bottom side (b).

7.2.2 Spacer

The SPACER layer is the middle layer of the sensing unit as shown in Fig. 7.1 , it is a single fibre-glass planar surface of 460um thick without copper-clad. The two sides of the spacer are equal to each others. Principal function of the spacer, is to create the circular cavity in which the membrane deflects when pressure loads are applied. The first step to create the SPACER has been to design the structure by a CAD software. The Fig. 7.5 shows the gerber files produced.

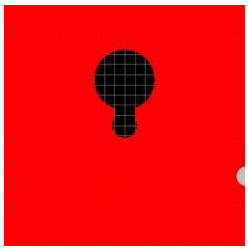

Figure 7.5 : Sensor: SPACER gerber file;

The second step has been to remove the copper from each side of 460 um FR4 laminate by chemical etching. Final step has been to cut out, by prototype machine milling tools, the SPACER layer.

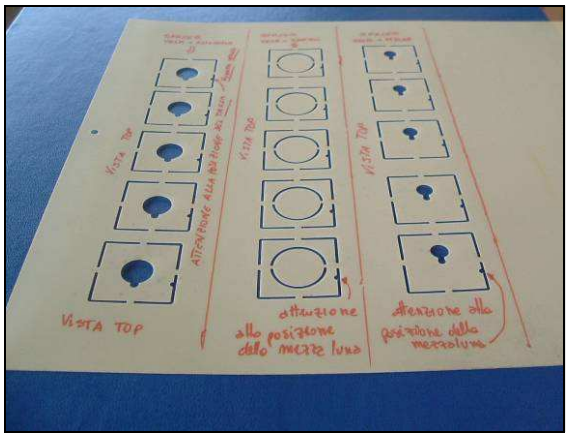

Figure 7.6 : the fabricated Spacer layers for different sensor prototypes dimension.

The base-spacer and spacer-membrane junctions are made with special spray glue sprinkled above the surfaces to joint. The most critical aspect of this layer, during the assembly process, is the risk that liquid glue penetrates inside the cavity. This event would affect the sensor efficiency both from the electrostatic and mechanical point of view. The presence of glue inside the cavity, in fact, would alter the dielectric constant of the means between the plate of the capacitor, and it would have an effect on the mechanical deflection of the diaphragm inside the cavity. To overcome the two problems, different FR4 shapes, 400 um larger than the cavity of the sensor, have been realized to protect the electrode in the base and the cavity of the spacer Fig. 7.7 (a), (b). The small FR4 shapes are then removed after the sprinkling of the adhesive glue.

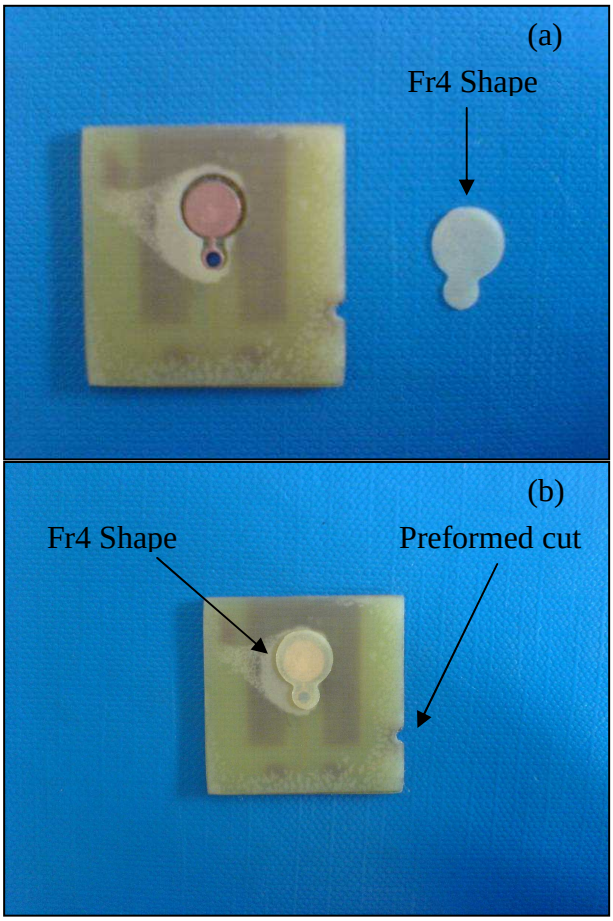

Figure 7.7 : Spacer layers fabricated for different sensor prototypes dimension.

Also in the SPACER layer one of the edge presents a semicircular cut realized to allow the signal, of the conductive membrane, to be lead to the bottom side of the base through the whole sensor thickness.

7.2.3 Mylar

Mylar is the active layer of the structure: it deflects inward and outward the cavity of the sensor, in response to the differential pressure input.
The assembly of MEMBRANE layer is a critical sensor fabrication process, this is due to the need of pre-stressing the thin film. The initial stress forced on the film is a

key factor in reducing instabilities around the zero pressure loads, and hysteresis along full span pressure input.

7.3 Plinth

The plinth is the junction element between sensor and the final electronic board. It has to lift the sensor from the electronic board plane, without breaking the electric paths.
To guarantee the electrical connection, the plinth takes sensor signals using the contacts on the long edges and it leads them to the electronic board through the vertical contacts on the short edge (see Fig.7.8). To avoid ground loop, just one of ten sensor shield ground contacts is connected to the electronic board ground through a vertical contact (the electrical path is shown in the upper side of Fig.7.8).
The two pads, allowing the contacts of capacitor electrodes, will be connected to the electronics board through two vertical contacts (the electrical paths are shown in the bottom side of Fig.7.8).
Like in the junction plinth-sensor, the contacts on the short edges without electric paths on the plinth upper side are used only to bond stiffly the plinth to electronic board and they are connected to ground.
In the middle of plinth there is a 2mm hole: it leads the pressure to the sensor static tap.
To create the plinth we used a 1.6mm FR4 laminate. The plinth is 5mm wide and 24 mm long.

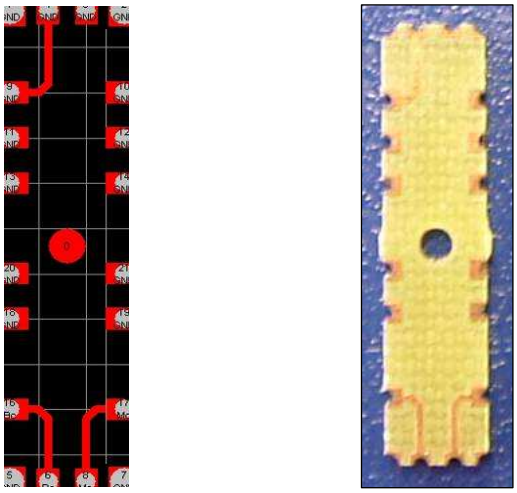

(a) (b)

Figure 7.8 : Plinth: gerber upper side (a), real upper side (b).

7.4 Methods

7.4.1 Base – Spacer, bonding

Aim of the junction between the BASE and the SPACER layer is to realized the cavity of the sensor. In this phase the concentric assembly of the circular fixed plate and the circular through cut of the spacer must be performed. The second important issue is to avoid glue to penetrate inside the cavity and above the electrode (like described in the paragraph 7.2.2). The concentric assembly has been performed by means of two precision steel blocks leaned to each other to form a reference square corner Fig 7.9 (a). In this way one of the four corners of the base has been leaned to the reference structure and after the glue has been sprinkled above the upper side of the base. Also the spacer layer has been leaned to the reference corner above the base Fig 7.9 (b).These easy self alignment of both the edge layers, let the circular cavity and the square copper plate to be concentric.

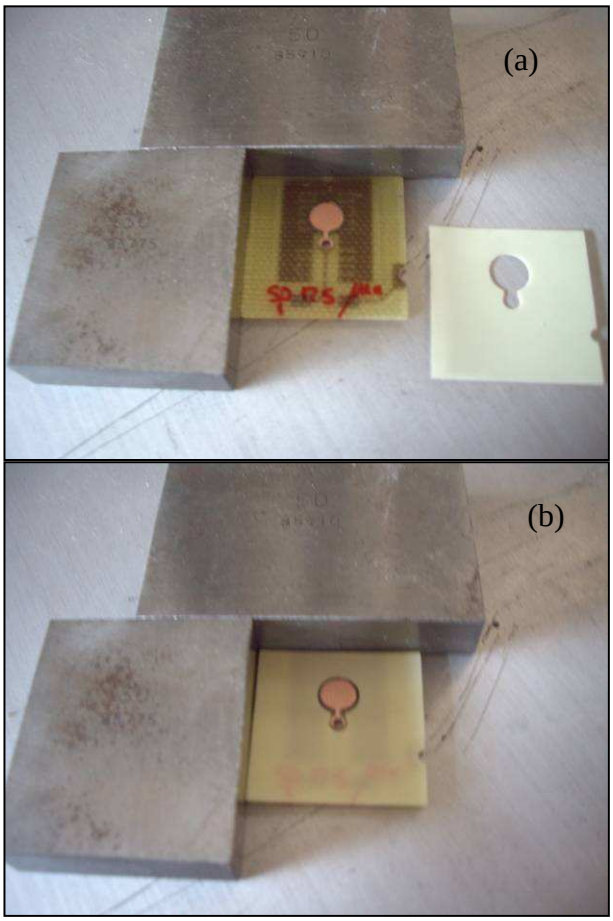

Figure 7.9 : BASE self alignment (a), SPACER self alignment (b)

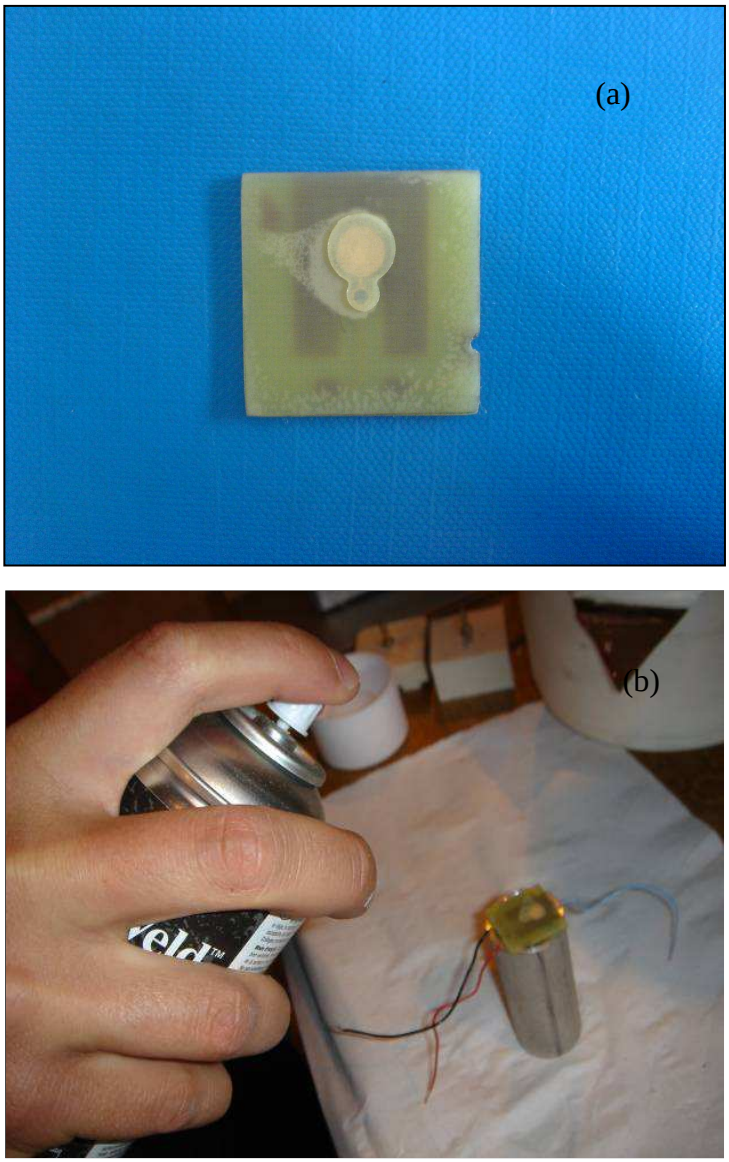

Figure 7.10 : FR4 Glue Shaper (a), Glue sprinkling process (b)

The second issue realized before the alignment procedure is performed by means of an FR4 cavity-shape 400 um larger than the cavity perimeter; the small shape protects the electrode during the glue spraying process, and it avoid the glue to penetrate inside the cavity when the adhesion compression load is applied, in Fig. 7.11 the final assembly is shown.

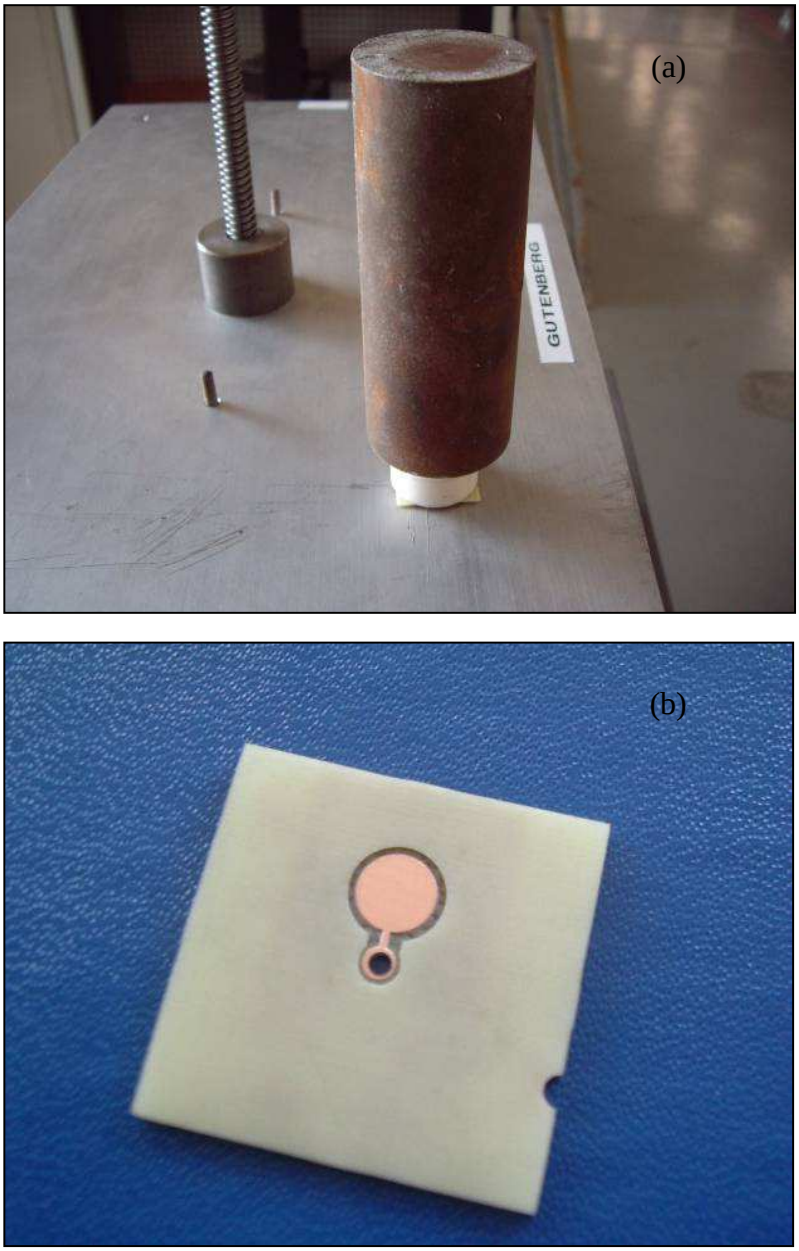

Figure 7.11 : Normal weight to ensure adhesion (a) , Base and spacer Bonded (b)

7.4.2 Mylar – Spacer, bonding

The main critical part of the assembly process is the junction between the membrane and the spacing layer, because a predefined homogeneous and repeatable pre-stressed level must be forced in order to reduce instabilities of the membrane causing hysteresis error. For the purpose a special pre-tension device has been developed and built. It consist of three different parts : a *circular cave cylinder*, a *circular ring*, and a *plunger* Fig 7.12.

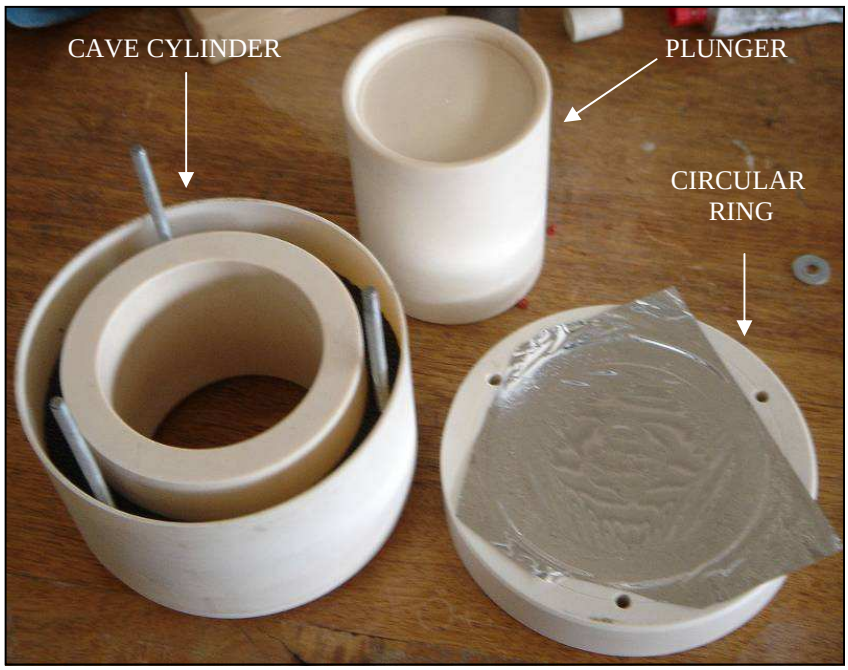

Figure 7.12 : Circular cave cylinder, circular ring, and a plunger

The used material to produce all the above mentioned devices has been manufactured in the laboratories of the faculty. Inside the cave cylinder a toroidal cavity is realized to house an amount of lead necessary to let the required tension be imposed Fig. 7.12.
The assembly routine must be performed with carefully attention in order to guaranty an homogenous and repeatable stress level in the membrane.
First step to perform the bonding is to clean and to degrease all the contact surfaces with a special cleaner and degreaser to avoid impurity or dirty to affect bonding process.
Successively a sheet of Mylar 840® is prepared and pre-stretched by means of a vacuum plane (Fig.7.14). Using an electric tester is necessary to ensure that the non-conductive side of the sheet is the one in contact with the suction surface(vacuum plane) while the other is free to get the glued SPACER surface where it has to be bond.

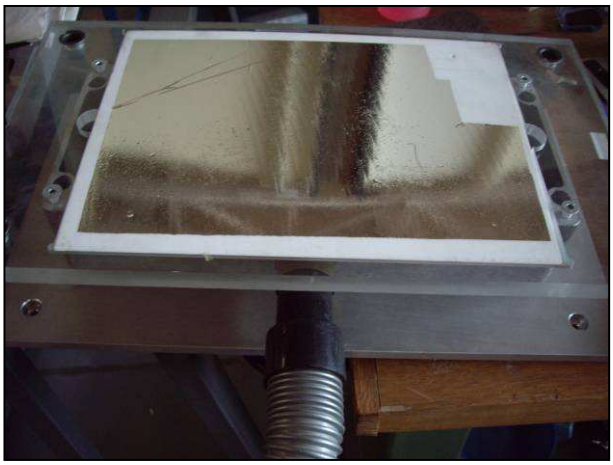

Figure 7.13 : Mylar sheet above suction surface

At the same time, when the air suction is in progress, the pre-streched sheet of Mylar is glued, with a soft adhesive, on the circular ring. This process is used to let the thin sheet surface to be as planar as possible before to be positioned above the cave cylinder, which is the device that will impose the required amount of stresses in the MEMBRANE.
The Mylar and the circular ring are joint to the cave cylinder by means of three screws and nuts able to ensure a strong mechanical junction between the circular ring the Mylar sheet and the cave cylinder. The two assembled objects shown in Fig 7.14 are then inserted inside the plunger along which vertical translation is allowed.

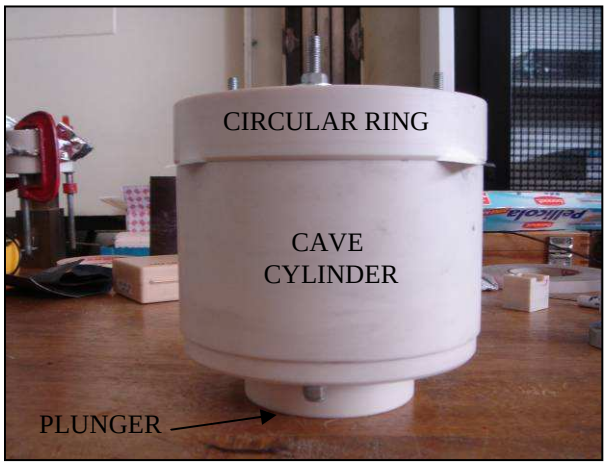

Figure 7.14: Circular ring and cave cylinder leaned on the plunger top

The plunger has been built few centimetre longer than the cave cylinder height, so the cylinder slides along the piston later walls until the diaphragm touches the top of the piston. When this condition is reached the cylinder stops its vertical movement and the gravity force acting on it let the thin Mylar film to be pre-stressed (Fig 7.15).

Figure 7.15 : Stretched MEMBRANE

After this action, the cavity of the spacer is protected by means of the small shape used in the base-junction and the spray glue is sprinkle over the upper side of the spacer. This action performed before the glue spraying process is fundamental to avoid the glue to penetrate inside the cavity when the adhesion compression load is applied. The small protection shape is then removed and the sensor frame is leaned on the stretched diaphragm (Fig 7.16 (a)).
Above the bottom part of the base a known weight acts a normal compression stress on the layers to ensure the layer bonding (Fig. 7.16 (b)). At room temperature, approximately 50% of the ultimate adhesion strength will be achieved after 30 minutes and 100% after 10 hours.

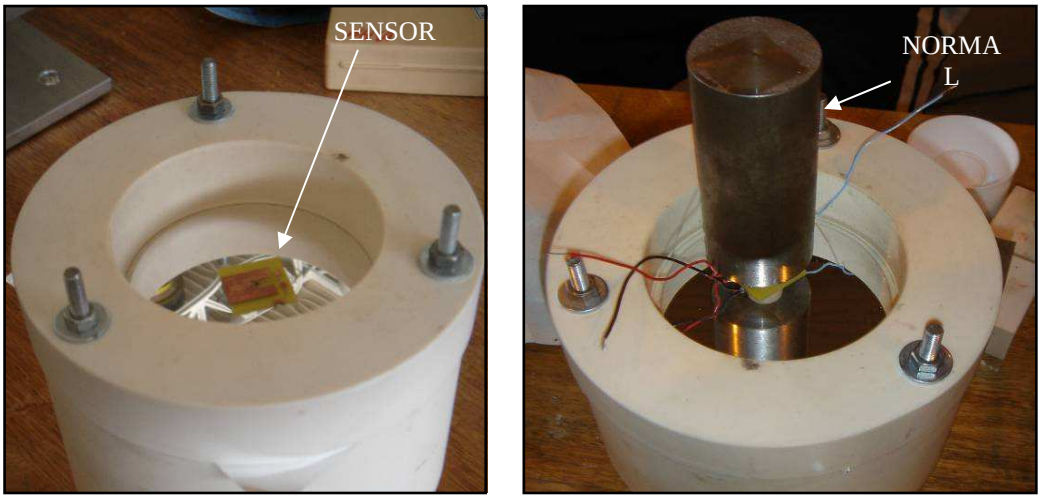

a) b)

Figure 7.16 : a)MEMBRANE bonding process; b)Normal weight to ensure adhesion

When the bonding process is completed a special conductive epoxy CW 2400 is applied in the through cut, shown in Fig 7.4 and Fig 7.7, to let the electric signal of the membrane to be lead through the thickness of the sensor to the relative electrode in the base of the sensing unit. The conductive glue requires, at room temperature, 4 hours to reach the ultimate strength and a low electric resistance(0.1Ω).

Finally, the weight used to impose the normal action to reach the adhesion of the layers is removed and the Mylar film in excess around the sensor edges is cut away using a cutter. The final assembled sensor is shown in Fig. 7.17.

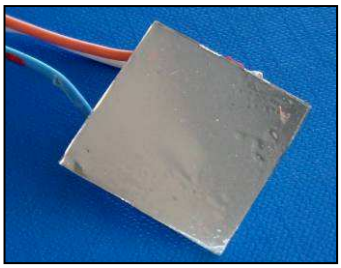

Figure 7.17 : Sensing unit assembled

In Table 7.1 the overall geometrical characteristics of the fabricated prototypes are presented.

	Type 1	**Type 2**	**Type 3**	**Type 4**
With	24 mm	24 mm	24 mm	24 mm
Length	24 mm	24 mm	24 mm	24 mm
Cavity Radius	5 mm	3 mm	5 mm	3 mm
Fixed electrode Radius	4,5mm	2,5mm	4,5mm	2,5mm
Spacer Thickness	110 um	110 um	75 um	75 um

Table 7.1 : Fabricated prototypes dimension

The full thickness of multi-layer sensor is about 1mm.

Chapter 8

Sail pressure sensor: experimental setup and results

The fabricated sail pressure sensor, as described in chapter 7, has been tested. The analysis set up has intended to validate the fem tool capacity to predict the transduction characteristics of the device and to estimate the actual behaviour of the sensor. The experimental program have been entirely performed in the laboratory of the Second School of Engineering of the University of Bologna.
Two types of analysis have been set up. The first one is intended to evaluate the static characteristic of the sensor and the effect of the pre-stress tension in the transduction chain.
The second test was set up to investigate some critically issues emerged from the first run of test in which problems concerned with viscoelastic drift and instabilities of the membrane, close to low value of pressure input, have been observed.

8.1 Experimental setup

The experimental test targets have been to obtain the static characteristics and testing the long term behaviour of the sensor, in order to depict the viscoelastic behaviour of the sensor membrane. The setup to perform the tests is composed by:

- a wind tunnel,
- a Pitot tube,
- sealed chambers for applying loads independently on the sensor membranes,
- a conventional silicon-based pressure transducer,
- an LCR meter,
- a Labview® interface control system.

The complete setup is shown in Fig. 8.1.

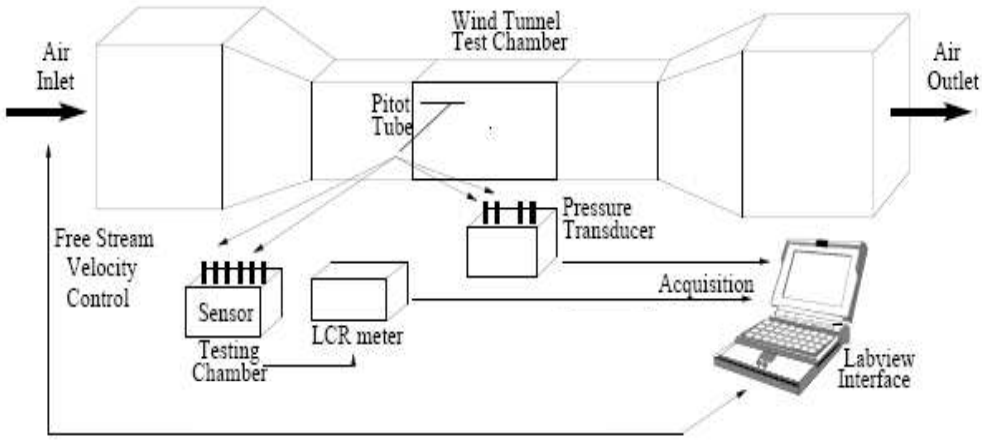

Fig 8.1 : the measure setup

It's clear like the experimental setup is very similar to the experimental setup performed for wing pressure sensor analysis. The only differences are in the structure of sealed chamber and in the pressure range led into the chamber (+/- 300 Pa)
The sealed chambers, for applying loads independently on the top of the sensor membrane, has been built again using PVC by means of a numeric-controlled milling machine in our laboratories. The PVC device is composed by a base (Fig. 8.2) where the sensor is placed and a lid. Below the sensor, inside the base, it was created a channel to lead the static pressure to the sensor static tap. In the lid has been created a channel to lead the total pressure.

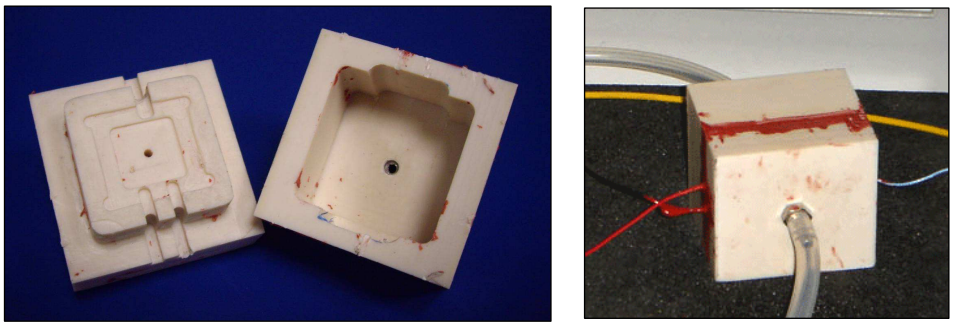

a) b)

Fig 8.2 : sealed chamber a) opened without sensor, b) after sealing

Every sensor has been connected electrically to the measure instrument by three wire (GND, fixed electrode, flexible electrode), soldered on the sensor contact pads.

8.2 Static characteristic measurement

8.2.1 Comparison between experimental data and fem static model

A set of different constant pressure values have been exerted on the sensor membrane, each value has been applied for an acquisition period of about sixty second , by mean of the sealed PVC chamber shown in Fig. 8.2. The static sensor experimental characteristic is thus obtained and compared with static simulations. In Fig. 8.3 the fabricated prototypes, named Type 4 with the geometrical characteristic specified in table 7.1 (Chapter 7) and a pre-stress level of 2.8 Mpa, is shown.
During the sensor assembling we have a geometrical dimensional tolerance of +/- 30um due to the thickness uncertainty of BASE and SPACER layers and the glue employed in the bonding process. Through the geometrical dimensional tolerance we have simulated the upper and lower bound: it's possible to note that the experimental capacitance trend (blue line) is in good agreement with the FEM static model (black line - Fig.8.3).
The experimental curve is compose by two closely spaced curves, this is due to the experimental characteristic affected by a certain level of hysteresis as shown in Fig 8.4.

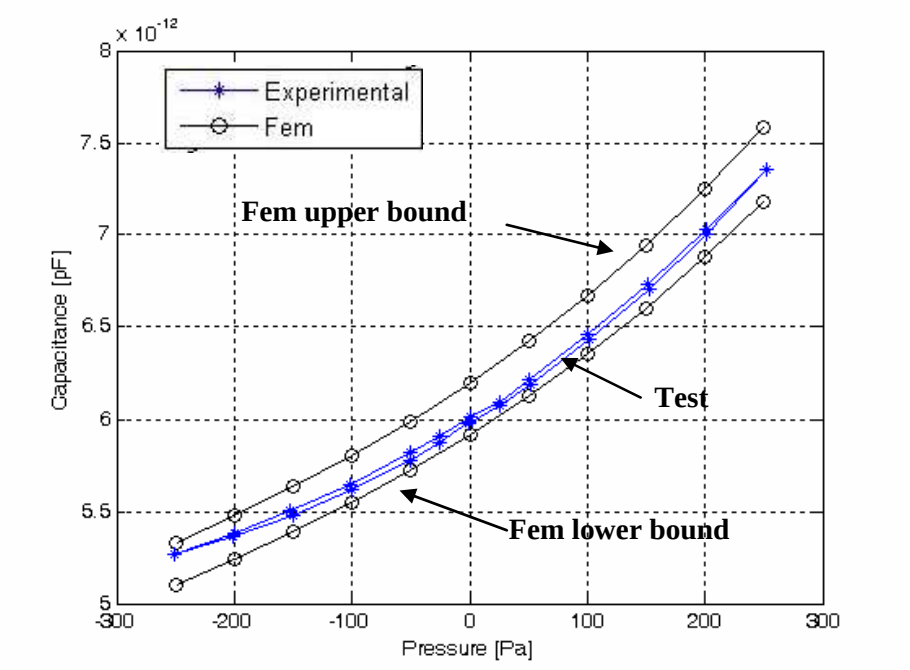

Figure 8.3: Static characteristic of the sensor Type 4

8.2.2 Comparison between several static characteristic

In order to observe the behaviour of the static characteristic, the Mylar membrane of the Type 4 prototype sensor (discussed above) has been assembly with different pre-stress load, by means of known amount of lead.
The behaviour of the static characteristic is function of different parameters: mean sensibility, accuracy, percentage hysteresis. Moreover it's important the capability of solder glue to keep the required tension in the membrane.

In the chapter 6 it has been observed, by FEM simulations, as if the pre-stress load increase, the transduction function loses its typical non linear shape. In fact the displacement becomes comparable to the thickness and the behaviour of the membrane tends to a thin plate subjected to small deflections. In Fig.8.4 three static characteristics related to three pres-stress loads imposed are presented.
If we consider the hysteresis error, it appears as a function of the pre-stress tension and in the performed experiments it had a ranges from 20,96% of FSO (Full Scale Output, the capacitive range) with zero pre-stress load, to 1.82% of FSO at 2,8 MPa. (Fig.8.4)
It's really important point out that the increasing of the pre-stress load decreases the mechanical sensitivity. In fact, the same pressure input produces a lower output capacitance and the FSO is reduced (Tab. 8.1)
A different trend appears if the linearity error, in particular if the zero pressure ones is considered. Increasing the pre-tension level we allow the sensor to manifest a lower linearity error at every pressure. This characteristic is clear especially close to the zero pressure input where the percentage error is reduce from 17.34% to 6.49% of FSO. Without initial stress the membrane appears to assume different equilibrium shapes depending on the load time history, this cause the membrane to present a zero pressure capacity value extremely unpredictable and unrepeatable.

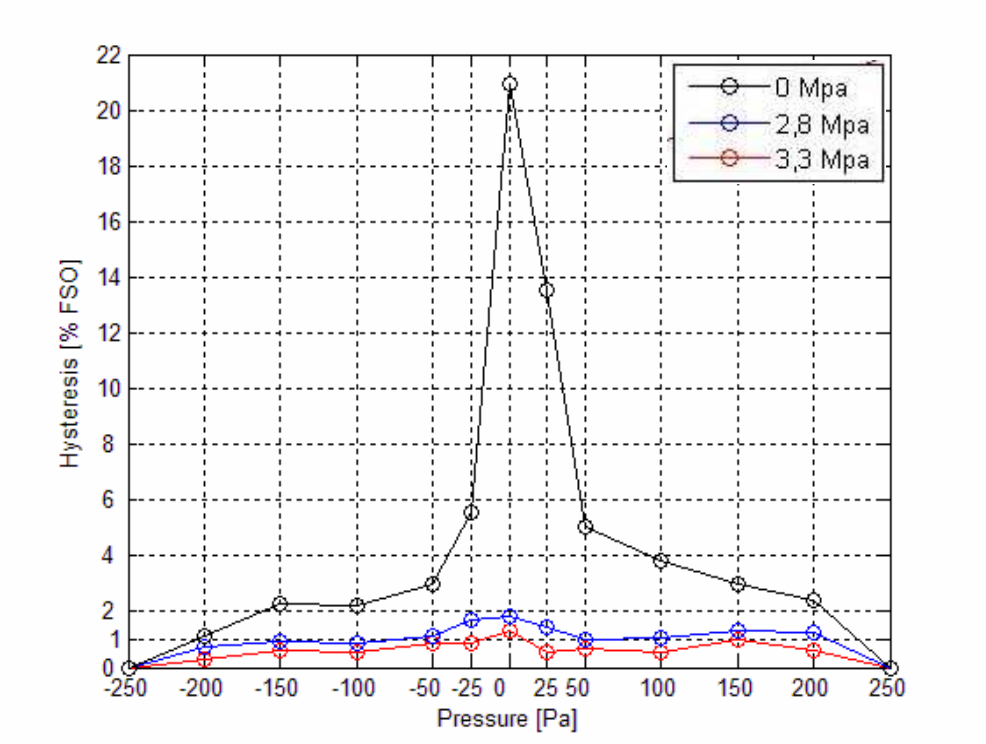

Figure 8.4: hysteresis sensor Type 4

Pre-stress Load	Absolute Hysteresis	Percentage Hysteresis	FSO	Mean Sensitivity	Linearity Error
0 MPa	551,58 fF	20,96%	2,63 pF	5,26 fF/Pa	17.34%
2,8 MPa	37,94 fF	1,82 %	2,08 pF	4,16 fF/Pa	12.98%
3,7 Mpa	11,90 fF	1,34%	0,89 pF	1,79 fF/Pa	6.49%

Tab.8.1: hysteresis error, sensitivity, and FSO for the three pre-stress load tested

Another important parameters to consider in the trade off process, is the capability of the solder glue to keep the adhesion of the membrane when the initial stress and pressure load are applied.
A membrane stretched with 5,5 Mpa has been tested with several cyclic load within the full scale input (Fig.8.5):

- in the first cycle (blue curve) a low sensitivity and a dead band zone in the range +/- 50 Pa have been found;
- at the fourth cycle (red curve) of the same sensor, the static characteristic changes; it shows the highly non-linear shape of the un-stretched ones with great hysteresis in the proximity of the zero input.

Experiments have shown that for stresses exceeding 5,5 Mpa the solder glue employed is not able to keep the tensions causing lack of long term repeatability or in the worst case the loss of adhesion among membrane and solder glue.

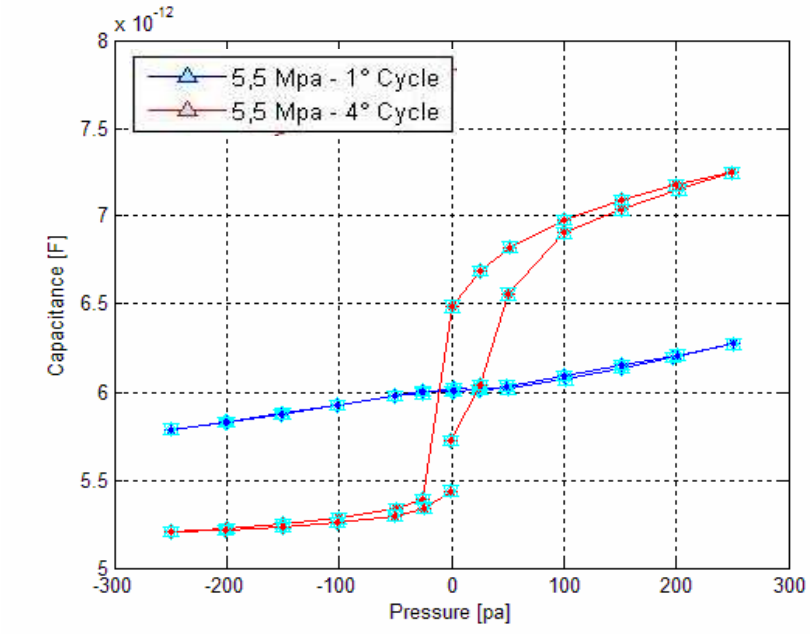

Figure 8.5: loss of repeatability due to lack of adhesion

Experimental tests have been performed on sensors prototypes with different radius, initial distance between plates and pre-stress level in order to tune the fem static

model, and to get parameters useful to infer a first order estimation about the inaccuracy of the sensor due to the viscoelastic phenomena. The geometry of the sensor to be employed in the sensing unit of the wireless sensor network has been chosen as trade off among these parameters to allow a reasonable accuracy an adequate sensitivity, and long term repeatability.

8.3 Creep behaviour experimental result

In order to understand the viscolelastic behaviour of the sensor a series of long term experimental tests has been performed. The experiments has been carried out by applying four different steps of constant pressure over the membrane, for the whole required time interval to reach an asymptotic constant value of capacitance output. The four imposed pressure loads in the test procedure have been: +50, +100, +150, +200 Pascal. The loads chosen are defined positive when the membrane deflect itself inside the cavity of the sensor, producing the higher value of capacity output.
Positive constant pressure loads was chosen because this is the condition where the time dependent viscoelastic deflection of the membrane is more amplified by the closer distance between electrodes.
As represented in Fig 8.6 it is possible to distinguish two superimposed dynamics: an instantaneous response due to the elasticity of the membrane and a slower rise due to the viscoelastic behaviour.

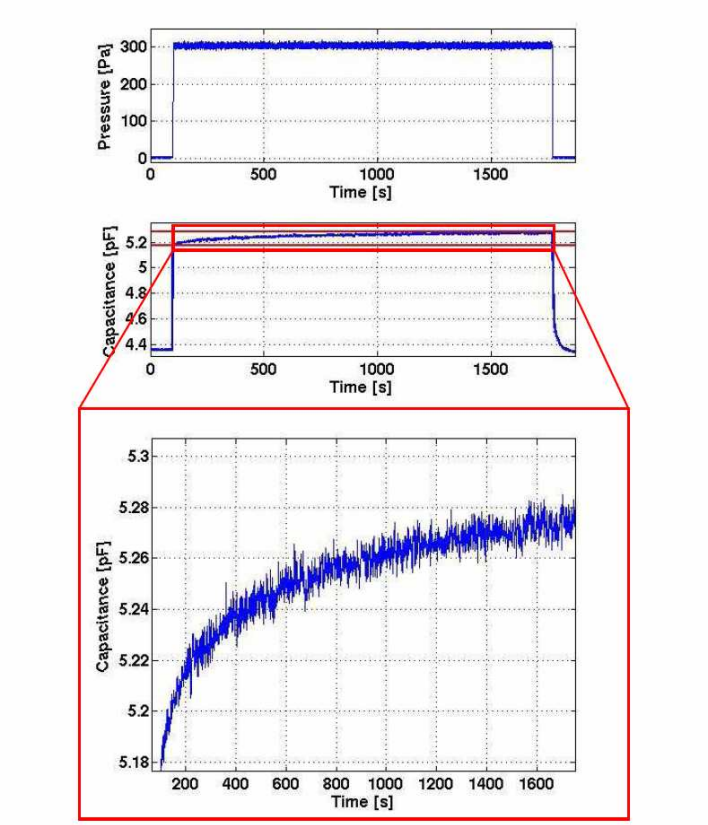

Figure 8.6: Membrane capacitive response to applied pressure step of 250 Pa.

In order to simulate the latter phenomenon, a time dependent creep modulus has been used, as described in chapter 6: to find out the creep modules parameters an iterative procedure based on experimental test (several pre-stress level in the membrane) is

required. Thus is possible to extract a viscoelastic error model described by the creep module. Coupling the viscoelastic error model with FEM static model, it is possible to find out the better sensor characteristic trade off in terms of cavity radius, initial distance between plate, and pre-stress level, able to minimize the creep dependent error in the whole FSO.

8.3.1 Unstressed membrane

As mention in the chapter 4, unstressed membrane are bond to the sensor frame by means of a suction surface therefore a low residual stress in the membrane is imposed but its magnitude is unknown and unrepeatable.
The static Fem model fail to evaluate the membrane behaviour in the proximity of zero pressure input this is due to the un-planar shape form of the membrane, this because of high value of hysteresis error close to zero pressure inputs. Long term experimental test has shown a creep dependent variations of approximately 330 fF resulting in a 17% degradation of dynamic range in 36 min for a pressure of 250 Pa (Fig.8.7).

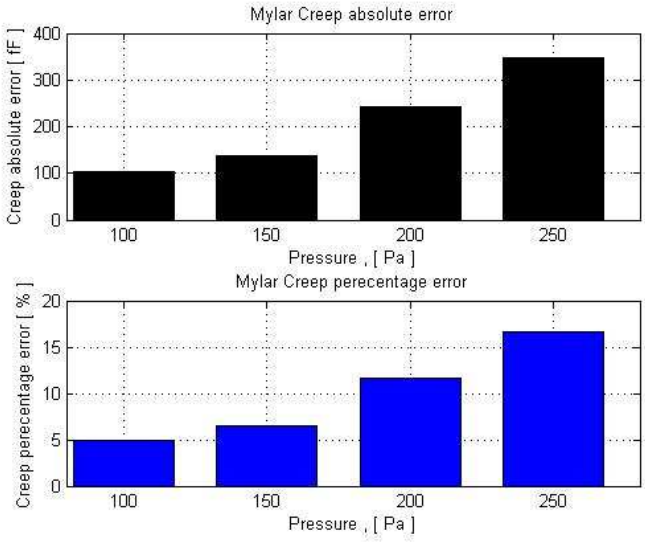

Figure 8.7: creep absolute and percentage in the unstressed membrane

Finally the Fem static model and the associated viscoelastic time dependent error model are compared with the experimental acquisition. It's possible to point out how the static model fail to estimate the trend and absolute value of the sensor behaviour for the lowest pressure input Fig.8.8 .

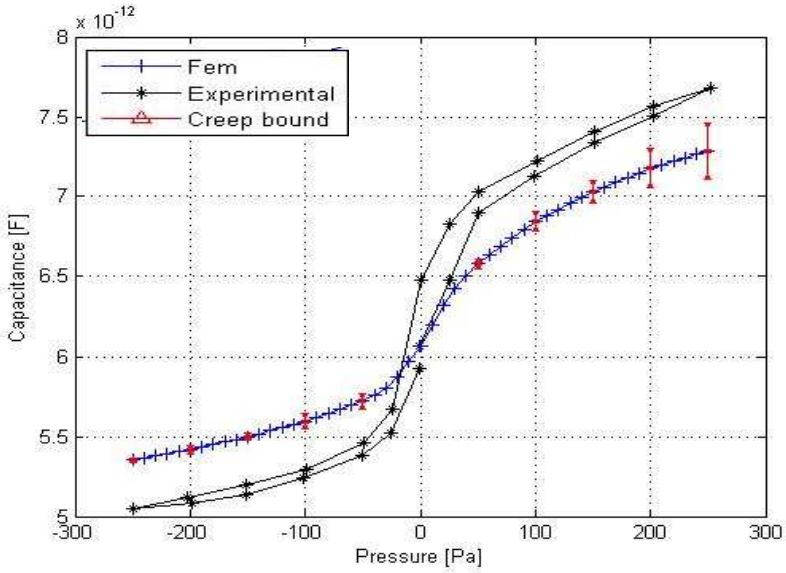

Figure 8.8: Un-stressed diaphragm : Fem static model, Creep Fem estimation, Experimental characteristic

It is important to note that the main error affecting unstressed membrane is the un-repeatability due to the different un-planar shapes assumed whenever the zero pressure input is applied.

8.3.1 Stressed membrane

The behaviour of stressed membrane have been also investigated. How described in the chapter 7, a repeatable pre-stress level was imposed during the fabrication.
When a certain pre-stress level is imposed to the membrane the FEM static model is able to reproduce with sufficient accuracy the experimental behaviour, both in terms of trend and capacity output values. Long term experimental test has shown a creep dependent variations of approximately 140fF resulting in a 6.5% degradation of dynamic range in 36 min for a pressure of 250 Pa (Fig.8.9).

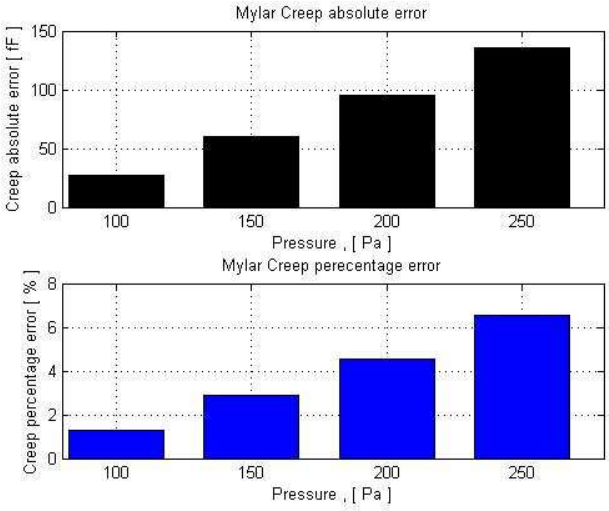

Figure 8.9: creep absolute and percentage in the stressed membrane

It is possible to appreciate how the high hysteresis value associated with the unstressed membrane disappears. The FEM static model reproduce the experimental shape and is able to predict the reduction of sensibility and full scale output due to the new behaviour of the membrane.
If the error bound predicted by the viscoelastic model are superimposed to the FEM static model and compared to the experimental uncertainty due to the actual viscoelastic behaviour. It is possible to see how the FEM error bound slightly overestimate the actual error (Fig.8.10).

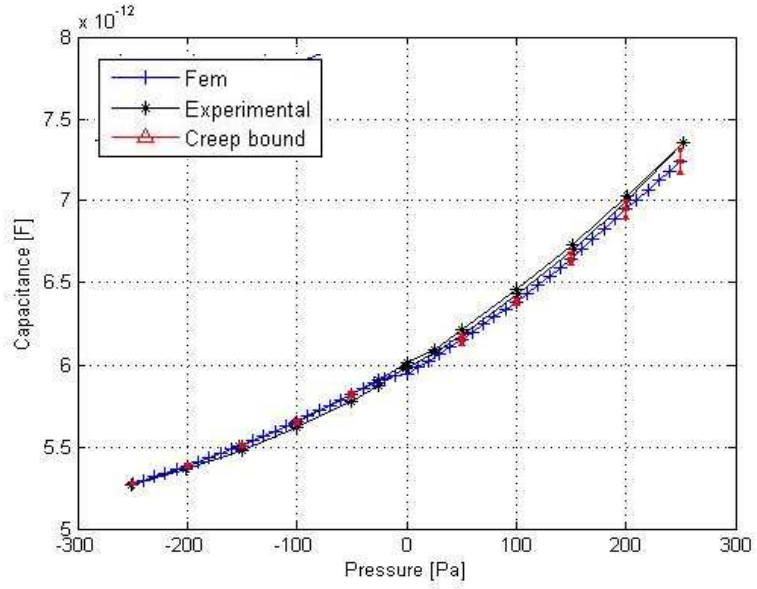

Figure 8.10: Pre- stressed diaphragm : Fem static model, Creep Fem estimation, Experimental characteristic

The reported data concern with the best sensor geometry and pre-stress level, provided as output of a numerical campaign performed by means of the Fem static model and viscoelastic error model obtained by means of acquired data through four pre-stress experimental tests.
The table 8.2 summarizes the characteristics of the best sensor developed (Type 4). We will use this sensor to realize the pressure sensing inside our system

Pre-stress Load	Absolute Hysteresis	Linearity Error	% Hysteresis	FSO	Capacity Zero-pressure	Mean Sensitivity
2,8 MPa	37,94 fF	12.98%	1,82 %	2,08 pF	6 pF	4,16 fF/Pa

.

Tab.8.2: characteristic of the sensor we have chosen to develop the system

Chapter 9

Sensing system

Designing the devoted electronic to perform the sensing of the sail pressure sensor, we have to remember, as it has been noted in Chapter 1, that the dimension and power consumption are important. Therefore the sensing circuitry must be developed to spend few energy allowing a long node life time using small battery. At the same time it must perform a fast, reliable and careful data acquisition, using less space (area) possible, so it will be important to use SMD components.
The electronic management has been performed by means of the microcontroller embedded in the Zensys Node, considering to cut down the energy consumption.
Every wireless sensor node of the network will mount a sail pressure sensor described in the previous chapters (6,7 and 8).
In this chapter the electronic structure, to perform the data read-out, is discussed. It describes the sensing circuitry management and a prototype to perform the functional test. Finally a schematic of the wireless sensor node is proposed.

9.1 Available sensing circuitry and choice made.

The sensing of a capacitive sensor can be realized using many methods. Mainly it's possible to use a frequency generator, which changes the frequency proportionally to the capacity variation. Another method is to measure the charge or discharge time of the capacitive sensor. Finally we can use a charge amplifier circuit.[26]
The first method is really sensitive to the input capacity of components : the sail pressure sensor has a C_0 (capacity value when the differential pressure is zero, see Chapter 8) of 6pF so it's very near to the input capacity of components (approximately 10 pF) .Therefore it's difficult to perform a good reading of pressure because the frequency generation process is dominated by input capacity of components.
In the second method, also if the sensor capacity is charged by a resistance of some tens of MΩ we achieve rise time of some μsec. To measure the rise time a microcontroller must check the voltage level on the sensor. Making this operation is possible, if the ADC conversion time is smaller than charge time of sensor, but the ADC conversion time embedded in the Zensys node is some tens of μsec. Therefore it's impossible to use this metod.
The last one appears the best. Using a charge amplifier there are not parasitic capacity dangerous or problems using the ADC converter (the voltage levels are fixed).

9.1.1 Charge amplifier

The proposed charge amplifier circuit consisting of two stage: the fist is the real charge amplifier, the second is a simple voltage amplifier used to maximize the ADC converter input voltage range. The 12 ADC converter embedded in the Zensys node has been used.
Studying the circuit working proposed in Fig. 9.1 it's possible to identify five phases:

Phase 1. The switch is closed, the control signal Vin is zero and the control signal Vdd-Vin is one. Therefore Vch will be equal to Vdd/2

Phase 2. The switch is open. The Vch rise by means of switch charge injection. The charge injection is variable phenomenon so, during every measure, it must be evaluated

Phase 3. The ADC converter evaluates the Vout : it's the reading process after the switch charge injection. The voltage value is stored inside the microcontroller.

Phase 4. Vin and Vdd-Vin change state: Vin =1 , Vdd-Vin=0. The Vch voltage decreases proportionally to the sensor capacity (Csens). Changing voltage on Ccomp is important to remove the charge on Csens due to the value of C_0, where C_0 is the sensor capacity when the differential pressure is zero. The Comp must be equal to the minimum value of Csens.

Phase 5. The ADC converter evaluates the Vout: this is a voltage value proportional to the sensor capacity value but it's stained by switch charge injection. Inside the microcontroller we will perform a simple math operation, using the voltage value stored during the phase 3, to obtain the final voltage value. This value represents the pressure acting on the sensor.

When phase 5 is ended the evaluation cycle restarts from phase 1 or breaks off, in function of software management.

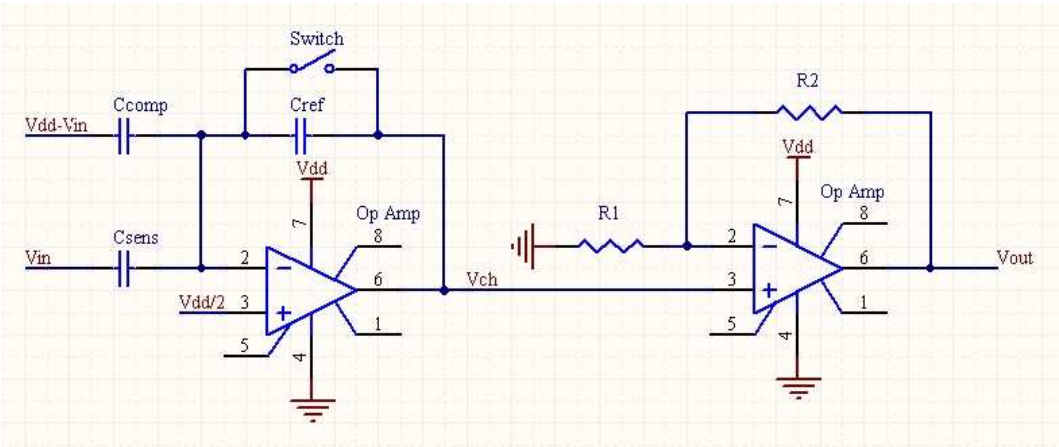

Fig. 9.1 : schematic of proposed charge amplifier

To understand the math expression describing the link between Csens e Vout we need to start from the phase 3. Calling Voff the voltage offset due to the charge injection, it's possible write the voltage sampled during phase 3 like:

$$V_{sw} = G\left[\frac{V_{dd}}{2} + V_{off}\right] \tag{9.1}$$

where G is the gain of voltage amplifier:

$$G = 1 + \frac{R_2}{R_1} \tag{9.2}$$

During the phase 5 the microcontroller acquires the Vout

$$V_{out} = G\,V_{ch} \tag{9.3}$$

where

$$V_{ch} = \frac{V_{dd}}{2} + V_{off} - V_{dd}\left(\frac{C_{sens} - C_{comp}}{C_{ref}}\right) \tag{9.4}$$

so it's possible to write:

$$V_{out} = G\,V_{ch} = G\left[\frac{V_{dd}}{2} + V_{off} - V_{dd}\left(\frac{C_{sens} - C_{comp}}{C_{ref}}\right)\right] \tag{9.5}$$

To obtain the final voltage value ($V_{\mu C}$) the microcontroller compares Eq 9.2 and Eq 9.5:

$$V_{\mu C} = V_{sw} - V_{out} = GV_{dd}\left(\frac{C_{sens} - C_{comp}}{C_{ref}}\right) \tag{9.6}$$

From Eq 9.6 it's possible to write Csens as:

$$C_{sens} = \frac{V_{\mu c} C_{ref}}{GV_{dd}} + C_{comp} \tag{9.7}$$

The capacity Cref has to be small to maximize the charge amplifier gain. It's interesting to note that charge injection increases the Vch range so it is a positive

factor in the measure cycle (but it has to be no so big to avoid the voltage amplifier saturation).
To manage the charge amplifier are necessary three digital line : two used for Vin and Vdd-Vin and the last one to conduct the switch state.

9.2 The developed charge amplifier

To design the charge amplifier we have to choose low power devices. In fact, as depicted in Chapter 1 and 2, it is really important to minimize the power consumption. To minimize the area used to build the circuit we make use of SMD components. To test the sensing circuitry we used the Zensys node ZM2106 (see Chapter 2) so it has been possible using directly the 12 bit ADC converter embedded, obtaining a two bytes voltage data.
To minimize the power consumption we have chosen to switch off the sensing circuitry when unused so we used devices with shut-down pin. To use them we had to use another digital line to manage the shut-down pin (just one for all electronic). In the design of the sensing circuit we have chosen the double operational amplifier TLV2763 [27] and single analog switch TS5A4595 (with a charge injection of 1pC) [28]. In fig 9.2 it's possible to see the developed prototype.

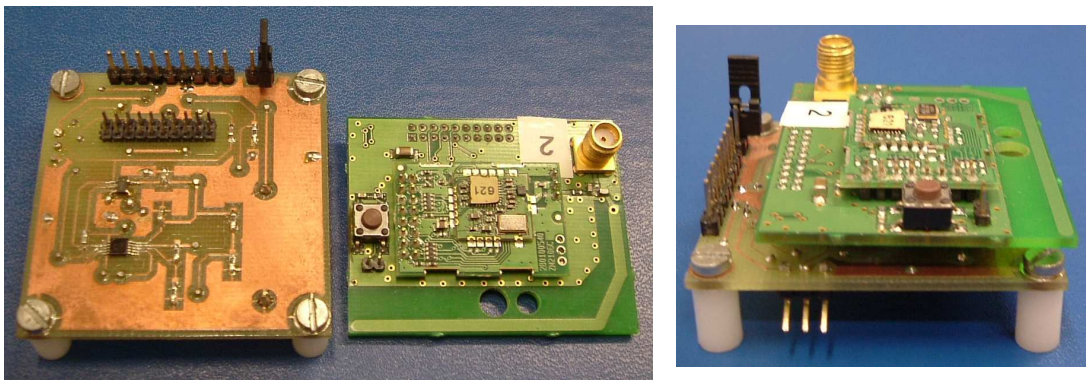

Fig. 9.2 : developed prototype to test the sensing circuit

9.3 Tests

The Zensys node ZM2106 has been programmed to perform the circuit management but also to transmit simply the collected data so that it has been possible to check the acquired data like in the final interface (see Chapter 10).
We have performed three types of test: the fist has been to check the functional phases and to acquire the sensing timing , the second has been to evaluate the linearity of the function voltage to capacity and finally we have estimated the power consumption.

9.3.1 Functional phases test

Using an Agilent 54641D Mixed Signal Oscilloscope, we have acquired the Vout waveform. In the Fig 9.3 is shown some sensing cycles where the five phases are clear.

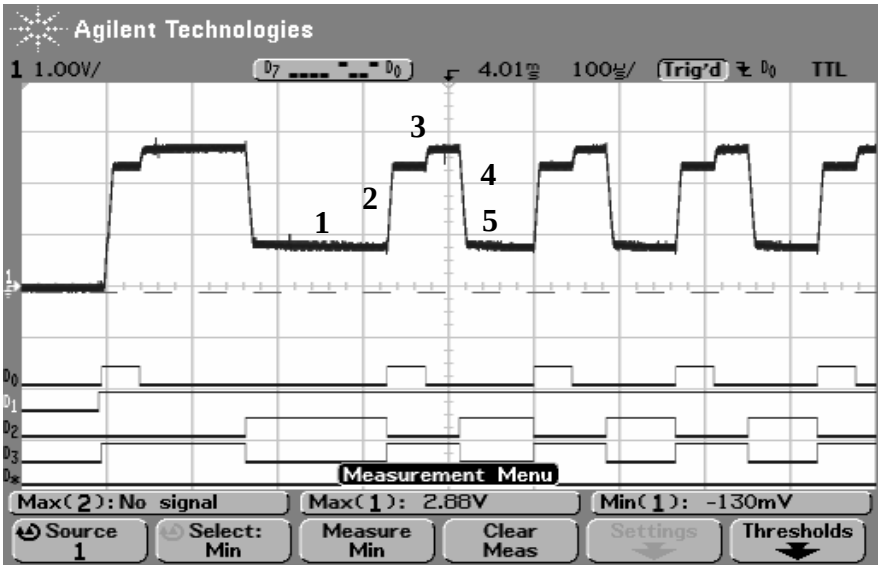

Fig. 9.3 : sensing cyles

Starting from the flat zone (1) we see the previous voltage level associated to the sensor capacity. The first rise voltage (2) happens when the circuit return in phase 1: switch closed , Vin=0 and Vdd-Vin=1. The second rise voltage (3) happens by the switch charge injection due to the opening of the switch. The subsequent drop (4) happens when Vin and Vdd-Vin change state and the flat zone (5) is the new voltage level accociated to the sensor capacity.
In Fig 9.3 are shown also the four digital line used to manage the sensing circuit: D0 is used to command the switch, D1 is used for the shut-down pin, D2 is the signal Vin and D3 is the signal Vdd-Vin.
Through this test has been possible to measure the time period for each cycle: it has been estimated nearly 100us. If we consider the ADC sample period equal to 96usec [12] and we remember that the sensing circuitry must perform two sampling during each cycle (Vsw and Vout) we can estimate a full sampling period for each acquired value equal to 300usec.

9.3.2 Linearity test

To estimate the linearity of the sensing circuitry, we have tested the developed prototype using capacity measured by Agilent 4284A Precision LCR meter, in the range between 2.2pF an 7pF . After it has been performed the sensing, programming the sensing system to realize sixteen, thirty two and one hundred an twenty eight sampling periods for each capacity value. The voltage value transmitted, for each capacitor tested, has been the average of the acquired samples.
The prototype has been powered by a 3.3V battery ad the ADC input voltage range has been tuned to be between 0.1V and 3V

We have discovered a good linearity because between the theoretic the measured values we find the follow mean error :

- mean of 16 samples the error has been +/- 3mV
- mean of 32 samples the error has been +/- 1.2mV
- mean of 128 samples the error has been +/- 0.3mV

In the Fig. 9.4 the C/V output graphic for 128 samples is shown.

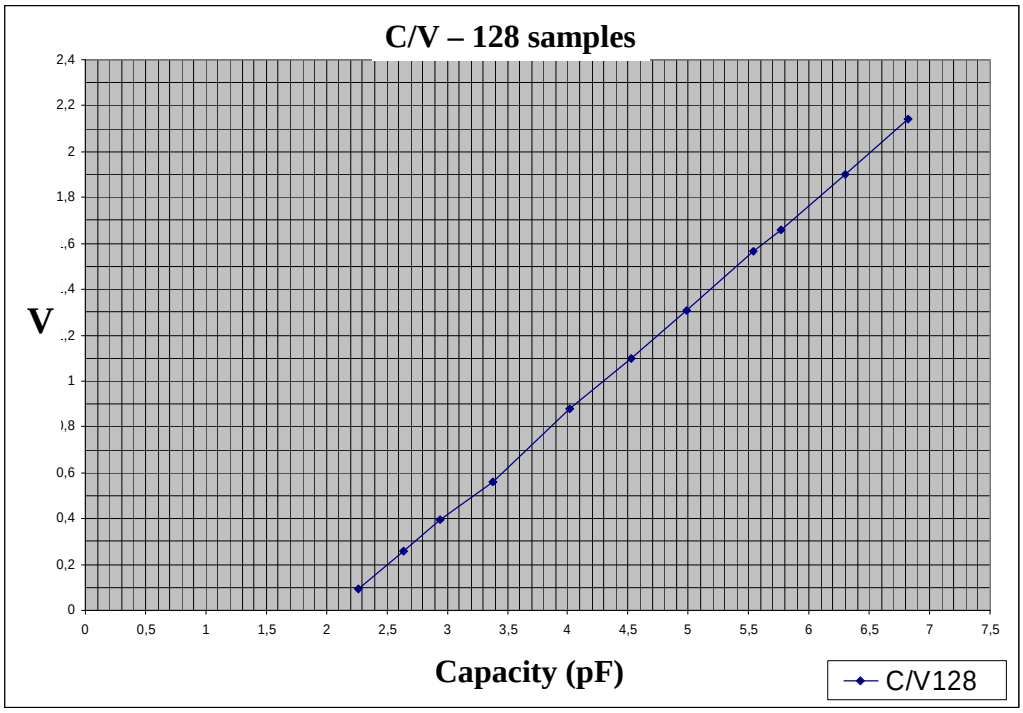

Fig. 9.4 : C/V characteristic using a mean of 128 samples

9.3.3 Power consumption

Finally it has been important to evaluate the real power consumption. To perform this measure simply we have programmed the Zensys node to realize sampling periods of some seconds (wake up mode) and the same for the periods when the electronic is switch off (sleep mode).
Powered the prototype circuit by a 3.3V battery, we have found the following consuption:

- sensing electronic in wake up mode : 100µA
- sensing electronic in sleep mode : <1µA
- Zensys node in wake up mode : 5,2mA
- Zensys node in sleep mode : 2,5µA

The values about the Zensys node consumption are the same depicted in the data sheet [12]

9.4 The proposed schematic of wireless sensor node

In the paragraphs above has been described the sensing system. It is suitable to be used in the developing of the wireless sensor node. Therefore now it's possible to create the full schematic of the wireless sensor node.
The final structure of the wireless sensor node will not use the Zensys node ZM2106, because too big, but the μboard ZW2102 with an area of only 2 square centimetres (Fig.9.5).

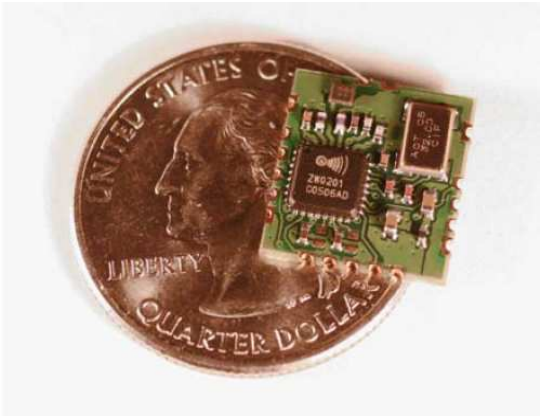

Fig. 9.5 : μboard ZW2102

In the full schematic, depicted in Fig. 9.6, there are some components, as the battery and the antenna not still described. This elements will be treated in the chapter 10 and 11.
In the Fig.9.6 it's interesting to note the sensing circuit builds by double operational amplifiers and the analog switches with some resistor and capacitor (red square).

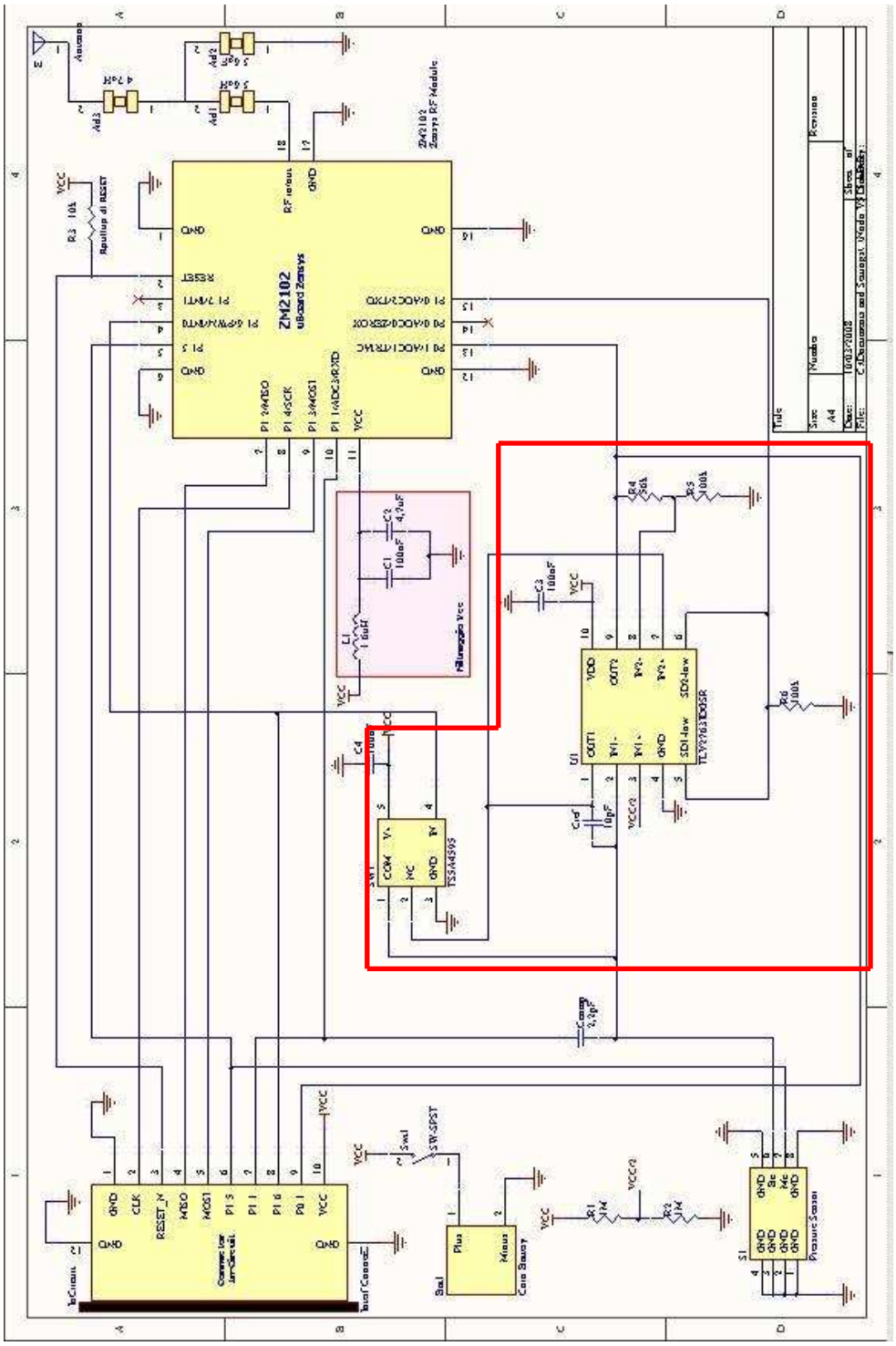

Fig. 9.6 : wireless sensor node:final schematic, inside red square the sensing circuitry

Chapter 10

The network of wireless sensor nodes

The sail is a particular place where creating a wireless sensor network. As described in the Chapter 2, heavy geometrical bonds affect the design of the wireless sensor node. The electronic board, the sensor, the antenna and the battery must be chosen to create the smaller structure but, at the same, the most reliable and careful .
In this Chapter we suppose to have all features above depicted, but in particular to have an omnidirectional antenna.
Working with an omniditectional antenna is one of the most important features in our wireless sensor network. In fact, if we think to put the wireless sensor nodes on the top of a sail, we are creating a network where the end devices are not fixed in a point, but they change the position with the sail, while the network controller is fixed in a point on the boat.
Therefore to have a good omnidirectional antenna, in the wireless sensor node, allows to have the same signal power transmitted in every direction, so that the wireless sensor node has the same radio link distance in every direction.
If we think to a racing sail-boat, it's simple to note that 30 metres can be the maximum radio link distance between the controller and a wireless sensor node; for a wireless sensor network this is a short range if it works in open space condition (Chapter 2). Therefore it will be possible to don't use the maximum power transmission, and so saving battery energy.
Thinking to the sail, we have chosen to implement the network on the top of the mainsail, because it's possible to embed the wireless sensor nodes in the battens. To obtain a good pressure map, the network needs a number of 30-50 nodes (dependently from sail surface) and a whole data refresh time every 3 seconds (this data it has been obtained by interview to testers ad shipbuilders). This conditions impose at the collector to receive a pressure data every 60msec.
To avoid delays in the data collection process we have chosen to implemet a simple star network topology. In fact, using a mesh network or a hybrid network, the hops between the end device (wireless sensor node) and controller can delay the data stream of an amount of time greater than 70msec as described in the Chapter 2. Working with a short radio link distance, the controller can directly communicates with every wireless sensor node.

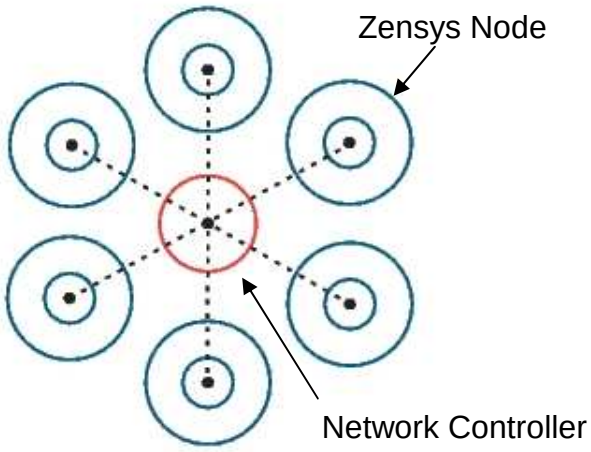

Figure 10.1: Star network topology

To realize a reliable network it's important to explore it with a efficient method, having in mind to save, in each moment, more energy possible on the wireless sensor node.
Working in the 868MHz ISM band, it's important also to don't crowd the band.

10.1 The elements of the Network

The network will be composed by the controller, the wireless sensor nodes and the graphics interface.

10.1.1 Graphics interface

The graphics interface is the tool by means of the user can control the network and to check the sail pressure map.
In the Fig.10.2 the graphics interface is shown.
It has been created by LabView® interface. It is only the beta version, in fact the pressure data are shown like voltage level (1). It's possible to set the number of nodes to check (2) and the synchronization character between controller and graphics interface (3) (useful during the system development). The number of acquired pressure data send from each node can be showed (4) and finally an output array with the last data arrived is present (5) (another tool useful during the system development). All the pressure data are stored in a file.

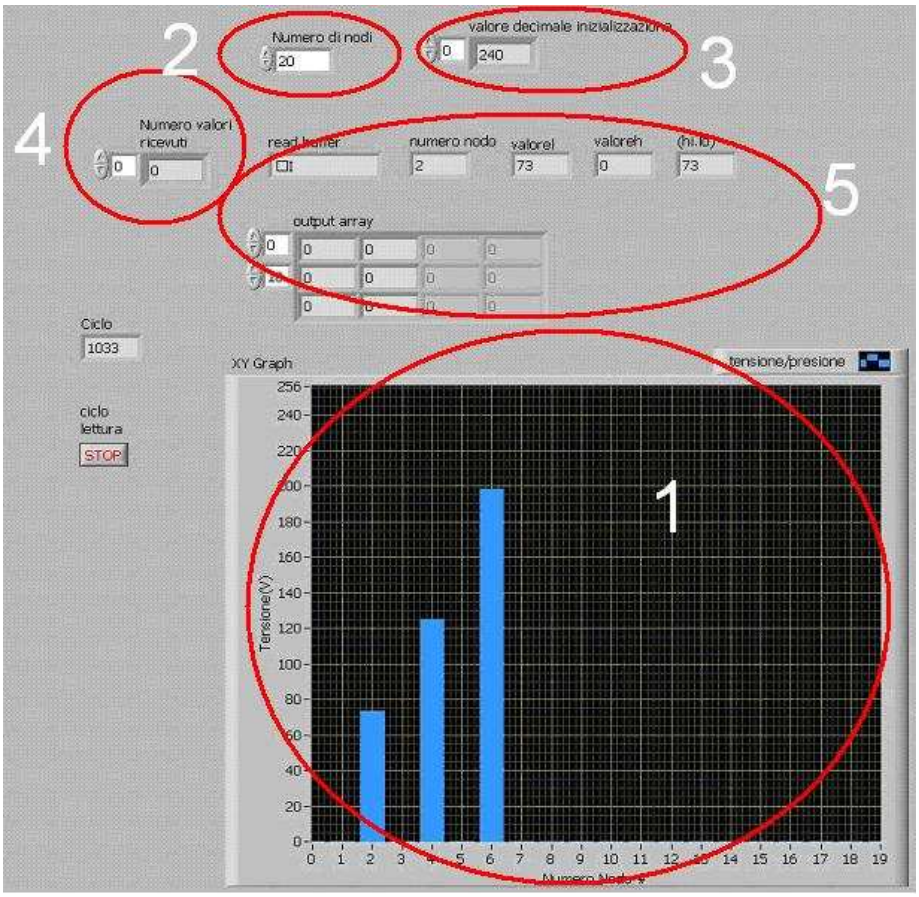

Figure 10.2: graphical interface

10.1.2 The controller

The controller is a Zensys node with around electronic to connect it to a computer by a cable.
We didn't created a devoted structure, but we have used a board available with the developer kit Zensys.

Figure 10.3: network controller

The controller needs to be powered by net supply because it spend a lot of energy being always power on. This normally it isn't a problem, because it works connected to the computer using the graphics interface.

10.1.3 The wireless sensor node

The wireless sensor node is the end device which must to check the pressure on the top of the sail. It was built following the bonds depicted in the chapter 2 and it's described in the chapter 11.
The main network target is to create a system able to maximize the node life time (further a reliable communication).

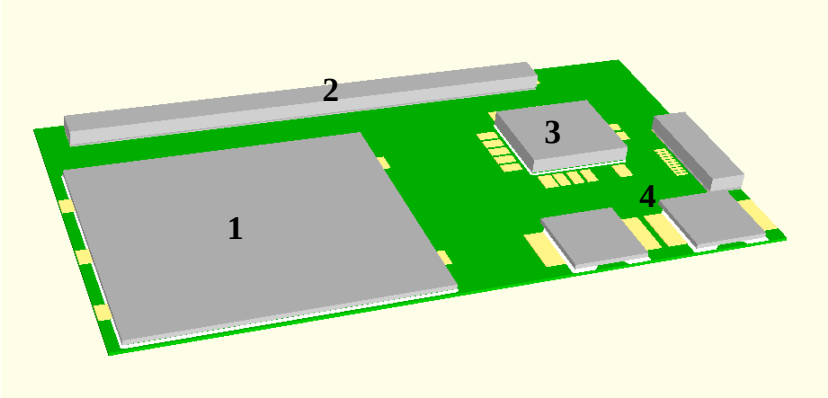

Figure 10.4: wireless sensor node: 1 sensor, 2 antenna, 3-4 sensing circuitry

10.2 The network management

To manage the network we have tested three methods:

- Free broadcast transmission of each node, using the Collision Avoidance implemented in the Zensys protocol.
- Transmission using time slot dedicated to each node
- Free transmission of each node with acknowledge

10.2.1 Free broadcast transmission

This free broadcast transmission has been the first method used to manage the network because, the Zensys protocol has a Collision Avoidance system , so we thought to use it.[12]
We have tested the network using four nodes and each node has been programmed to transmit every 240msec so that in a period of three seconds fifty transmission have been performed.
The result has been that, after some seconds the transmission is started to collide and after few tens of seconds we had only collision. We have concluded that Zensys Collision Avoidance system is not the right tool to have a reliable network. This

behaviour is understandable if we think to the target of generic wireless sensor network: it has been created to perform home control with low duty cycles (see Chapter 2) so the random time generated, to perform the Collision Avoidance system, can be to big compared to our activation times.

10.2.2 Transmission using time slot

The second method used has been based on the creation of a number of time slot, equal to the number of wireless sensor nodes, in a period of three seconds. Each time slot has been used to transmit the pressure data from only one node. To perform this network management the controller had to control the synchronization of the whole network using periodic frame transmitted to the nodes.
Without describing the synchronization methodology , we have discovered that the timer, used on the wireless sensor node to measure and creating the time slot, is really inaccurate. In fact, this system needs at least two synchronization frame every data pressure refresh period. To use this method is impossible because the synchronization procedure need nearly one second.

10.2.3 Free transmission with acknowledge

This method is very simple. When a node has to transmit a data, simply it does it, waiting an acknowledge frame from the controller. If the acknowledge doesn't arrive before some tens of milliseconds from the transmission, the node repeats the transmission after a random time, otherwise it put itself in sleep mode. The controller transmits the acknowledge if the arrived data is no corrupted.
This method is the one used to manage the wireless network.
Using this method there is a problem: it's impossible to manage a network with 50 nodes.
In fact, if we consider the transmission to be a Poisson's process, it's possible to write the probability to have no collision as:

$$P_o = e^{-2\lambda_r T} = e^{-2G} \tag{10.1}$$

where T is frame length transmitted in seconds and λ_r are the retransmissions.
The average number of transmission with success S will be equal to:

$$S = Ge^{-2G} \tag{10.2}$$

Drawing this function (Fig.10.2) is possible to discover the maximum value of S when G is equal to 0,5. [29]

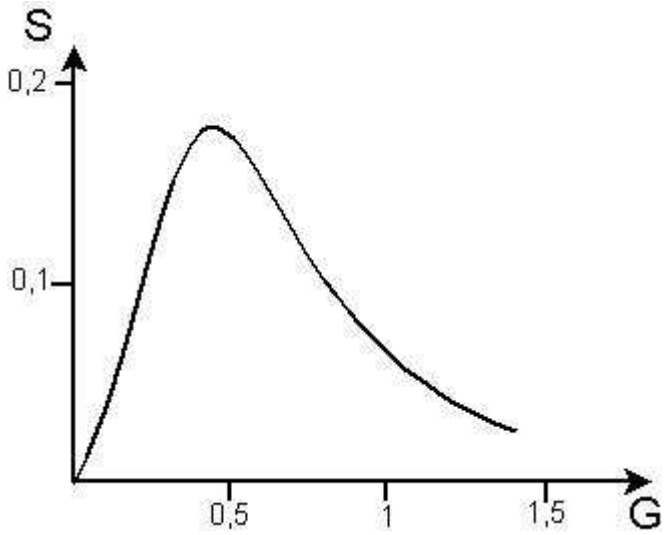

Figure 10.5: function of average number of transmission with success

The maximum value of S is 0.18erl: it's the maximum amount of transmissions with success per second in the network.
Working with the Zensys platform and having to transmit 2 byte with a data rate of 9,6kbps [12] waiting the acknowledge, it's possible, using the Zensys developer kit documentations, to compute the full time of transmission and answer: 40msec. Calling this value T it's possible to identify the number of transmission in a period of one second (λ_i):

$$\lambda_i = \frac{S_{Max}}{T} = 4{,}5tx/s \tag{10.3}$$

therefore, working on a period of 3 seconds (T_{tot}), it's possible to find as no more of 13 wireless sensor nodes can transmit in a data refresh period (Eq. 10.4)

$$N = \lambda_i T_{tot} = 13{,}3 \tag{10.4}$$

These reflections appear dramatic, but there is a solution. We are working with the 200 series Z-Wave single chip (ZW0201) but it isn't the best Zensys solution. Indeed on the market it's present the new 300 series Z-Wave single chip (ZW0301). This is a new generation of Zensys node fully compatible with the hardware and software developed on the 200 series Z-Wave but with a data rate increased to 40kbps[30]. Considering a transmission using the new hardware the period necessary to the transmission to receive the acknowledge is 10msec (T). Now, from the Eq.10.3 it's possible to achieve:

$$\lambda_i = \frac{S_{Max}}{T_{new}} = 18tx/s \tag{10.5}$$

so the number of wireless sensor nodes able to transmit in a data refresh period will be 54 (Eq. 10.6)

$$N = \lambda_i T_{tot} = 54 \tag{10.6}$$

To solve the transmission problems it's therefore sufficient to change the Zensys node series.

10.3 Controller and Wireless sensor node programming

Identified the method to perform the data exchange between controller and wireless sensor nodes, it's necessary to explain how the controller and the end devices have been programmed.
It's possible to recognize four different network phases:

1) *Creating the network*. This phase starts with the controller switching on and the start of graphics interface. The controller waits the power on of each node: every time a node switch on, it sends a frame to ask to the controller of being joined to the network. The controller knows the number of nodes to join in the network: it receives this information from the graphics interface.

2) *Waiting to wake up*. When a node has been joined to the network, it receives an acknowledge from the controller and after it goes in sleep mode. Every four minutes the node wakes up and it waits during a period of 90msec the START data frame from the controller

3) *Working*. When the user push the START button in the graphical interface, the controller starts to send, every 50msec, the START data frames during a period of four minutes. Each wireless sensor node, received the START data frame, sleeps during the next four minutes, to avoid to overlap its transmission to the START data frame. When the controller finished the network wake up, it starts to wait the pressure data from the nodes and it sends the acknowledges. The controller transmits each data received to the graphics interface. The graphics interface stores the data into a file and it shows also the pressure values at the user. Each wireless sensor node wakes up every three seconds and it check the pressure data. If the new data is different from the previous more than a threshold programmed, the node transmit the new information, otherwise it returns in sleep mode. Using this method the node is able to save the battery, because it transmits only if the data is important, and the transmission is the most expensive action for the battery. At the same, the node uses the band only if necessary. If the node doesn't receive the acknowledge, it retries the transmission after a random

time. This action is repeated another time. At the third transmission without acknowledge the node thinks lost the data and it goes in sleep mode.

4) *Waiting to sleep*. Every sixty wake up, each node set itself in reception mode during a period of 90msec, waiting the SLEEP data frame from the controller. If the user push the STOP button in the graphics interface, the controller stops to wait pressure data and it starts to sends SLEEP data frame every 50msec during a period of four minutes. To be sure that all wireless sensor node are in sleep mode the controller listens to the network during five seconds. If there are no transmissions the controller wait a START command from the graphics interface, otherwise it restarts to sends the SLEEP data frame. The wireless sensor node, received the SLEEP data frame, set itself in SLEEP mode. The network is returned in the phase *Waiting to wake up*.

From these four phases is clear like the real wireless sensor nodes power on is done only when the network is created. The SLEEP mode is only an ultra-low power state.

10.4 Energy consumption

To estimate the power consumption we suppose ,during a day, the network working eight hours and the other sixteen it stays in sleep mode. We suppose to transmit with -5dBm power using 23mA and to spend the same to receive [12]. We have chosen this transmission power by means of transmission tests using the ZW2106 module using a printed circuit board monopole antenna (see Chapter 11), an after to have estimate the transmission range [31] in function of power transmission.. If the sensing circuit works with 32 samples using 300μsec per sample cycle uses 10msec to create a pressure data using 5,3mA(see Chapter 9). To transmit and waiting the acknowledge the node spend 23mA during 40msec.
If we use the “mAh” to describe the power consumption it possible to estimate the following value:

- During the 16 hours of Sleep mode, considering also the periods where the node wait START data frame the node uses only 0.2mAh
- During the 8 hours of Working mode the node creates 9600 pressure data. If we suppose the node transmits every data, and we consider also the periods when the node waits the SLEEP data frame, the node uses only 2,7mAh

The node power consumption, during a day, without retransmission, is less than 3mAh. To be conservative we suppose to have the 50% of transmission retransmitted, so the power consumption will be 4.2mAh every day.

Chapter 11

The wireless sensor node

The wireless sensor network, to operate on the top of the sails, must to guarantee the lowest level of invasivity. The node dimensions are an important issue of the network, because geometrical variations or discontinuity over sail surface may affect the characteristic of the flow and, as a consequence, to modify the pressure field of the sail. For these reasons the most convenient way to place the wireless sensor nodes over the sail is to integrate them in the battens of sail. This topic, due to the natural shape and dimension of battens, will dramatically affect the design of the single node.
The battens width usually ranges from 20 to 40 millimetres , for the node design the higher battens limit of 40 millimetres has been chosen. The pressure sensor is 24millimeters wide, therefore the sensor node board width must to be greater than 24millimeters but less than 40millimeters.
To fix the sensor node board length we have to consider how to integrate the node inside the batten. We have chosen to create a pocket where housing the node. If the pockets are too length and deep, they can weaken the batten structure. The maximum thickness of a batten is about four millimetres. We have chosen to create pocket deep nearly three millimetres with a length smaller than ten centimetres.
To build a wireless sensor board compliant to the geometric bounds, after the sensor and the sensing system, it has been necessary to choose the optimum antenna. Moreover it has been fundamental to establish the value of power supply and the type. Finally it has been important to minimize the wireless sensor node layout, to achieve the board with the smallest area possible.

11.1 The antenna

Having to mount the antenna over a miniaturized board we have to save space without losing radio link distance and omnidirectionality (see Chapter 10).
The antenna types useful using a wireless sensor network are mainly:

- $\lambda/4$ or $\lambda/2$ whip antenna
- $\lambda/4$ monopole
- chip antenna
- planar antenna

The whip antenna is the best between the antenna proposed [32] with good omnidirectionality and a good gain, but it's impossible to use it because too big (Fig.11.1). At the same every external antenna cannot be used.
Working in the 868.4MHz ISM band the wave length λ is 34,5cm, therefore the planar antenna (patch) is too big (because the area surface is proportional to the λ [33]) but also really directional, so it doesn't fit with the design bounds.
The chip antenna is the smallest antenna, but at the same time its performance are really dependent from electric parameters (ground plane dimension, electronic too close, ecc.) so it complicates the board design. Another big problem is its poor omnidirectionality [32] [34], with a short radio range.
The λ/4 monopole, internally mounted, can be directly created as a trace on a printed circui board.

Fig.11.1: ZM2106 node using a λ/4 whip antenna

This antenna is the most similar to a whip antenna, because it has a good omnidirectionality , a good gain and so the radio range will be good [33]. The main problem, using this kind of antenna, is the design: the material (FR4) used to build the board or the available space can be unsuitable to the antenna tuning.
Based on the antenna features above described, it has been chosen to implement a λ/4 monopole directly on the printed circuit board.

11.1.1 The design conditions

The wireless sensor node is little system where a sensor with the sensing electronic, a microcontroller, a transceiver, an antenna and the power supply have to work together in the smallest area possible. Therefore it's necessary to use the least surface for each system electronic part, and during the design of antenna can be a dramatic bound.
If we want to use a simple λ/4 monopole is necessary to create a trace on the printed circuit board of 86millimeters (working in the 868.4MHz ISM band the wave length λ is 34,5cm) with a free space all around (no electronic or ground plane). These are dramatic conditions, because it would be impossible to stay within the bounds described above.
To solve this problem we chose to draw the antenna trace wrapping it around a corner. Using this method the length of the monopole should be 10 to 20% shorter

than then full size monopole (depending on the dielectric and the thickness of board) [34]. The antenna shape will be like an “L”. Moreover drawing the antenna on the board edges, it has been possible to cut down the necessary free space on the board.
The next step has been to cut out a free area where create the antenna, inside the wireless sensor board.
We have chosen a board 30millimeters wide (to leave at least of 5 millimetres of batten, up and down the node) and a board 90-100 millimetres long. It has been possible to estimate the free area available to the antenna design after some board layout test, the shape and the dimensions are depicted in Fig.11.2.
Before starting the design it has been essential to define the substrate used to create the board. Like it will be explained in the paragraph 11.3, the node needs a flexible board so we chose a thin FR4 used also in the sensor fabrication: the FR4 DURAVER-E-CU 104ML : 460 μm thick with copper 35 μm thick (both side).
To design the antenna we have used the software CST Microwave Studio.

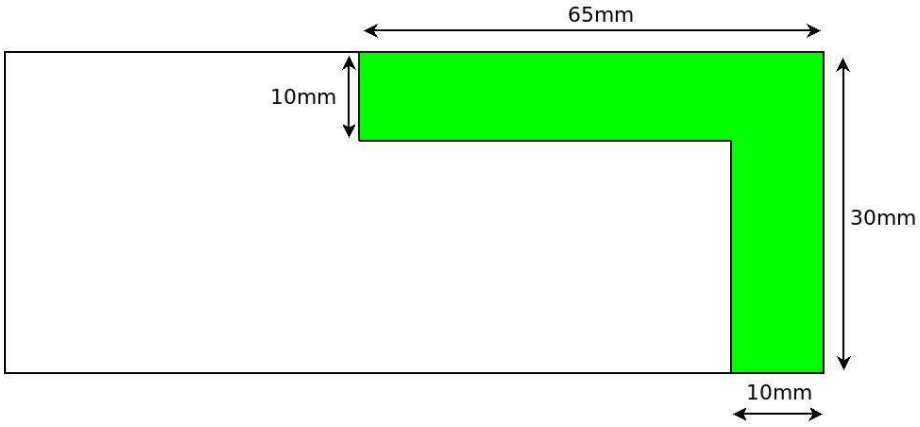

Fig.11.2: free area available to the antenna design

11.1.2 The antenna design

The antenna design aim has been to create a device with the same impedance, 50Ω, of the μboard ZW2102 transceiver output used. Unfortunately the design conditions described (free area available, FR4 thickness) are not the best to reach the target and so, we have worked to create the best antenna possible.
During the simulations we have kept in mind that a matching has bee necessary between antenna ad radio frequency output of the ZW2102, so we optimized the real S_{11} antenna parameter, referred to S_{11} antenna parameter conditioned to matching condition.
The antenna designed is shown in Fig 11.3; the S11 parameters are shown in Fig 11.4.

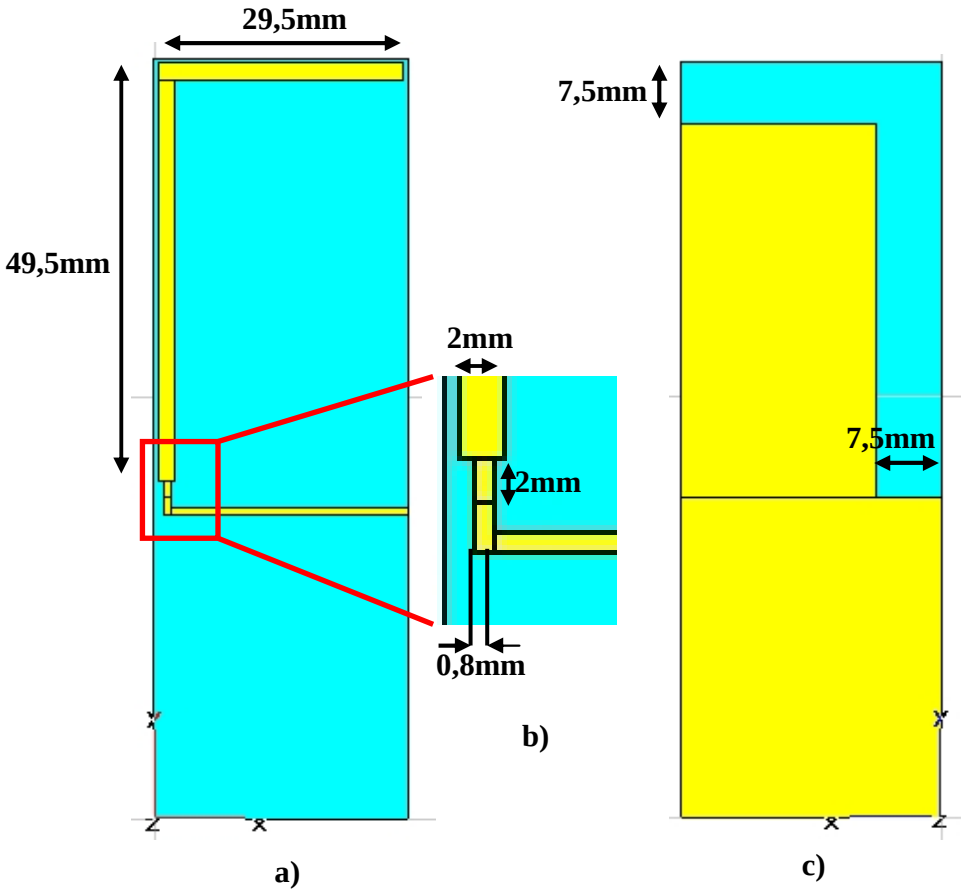

Fig.11.3: The antenna designed: a) top view , b) antenna feed , c) bottom view

The main trace length of the "L" monopole is 49,5 millimetres, the second trace is 29,5millimettres, the traces are 2mm wide. It's important to note that the free area available to build the antenna has been reduced to 7,5 millimetres.
If we observe the Fig.11.4 a) we see a poor resonance around the 900MHz, but like depicted in Fig.11.4 b) using a matching network we can achieve a really good resonance (-25dB), but with a narrow band. Working in the 868.4MHz ISM band is necessary only a 10MHz band and so narrow resonance can be acceptable.

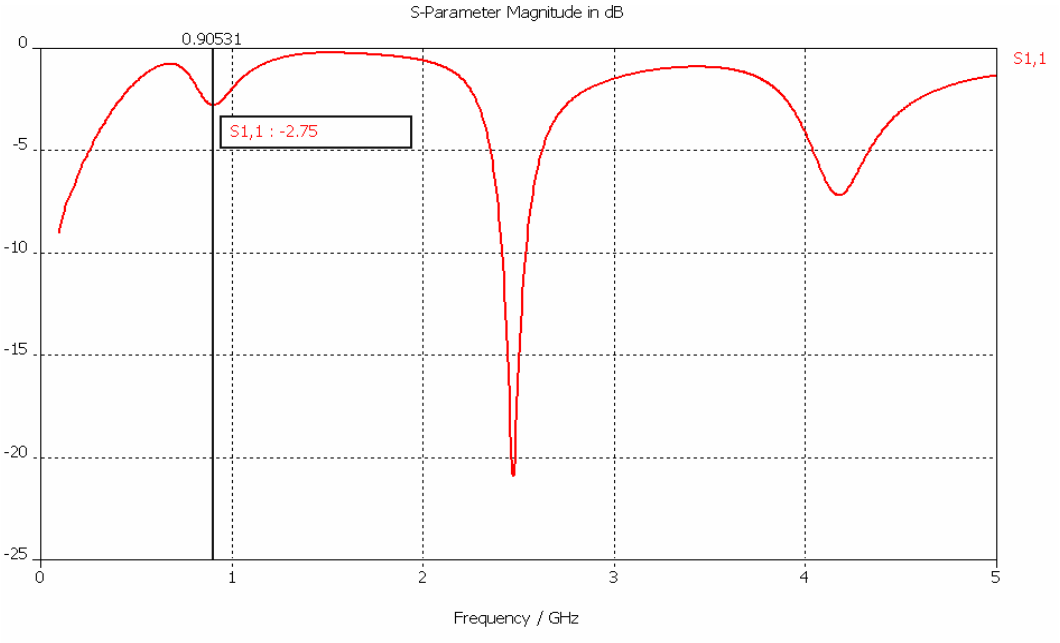

a)

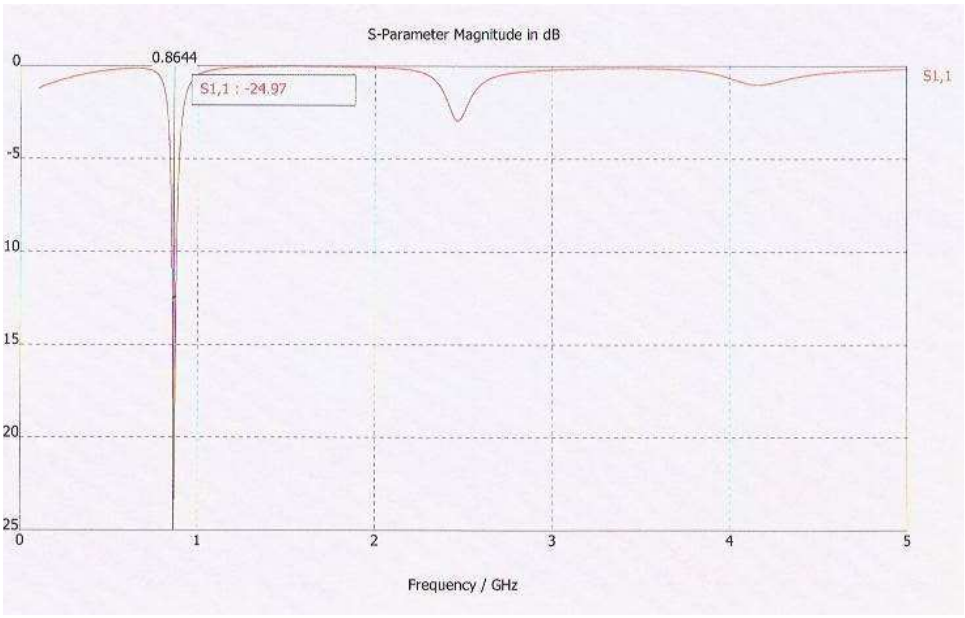

b)

Fig.11.4: The S_{11} parameters : a) real condition , b) matching condition ,

It’s important to point out that antenna has a good Gain. In fact, like depicted in Fig11.5, the ABS Gain is 0dB.

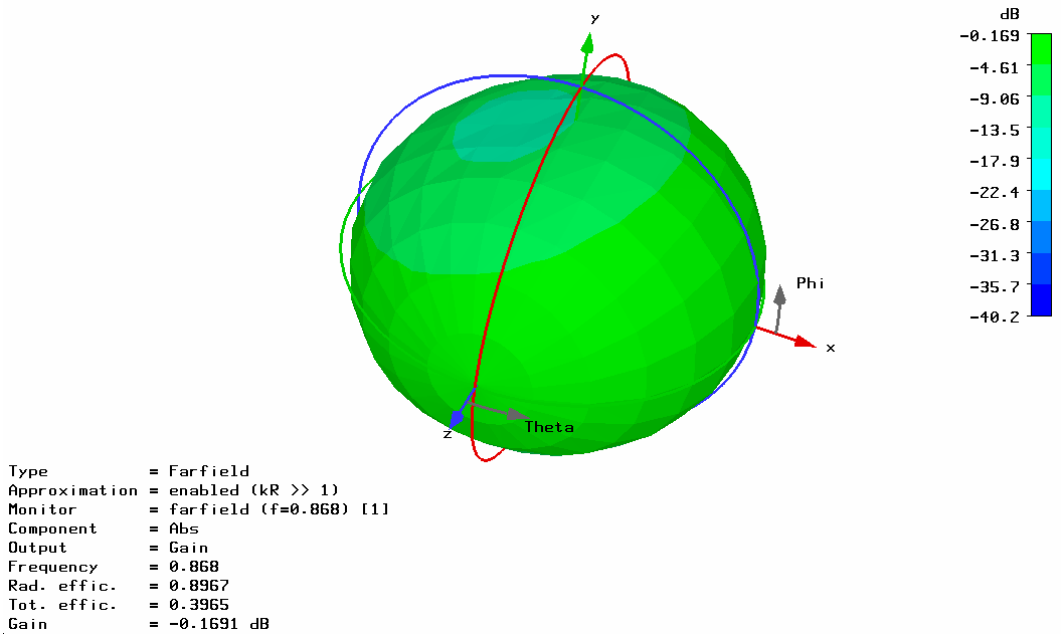

Fig.11.5: The antenna Gain

11.1.3 The matching network and antenna test

During the design, to accelerate the simulations, we use the ground plane only in the bottom side of the project, but when realize the antenna, by the LPKF Protomat S62 fast prototype machine (the same used in the fabrication of the sensor), we created a structure similar to the final board (Fig.11.6). Therefore we put the ground plane also on the top side, but this act changed slightly the antenna impedance

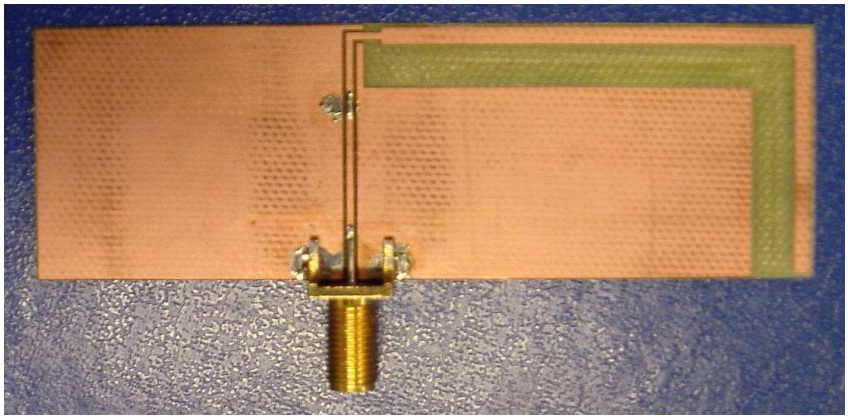

Fig.11.6: antenna realized without matching network

In fact, the impedance simulated at the frequency of 868.4MHz was Z_{sim}= 28+j81 while the impedance measured became Z_{mea}=21-j64.

Starting from this value it was possible to design a matching network using lumped components. Using the matching network theory, we studied a Π network a a T network [35]. The T matching network, with a shunt capacity an two inductors series was the best, because with component values near to the commercial values.
We have developed a new antenna with the footprints to implement the matching network near the antenna feed (Fig.11.7).

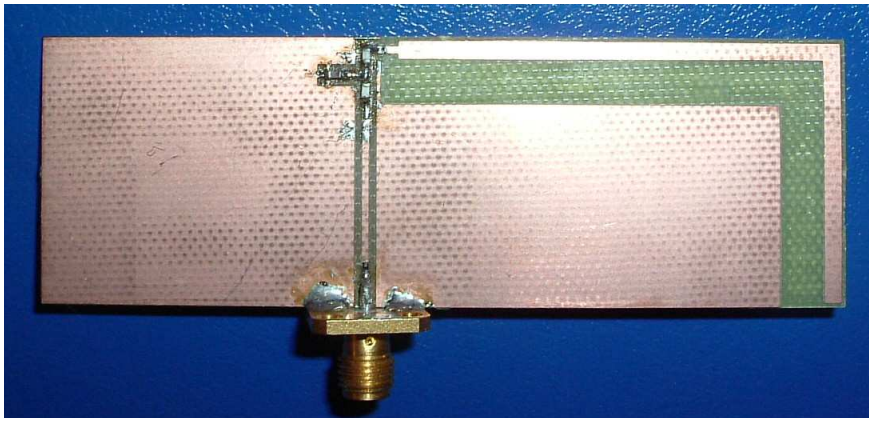

Fig.11.7: antenna realized with matching network

The tests were performed by means of Agilent Technologies E5071B 300kHz-8,5GHz Network Analyzer, the data saved as CSV files and after drawing by means of Matlab®. We have discovered that to change a bit the matching network components values has been necessary. The final values and the structure are shown in Fig.11.8.; the resonance achieved shows a good agreement with the simulation and a 10MHz band (Fig.11.9)

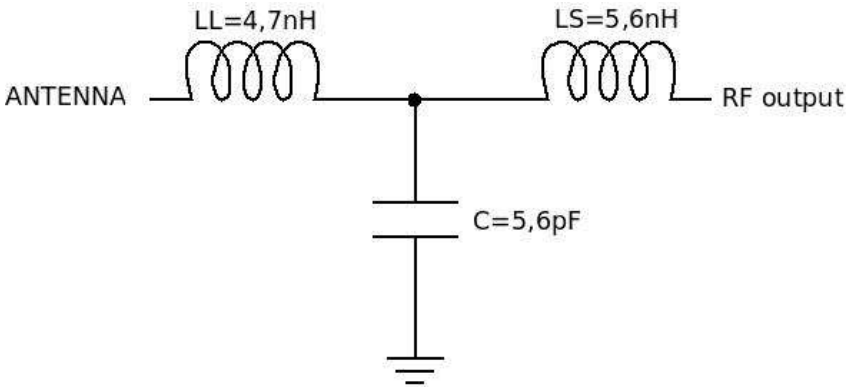

Fig.11.8: the implemented matching network

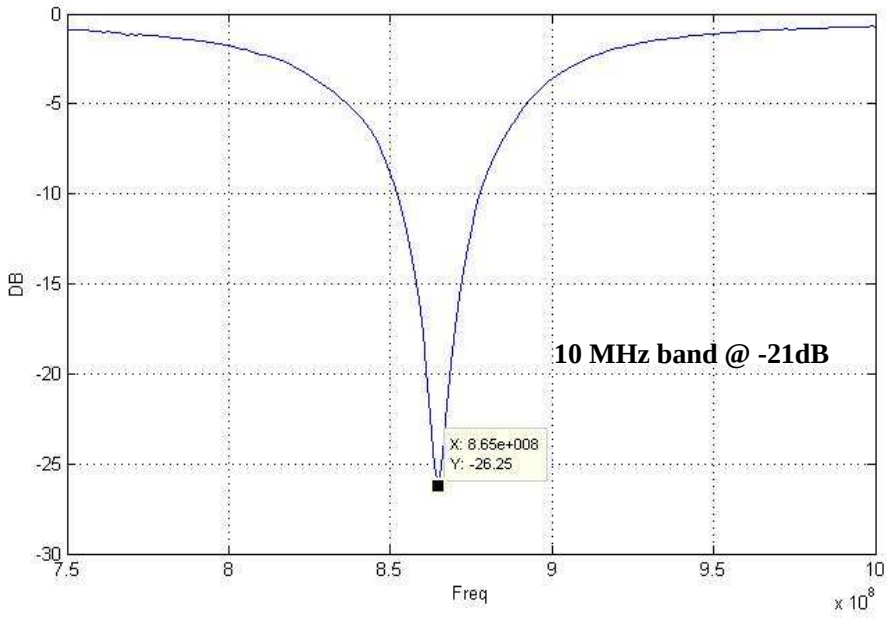

Fig.11.9: measured S_{11} parameters under matching condition

11.2 The power supply

To supply the wireless sensor node we have considered several cases.
The fist one was to implement on the board a simple energy harvesting based on solar cells. We have thought to store the energy harvested inside supercapacitor and so creating a board without battery able to have an unlimited life time. But we quickly left this idea. In fact, to supply the node during 24 hours 4.2mAh (equal to a charge of 15 Coulomb) are necessary (paragraph 10.4). To store so many charge we need at least of 5F capacitor, 3 volt charged. Searching between the available devices on the market [36] [37] it was clear as the dimensions exceed the node geometrics bounds. Moreover the typical working voltage in 2,5V and the best device has a 20µA leakage current (an high leakage current exacts a greater capacity value to be able to supply the node with the same charge).
The next solution considered was to use the smallest battery possible. Before we have tried watch batteries[38]: really small and with a good discharge curve, they have a little charge (nearly 20-25mAh) but mainly the current capable to be drained is very low. We considered also a flexible battery [39]: really thin with a small area, it has poor capacity and a big internal impedance. A big internal impedance cut off the nominal voltage during the peak current (when the node transmits), therefore it has been impossible to use it.
Finally we have chosen a classic coin battery. Using this device it has been possible to have a good amount of energy without being too invasive. We used a 3V 220mAh coin battery 32millimetres diameter and 2,6millimetres high.
In the Chapter 10 , we have evaluated the wireless sensor node energy consumption, with a 33% duty cycle (8hours in wake up mode every 24hours), is equal to 4.2mAh, therefore the node life would last 50days. This is the right node life time if the wireless sensor network user, powers on every node (acting on the switch mounted

on every board) and it uses the network until the batteries are exhausted. Powering off the whole network, if unused for many days, it's possible to increase the life time

11.3 The wireless sensor node

Fixed the power supply and designed the antenna, the last step has been to create the board layout, depicted in Fig 11.10.

a)

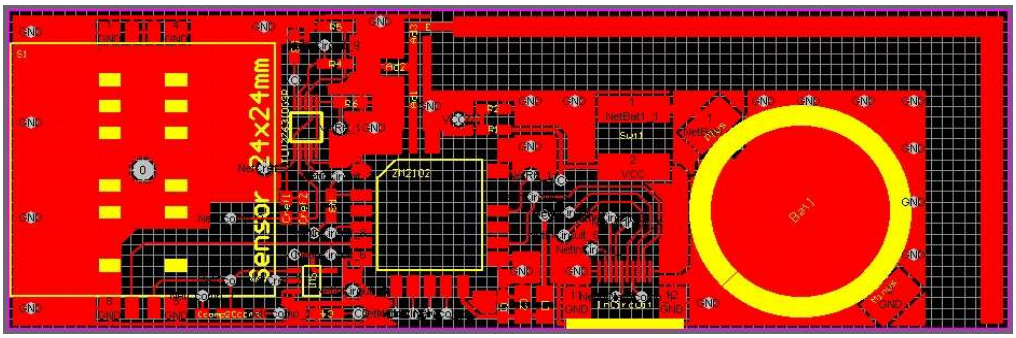

b)

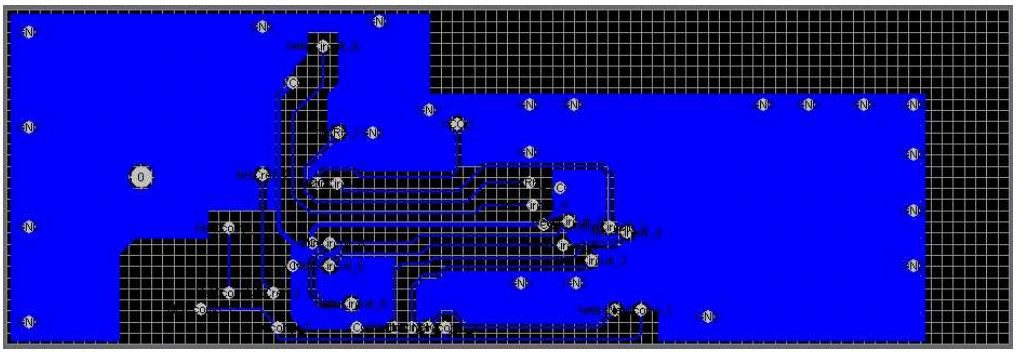

Fig 11.10 : wireless sensor node layout : a) top view b) bottom view

It's important to note that there are not components in the bottom side. In fact, it's basic to guarantee the board flatness in the bonding surface with the batten to improve adhesion.
Moreover, housing the node on the sail, it needs to create a board flexible to adjust itself to the sail curving without breaking electronic or the sensor.
To minimize the dimensions we have used the smallest components and we have designed a dense electrical routing.
In the Fig.11.11 the final wireless sensor node is depicted.

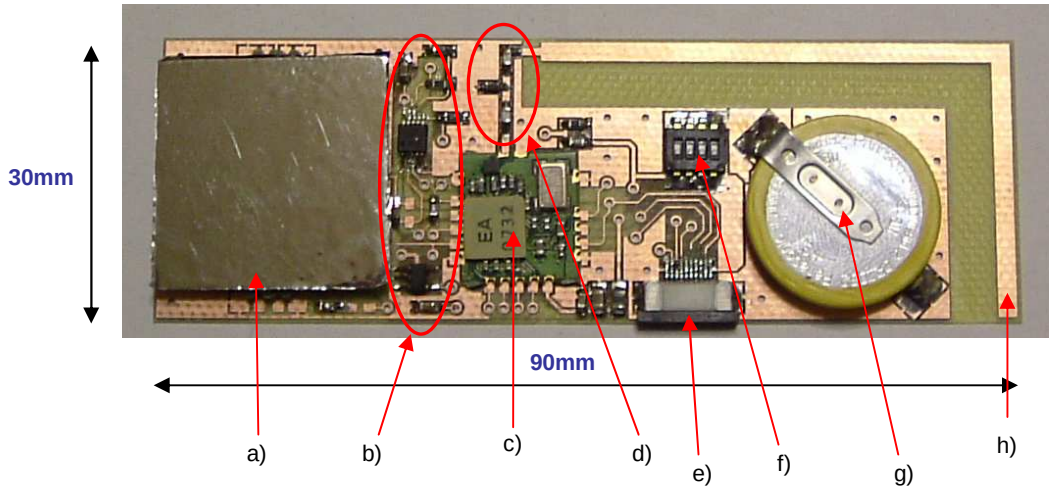

Figure 11.11: final wireless sensor node – top view

In the Fig.11.11 it's possible to note:

a) pressure sensor;

b) developed sensing circuitry;

c) ZW2102 Zensys node : it's the "mind" of the node: it translates the analog voltage value in a digital value, manages the sensing circuit and perform the radio transmissions;

d) matching network;

e) programming connector : connector to program the ZW2102;

f) switch ON/OFF: it's the switch dedicated to power on the node. The Sleep a Wake up mode are possible only if the node has been powered on by the switch;

g) 3V 220mAh coin battery

h) 868MHz ISM band "L" λ/4 monopole antenna created directly on the PCB.

The board has been created using a FR4 DURAVER-E-CU 104ML substrate, 460 μm thick with copper 35 μm thick (both side). The small thickness is necessary so that node is real flexible an capable to follow the sail curving.
All components are housing on the top of the board: then bottom is free to allow a perfect bonding with the sail batten. The figure 11.12 show the bottom layer of the wireless sensor node. We can note as below the "L" λ/4 monopole antenna there isn't metal plane, to allow the right behaviour of antenna, and it's possible to see the static tap to lead the pressure inside the sensor (the biggest hole on the right side).

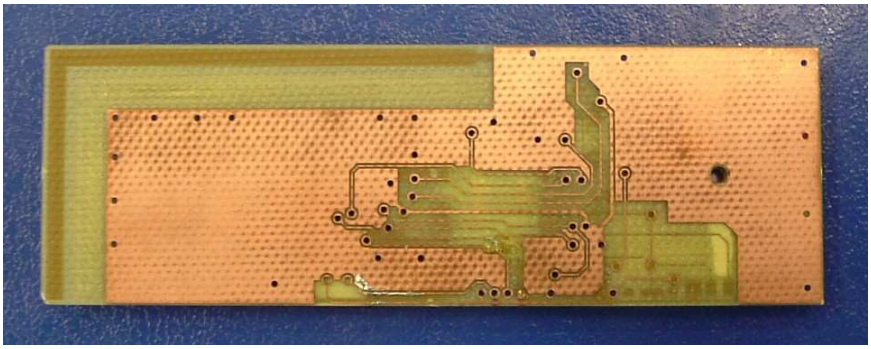

Figure 11.12: wireless sensor node - bottom view

It's important underlining as the sensor isn't bonded directly on the board. In fact, the sensor is too wide: every board strain, due to the batten curving, changes the sensor membrane tension, distorting the pressure value. To avoid this event we use a mechanical solution: below the sensor we have bonded a narrow plinth but with a length equal to the sensor width.

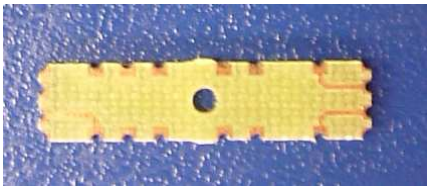

Figure 11.13: Plinth - top view with electrical paths

The plinth is 5mm wide, 24mm long and 1,6mm thick (the fabrication has been described in Chapter 7). Using this structure the board strain doesn't act on a surface of 24x24mm (sensor surface) but on a surface of 5x24mm

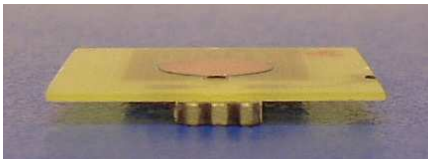

Figure 11.14: plinth bonded to sensor base, the edge electrical paths are evident

It's important point out that the electrical contacts between sensor and board are bypassed by electrical paths on the top plane and on the edges of plinth.
Using the plinth, the sensor is the highest component of the board. On the whole developed wireless pressure node the maximum high is only 4 mm; it is 30mm wide and 90mm long.

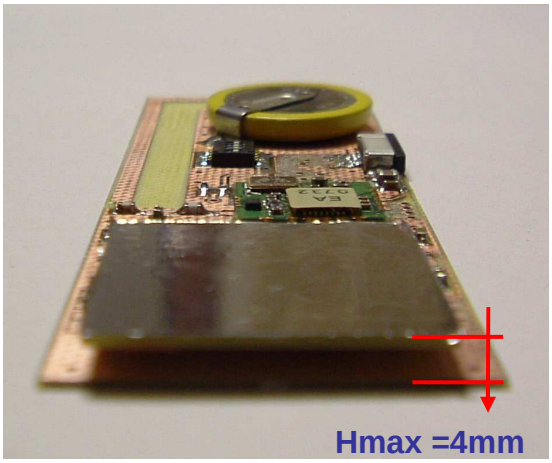

Figure 11.15: wireless pressure monitoring node – sensor side

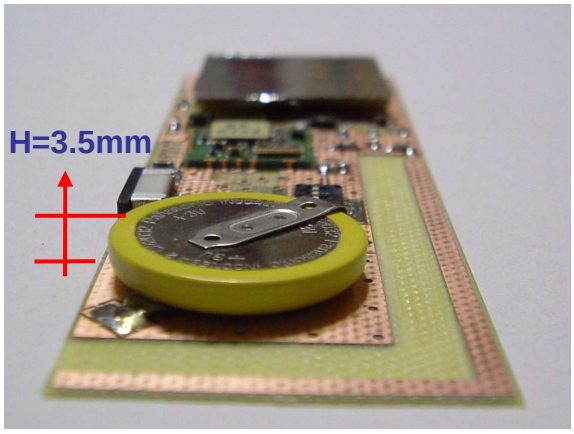

Figure 11.16: wireless pressure node – battery side

As described, the pocket, where the wireless sensor node will be housed, has a depth of 3millimetres. Therefore the sensor sticks out nearly one millimetres: this value is sufficient so that the sensor will be at the same sail level, if we consider a sail cloth thickness nearly 1millimetres. The sail will must have a window shaped with the same dimensions of the sensor.

11.4 The wireless sensor node performances

To qualify the node behaviour in the pressure reading process, basic it is to know the minimum pressure value detectable.
In the previous chapters we have described as the sensor capacity over a range of 2.08pF detects a pressure range of 500Pa (-250Pa,+250Pa) with a mean sensitivity of 4,16fF/Pa. The sensing circuitry translates sensor capacity range over a 3V voltage range, so that a 1mV variation is equal to 0.693fF variation.

The 12bit ADC embedded in the Zensys node has a ±3LSB intregral nonlinearity [12], so that the 3V sensing circuit output voltage range will be quantized over 512 levels. The minimum voltage step detectable will be 5,86mV (noiseless condition). Therefore the minimum voltage step is equivalent of 4,06fF or 1,02Pa. In Tab. 11.1 are summarized these remarks.

ΔC Sensor	**Pressure Range**	**Mean Sensitivity**	**Sensing voltage range**	**Quantization levels**	**Minimum voltage level**	**Minimum ΔC detectable**	**Minimum ΔP detectable**
2.08pF	500Pa	4,16 fF/Pa	3 V	512	5,86mV	4,06 fF	1,02Pa

Tab.11.1: the wireless sensor performances

The performed hypothesis, speaking about the minimum pressure level detectable by the sensor (in the Chapter 6) has been to detect 1-2Pa and, under the best conditions, to reach this sensitivity level is possible.
Finally the node dimensions and the good agreement with the geometric bounds (Fig.11.17), the life time obtained and the completeness, describe the system quality.

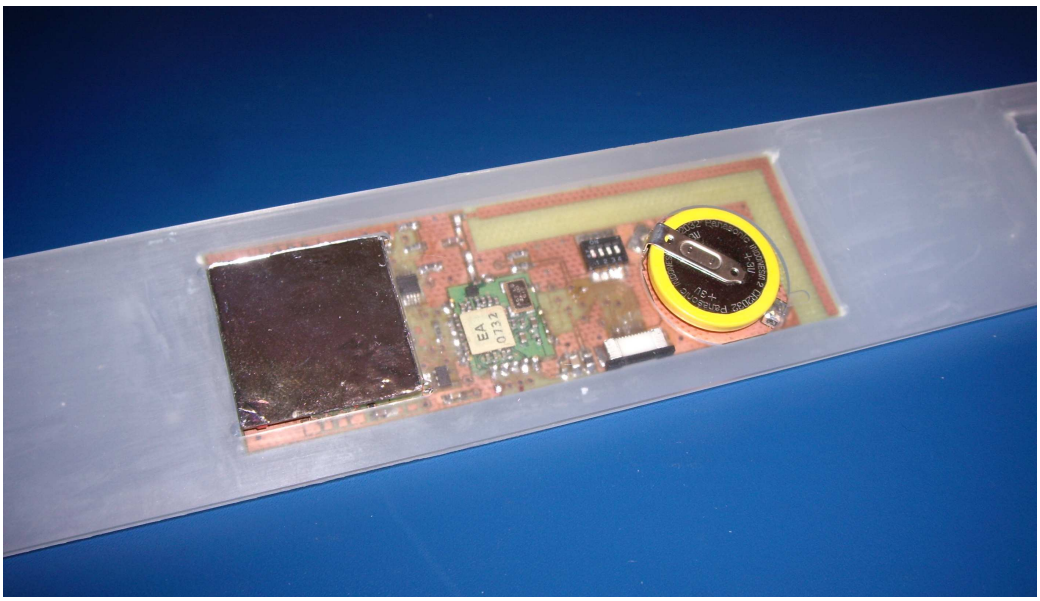

Figure 11.17: wireless pressure node inside the batten

Conclusions

In this thesis a wireless sensor network for fluid fields pressure has been designed, built and tested.
To develop the system, a capacitive pressure sensor, based on polymeric membrane, and read out circuitry, based on microcontroller, have been designed, built and tested. The wireless communication has been performed using the Zensys Z-WAVE platform, and network and data management have been done. Finally, the full embedded system with antenna has been created.
The experimental results, following the sensor testing, have shown good agreements with FEM simulations of the pressure-capacitance static function.
The sensor shows a large dynamic range of 2pF over a ±250Pa range with a capacitive variation of about 4fF/Pa. However the creep phenomenon affects the sensor behaviour: it can decrease the sensitivity for large time scales. In fact, experimental results show how a 140fF of capacitance variation that means 6.5% of degradation of the dynamic range in 36 minutes applied pressure of 250Pa. The viscoeleastic behaviour is due to the material used in the fabrication. The sensor represents a good trade off in terms of materials used, manufacturing and cost. Indeed the Printed Circuit Boards technology has been demonstrated to be low cost, allowing fast prototyping.
The sensor has also a good spatial resolution with a sensitive cavity radius of about 3 millimetres and a low invasive level.
The above remarks describe a device suitable to be used in a wireless sensor network created to perform pressure monitoring on the top of the sail.
To implement the network a star topology has been chosen to speed up the communication between each wireless sensor node and the controller. Several network management strategy has been studied, but none has allowed to reach a full pressure map refresh in a 3 seconds period over a network composed by 50 nodes. In fact the Zensys platform has been demonstrated to be a compact electronic structure (single chip), simple to use and with a excellent range radio, but it has also a poor data rate, so that it is possible to implement a network management strategy capable to work only on 13 nodes in a 3 seconds period. Nevertheless it has been described as to overcome this bound: it would be sufficient to upgrade the platform hardware, mounting inside the nodes the new single-chip version with a data rate four times higher.
Finally it has been created the wireless sensor node. The hardware is 30mm wide and 90 mm long with a thickness of 4 mm: so as to exactly be embedded inside a sail batten. The pressure sensor, the sensing circuitry, the antenna, the Zensys node and the power supply have been implemented on a single board.
It has been realized a low power device: using a 3V 220mAh coin battery , the node life would last about 50 days, operating 8 hours per day.
As described in the table 11.1, and neglecting the electronic noise, the system, is able to detect a pressure variation of about 1Pa.

To complete the work, we are developing a sail profile model to put inside the wind tunnel. The experimental tests will be fundamental to confirm the features of the system, before mounting the wireless sensor network on the top of a real sail.

Bibliography

[1] I. H. Abbot, A. E. von Doenhoff, *Theory of wing sections*, Dover Publications New York, 1958.

[2] R. Eppler, *Airfoil Design and Data*, Springer-Verlag, Hardcover, 1990.

[3] M. B. Cohn, R. Roehnelt, Ji-Hai Xu, A. Shteinberg, S. Cheung, *MEMS Packaging on a Budget (fiscal and thermal)*, Electronics, Circuits and Systems,2002. 9th International Conference on, Vol. 1, 2002, pp. 287-290.

[4] S.Rhee, S. Liu, *An Ultra-low Power, Self-organizing Wireless Network and Its Applications to Noninvasive Biomedical Instrumentation*, 2002 IEEE/Sarnoff Symposium on Advances in Wired and Wireless Communications West Trenton, NJ, USA, Mar. 13, 2002.

[5] M. Tubaishat, S. Madria.; *Sensor networks: an overview* , Potential, IEEE volume 22, Issue 2, Apr-May 2003 Page(s):20-23 Digital Object Identifier 10.1109/MP.2003.1197877 .

[6] M.Zoboli; *Lezioni di Campi Elettromagnetici*, Edizioni Sanra Croce

[7] Torfs, T.; Sanders, S.; Winters, C.; Brebels, S.; Van Hoof, C.; *Wireless network of autonomous environmental sensors*; Sensor, 2004. Proceeding of IEEE 24-27 Oct. 2004 Page(s):923 - 926 vol.2 Digital Object Identifier 10.1109/ICSENS.2004.1426322

[8] Polastre, J.; Szewczyk, R.; Culler, D.; *Telos: enabling ultra-low power wireless research*.Information Processing in Sensor Networks, 2005. IPSN 2005. Fourth International Symposium on. 15 April 2005 Page(s):364 - 369 Digital Object Identifier 10.1109/IPSN.2005.1440950

[9] ZigBee Technology Documents; www.sigbee.org

[10] Min R. and Chandrakasan A.;*Top Five Myths about the Energy Consumption of Wireless Communication.* Mobile Computing and Communications Review, Volume 7, Number I

[11] Prophet G.;*Is ZigBee ready for the big time?*;EDN, Agust 2004

[12] Z-WAVE Developper's kit documentation

[13] Rhee, S.; Seetharam, D.; Liu, S.;*Techniques for minimizing power consumption in low data-rate wireless sensor* networks.Wireless Communications and Networking Conference, 2004. WCNC.2004 IEEE Volume 3, 21-25 March 2004 Page(s):1727 - 1731 Vol.3

[14] M.Zagnoni, *Mixed Domain Sensor System*, Alma Mater Studiorum University of Bologna, March 06

[15] G. Mc Crum, C. P. Buckley, C. B. Bucknall, *Principles of Polymer Engineering*, seconded, Oxford University Press, Oxford, 2000.

[16] DuPont Kapton DataSheets, downloaded at http://www.dupont.com/kapton/

[17] V. E. Smirnova, N. A. Dolotova, V. I. Aleshin, V. P. Volodin, *Study of creep in polyimide film*, Polym. Sci., Ser. A 40, Is. 7, 1998, pp. 730-735.

[18] M. Zagnoni, A. Golfarelli, P. Proli, S. Callegari, A. Talamelli, E. Sangiorgi and, M. Tartagni, A Non Invasive Capacitive Sensor Strip for Aerodynamics Pressure Measurement, *Sensors and Actuators A*, Vol. 123-124 (2005), pp. 240-248.
[19] Wilkinson S., *"Static Pressure Distributions Over 2D Mast/Sail Geometries"*, Marine Technology, vol 26(4),333-337, 1989.
[20] *Encyclopedia of Polimer Science and Engineering*, Vol. 9, Mechanical Properties, p. 390, Copyright r 1987, by John Wiley and Sons, Inc.
[21] N. Soin, B. Y. Majlis, *An Analytical Study on Diaphragm Behavior for Micromachined Capacitive Pressure Sensor*, ICSE 2002, IEEE International Conference on Semiconductor Electronics, Proceedings, 2002, pp. 505-510.
[22] www.WB-sail.fi
[23] *http://www.comsol.com*.
[24] K. I. Arshak, D. Morris, A. Arshak, O. Korostynska, E. Jafer, Development of a wireless pressure measurement system using interdigitated capacitors, *IEEE Sensors Journal*, Vol. 7 (2007), pp. 122-129.
[25] Dupont Mylar DataSheet, downloaded at http://www.dupont.com/kapton/
[26] L.k. Baxter "*Capacitive Sensors*"; IEEE Press, 1997
[27] TLV276x DataSheets, downloaded at http://www.ti.com
[28] TS5A4595 DataSheets, downloaded at http://www.ti.com
[29] S.Tanenbaum;"*Computer Networks"*Prentice Hall.
[30] 300 series Z-WAVE Single Chip DataSheets, downloaded at http://www.zen-sys.com
[31] Rao S. *Estimating the ZigBee transmission-range ISM band*. EDN May 2007
[32] Buckley, J.; Aherne, K.; O'Flynn, B.; Barton, J.; Murphy, A.; O'Mathuna, C.;*Antenna performance measurements using wireless sensor networks*. Electronic Components and Technology Conference, 2006. Proceedings. 56th.30 May-2 June 2006 Page(s):6 pp.
[33] Warren L. Stutzman, Gary A. Thiele *Antenna Theory and design*. 1981 John Wiley and sons
[34] Smith,K.*Antennas for low power applications*. RFM, RF Monolithics inc. technical documentation
[35] Bowick, C. " RF Circuit Design"; Howard W.Sama. 1982
[36] BoostCap Ultracapacitor PC series Data Sheet. Maxwell Technologies
[37] Powerstor Aerogel Supercapacitor A series DataSheet Cooper Bussman
[38] 319 Watch Battery DataSheet Renata Battery
[39] LFP25 – Flexcard DataSheet Varta Battery